Modelling locust foraging

Fillipe Georgiou
BMath(Hons) BEng(Hons)

November 2022

Supervised by
Ngamta Thamwattana, Bishnu Lamichhane, J. E. F. Green, Jerome Buhl

A document submitted in fulfilment of the requirements for the degree of
Doctor of Philosophy
at
University of Newcastle, Australia

This research was supported by an Australian Government Research Training Program (RTP) Scholarship.

To my parents, who inspired and nurtured a love of mathematics.

Abstract

Locusts are short horned grasshoppers that exhibit two diametrically opposed behavioural types depending on their local population density. These are: solitarious, where they will actively avoid other locusts, and gregarious where they will seek them out. It is in this gregarious state that locusts can form massive and destructive flying swarms or plagues. However, these swarms are usually preceded by the aggregation of juvenile wingless locust nymphs. In this thesis we develop a mathematical model to understand how and why the distribution of food resources affect the group formation process.

We do this by first deriving a multi-population partial intergro-differential equation model that includes non-local locust interactions, local locust and food interactions, and gregarisation dynamics. The model is studied using a combination of analytical techniques, such as linear stability theory and gradient flow methods, and numerical simulations. The numerical solutions are obtained using an adaptive time-stepped finite volume based scheme combined with fast Fourier transforms to efficiently solve the non-local component. Our initial results suggest that food acts to increase the maximum density of locust groups, lowers the percentage of the population that needs

to be gregarious for group formation, and decreases both the required density of locusts and time for group formation around an optimal food width. Further, by considering foraging efficiency within the numerical experiments, we find that there exists a foraging advantage to being gregarious.

Next, we explore this foraging advantage of gregarisation within increasingly heterogeneous environments. We consider a single two dimensional simulation of a spatially heterogeneous environment to understand the mechanics of gregarious/solitarious foraging. We also investigate the steady state foraging advantage in environments ranging from homogeneous to very spatially heterogeneous. Finally, we perform a parameter sensitivity analysis to determine the model parameters that have the greatest effect on foraging advantage. We find that during the aggregation stage, prior to the onset of marching, in increasingly heterogeneous food environments it is better for a locust to be gregarious than solitarious. In addition, we find that this is intrinsic to the gregarious/solitarious behavioural dynamic as it occurs almost regardless of the model parameters.

In the final part of this thesis, we expand the model to include the effect of hunger on locust interactions and repeat our analyses. We find that the results are consistent with the less complex model and that hunger acts to decrease the maximum density of locust groups and raises the percentage of the population that needs to be gregarious for group formation.

Overall, this thesis demonstrates the advantages and power of continuum models in providing insights into biological systems. The results presented

here provide avenues of future exploration both in the mathematical and experimental spaces. Finally, it is our intention that this thesis will provide a guide for the creation and analysis of future models of collective behaviour.

Declarations

STATEMENT OF ORIGINALITY

I hereby certify that the work embodied in the thesis is my own work, conducted under normal supervision. The thesis contains no material which has been accepted, or is being examined, for the award of any other degree or diploma in any university or other tertiary institution and, to the best of my knowledge and belief, contains no material previously published or written by another person, except where due reference has been made. I give consent to the final version of my thesis being made available worldwide when deposited in the University's Digital Repository, subject to the provisions of the Copyright Act 1968 and any approved embargo.

Fillipe Georgiou

ACKNOWLEDGEMENT OF AUTHORSHIP

I hereby certify that the work embodied in this thesis contains published paper/s/scholarly work of which I am a joint author. I have included as part of the thesis a written declaration endorsed in writing by my supervisor, attesting to my contribution to the joint publication/s/scholarly work.

By signing below I confirm that Fillipe Georgiou contributed equally to the papers/publications entitled

[1] *Accepted*, Georgiou, F., Buhl, J., Green, J.E.F., Lamichhane, B., and Thamwattana, N. (2022). Modelling foraging competition between solitarious and gregarious organisms in increasingly heterogeneous environments. Journal of Insect Physiology.

[2] Georgiou, F., and Thamwattana, N. (2020). Modelling phagocytosis based on cell–cell adhesion and prey–predator relationship. Mathematics and Computers in Simulation 171, 52–64.

[3] Georgiou, F., Lamichhane, B., and Thamwattana, N. (2018). An adaptive numerical scheme for a partial integro-differential equation. ANZIAM Journal 60, C187–C200.

[4] Georgiou, F., Buhl, J., Green, J.E.F., Lamichhane, B., and Thamwattana, N. (2021). Modelling locust foraging: How and why food affects group formation. PLOS Computational Biology 17, e1008353.

[5] Georgiou, F., Thamwattana, N., and Lamichhane, B.P. (2019) Modelling cell aggregation using a modified swarm model, In Elsawah, S. (ed.) MODSIM2019, 23rd International Congress on Modelling and Simulation. Modelling and Simulation Society of Australia and New Zealand.

[6] Georgiou, F.H., Lamichhane, B., Thamwattana, N., Buhl, J., and Green, E. (2020). A numerical scheme for non-local aggregation with non-linear diffusion and approximations of social potential. ANZIAM Journal 62, C242–C255.

Ngamta Thamwattana

Acknowledgements

First and foremost, I would like to thank my supervisors Prof. Ngamta Thamwattana, Dr Bishnu Lamichhane, Dr Edward Green, and Dr Jerome Buhl. This endeavour would not have been possible without their continual collaboration, counsel, and care. In addition, thank you to A/Prof Mike Meylan and the team at ClimateRisk for the incredible placement experience.

I would like to also thank my fellow PhD students for interesting discussions, meetings about meetings, and making the process that little bit easier with their camaraderie. My friends and family, for giving me constant support and well needed diversions. Last (but certainly not least), my partner Vanessa who has helped me every step of the way and in capacity she could.

Contents

List of Figures

List of Tables

Chapter 1

Introduction

Locust swarms have plagued humankind for millennia, affecting every continent except Antarctica and impacting on the lives of 1 in 10 people [91]. A single locust swarm can contain millions of individuals [4] and in a single day is able to move up to 200 kilometres [38]; with each locust being able to consume its own body weight in food [99]. Locusts have played a role in severe famine [39], disease outbreaks [90], and even the toppling of dynasties [63]. More recently, in March 2020 a perfect storm of events caused the worst locust outbreaks in over 25 years in Ethiopia, Somalia and Kenya during the COVID-19 pandemic [57]. Damaging tens of thousands of hectares of croplands and pasture, these outbreaks presented an unprecedented threat to food security and livelihoods in the Horn of Africa. In addition, the onset of the rainy season meant the locusts were able to breed in vast numbers raising the possibility of further outbreaks [37].

Locusts are short horned grasshoppers that exhibit density-dependent phase-polyphenism, i.e., two or more distinct phenotype expressions from a single genotype depending on local population density [71]. In locusts there are two key distinct phenotypes, solitarious and gregarious, with the process of transition called gregarisation. Gregarisation affects many aspects of locust morphology from colouration [78], to reproductive features [82], to

Figure 1.1: **Photo of locusts by Prof Gregory Sword.** An exemplary image of the changes brought about by phase polyphenism. The locust on the left is in the solitarious phase and has taken on cryptic colouring, whereas the locust on the right is in the gregarious phase and has aposematic colouring.

behaviour [86] (see Figure 1.1). Behaviourally, solitarious locusts are characterised by an active avoidance of other locusts, whereas gregarious locusts are strongly attracted to other locusts. Gregarisation is brought about by locusts crowding together and can be reversed by isolating the individuals [99]. In the Desert locust (*Schistocerca gregaria*), gregarisation can take as little as 4 hours with the timeframe for reversal dependant on the length of time the individual has been gregarious (again, potentially as little as 4 hours) [71]. It is in the gregarious state that locusts exhibit large scale and destructive group dynamics with flying swarms of adult locusts being perhaps the most infamous manifestation of this.

Despite the destruction caused by adult swarms, the most crucial phase for locust outbreak detection and control occurs when wingless nymphs form hopper bands, large groups of up to millions of individuals marching in unison [99]. Depending on the species, these groups may adopt frontal or columnar formations, the former being comet like in appearance with dense front and less dense tail [17], and the latter being a network of dense streams [99]. As a precursor to hopper bands, nymphs will form gregarious aggregations or groups, i.e. a large mass of gregarious nymphs. Understanding the group dynamics of gregarious locusts are key to improving locust surveys and control by increasing our ability to understand and predict movement.

In addition to the group dynamics, better knowledge of locust interactions with the environment would help to improve the prediction of outbreaks [93]. On longer time-scales, environmental conditions such as rain events synchronize locust lifecycles and can lead to repeated outbreaks [71]. On shorter time-scales, changes in resource distributions at both small and large spatial scales have an effect on locust gregarisation [25, 31, 32, 33]. It is these short time-scale locust-environment interactions that we investigate in this thesis, using mathematical modelling to further understand both their effect on group formation and if there is any advantage to gregarisation in this context.

As all the mentioned behaviours arise from simple inter-individual interactions, understanding the group dynamics of gregarious locusts can also give deep insight into the underlying mechanisms of collective behaviour. Consequently they are an important subject of mathematical modelling efforts. Individual based models (IBMs) are the dominant approach in the locust modelling literature [4, 27]. In IBMs locusts are modelled as discrete individuals who update their velocity according to simple interaction rules. IBMs are categorised as second order models if they include particle inertia, and first order (or kinematic) if inertia is neglected [21]. For example, the second order model explored by D'Orsogna et al. [30] has individuals update their

velocity, with self propulsion, friction, and the distance weighted average of all other individuals. Given N individuals, each at position X_i we would write

$$\dot{X}_i = V_i, \tag{1.1}$$

$$\dot{V}_i = \alpha V_i - \beta V_i |V_i|^2 - \frac{1}{N} \sum_{j=1}^{N} \nabla Q(X_i - X_j), \tag{1.2}$$

where Q is termed the social potential, αV_i gives the individuals self propulsion and $-\beta V_i |V_i|^2$ represents the drag caused by friction. The social potential is a function $Q : \mathscr{R}^d \to \mathscr{R}$ that describes how the strength of interaction between individuals varies with the distance between them. It is worth noting that the distance may be topological and not just spatial distance [51]. Second order IBMs have been used in modelling collective behaviour in fish [7, 8, 50, 53, 56, 59], birds [26, 51], and abstract organisms [61, 64]. Second order IBMs can be constructed to simulate two key behaviours; flocking, which is the collective movement of individuals in a common direction, and milling, the collective movement of individuals around a common point (see Figure 1.2 for examples).

Within the realm of locust modelling, second order IBMs in conjunction with lab experiments and field data have teased out a variety of locust movement characteristics. In a 2006 paper, Buhl et al. used a combination of modelling and lab experiments to find that the critical density of locusts for the transition from disordered to ordered movement was between 17.2 and 24.6 locusts/m^2 and that as the density of locusts increases the stability of the movement direction increases [16]. This was supported using field data in 2011 [17], where it was additionally found that locust movement is mediated by combinations of social interactions such as avoidance, alignment, and attraction, and that the range of these interaction is 13.5 cm [17]. In addition, while the onset of collective behaviour may be brought about by

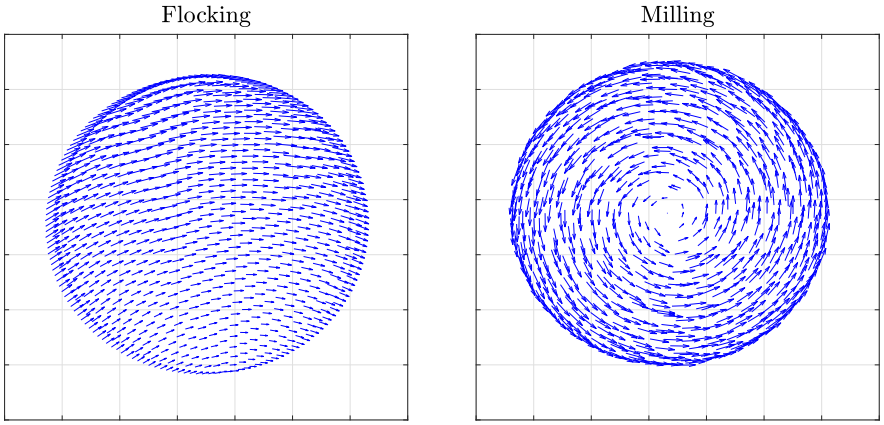

Figure 1.2: **Types of collective movement in 2nd order IBMs.** Flocking, which is the collective movement of individuals in a common direction, and milling, the collective movement of individuals around a common point. In both plots, $N = 800$, $Q(\boldsymbol{x})$ is given by 1.4 with $A = 1$,$R = 10/9$,$a = 1$, and $r = 0.75$. Finally, for flocking $\alpha = \beta = 0$ and for milling $\alpha = 0.1$, $\beta = 0.05$.

cannibalism [9] a study by Buhl, Sword, and Simpson showed that this model of movement was not valid where marching had already begun to occur [15]. An alternative study by Ariel et al. found that pause and go motion may be pivotal in the onset and maintenance of collective movement [5].

In contrast to second order IBMs, first order IBMs do not have the same dynamic steady states, instead settling into a crystal like structure (in the absence of other forces). However, first order IBMs are still useful for modelling the more disordered stages of locust behaviour [11, 96], and can give insight into the behaviour of higher order IBMs [20, 21]. The simplest first order IBM is given by,

$$\dot{X}_i = -\frac{1}{N}\sum_{j=1}^{N} \nabla Q(X_i - X_j), \tag{1.3}$$

where again Q is a social potential. A common social potential in locust

modelling is the Morse potential given by,

$$Q(\boldsymbol{x}) = -Ae^{-\frac{|\boldsymbol{x}|}{a}} + Re^{-\frac{|\boldsymbol{x}|}{r}}, \tag{1.4}$$

where A, R are the strength of attraction and repulsion, respectively, and a, r are the characteristic length-scale on which they occur. There are four possible combinations of A, R, a and r leading to five different behaviours [67]:

- If $R > A$ and $r > a$, repulsion dominates attraction and leads to aggregations failing to form.
- If $A > R$ and $a > r$, attraction dominates repulsion and leads to densely packed aggregations regardless of number of individuals.
- If $A > R$ and $r > a$, attraction is stronger at close range and repulsion is stronger at long range leading to a combination of the above two cases.
- If $R > A$ and $a > r$, repulsion is stronger close range and attraction is stronger at long range and can result in two differing steady state aggregations; H-stable, where as the number of individuals increases the spacing between individuals approaches a finite constant, and 'catastrophic' where the spacing of individuals goes to zero as $N \to \infty$.

We can determine the condition for H-stability by first considering the total potential energy of the system (in the absence of boundary interactions), this is total of the pairwise potentials Q, and is given by

$$E = \frac{1}{2N} \sum_{i=1}^{N} \sum_{j=1, i \neq j}^{N} Q(X_i - X_j), \tag{1.5}$$

we take a factor of $\frac{1}{2}$ so that each pair is only counted once. We note that (1.3) minimises the energy given by (1.5). For H-stability we require $E > -NB$

for some $B \in \mathbb{R}\ \forall N > 0$, or equivalently for an absolutely integrable Q [76],

$$\int_{\mathbb{R}^n} Q(\boldsymbol{x}) d\boldsymbol{x} > 0,$$

where n is the number of spatial dimensions. Thus, for the Morse potential given by 1.4, we have the condition in two spatial dimensions

$$\frac{a}{r} < \left(\frac{A}{R}\right)^{-\frac{1}{2}}.$$

We can then combine the H-Stability condition with the four cases given previously into one succinct statement, that is, the condition for H-Stable aggregations in two dimensions is

$$1 < \frac{a}{r} < \left(\frac{A}{R}\right)^{-\frac{1}{2}},$$

with the corresponding condition for the 'catastrophic' aggregations being

$$1 < \left(\frac{A}{R}\right)^{-\frac{1}{2}} < \frac{a}{r}.$$

Examples of the resulting steady states can be seen in Figure 1.3, for each type H-Stable and 'catastrophic' the red x's are a simulation of 100 individuals and the blue dots are 1000 individuals.

One downside of IBMs is that there are few analytical tools available to study their behaviour. In contrast, continuum models, in which locusts are represented as a population density that is a function of space and time, can be analysed using an array of tools from the theory of partial differential equations (PDEs). They are most appropriately employed when there are a large number of individuals since they do not account for individual behaviour, instead giving a representation of the average behaviour of the group. The latter (continuum) approach is adopted in this thesis.

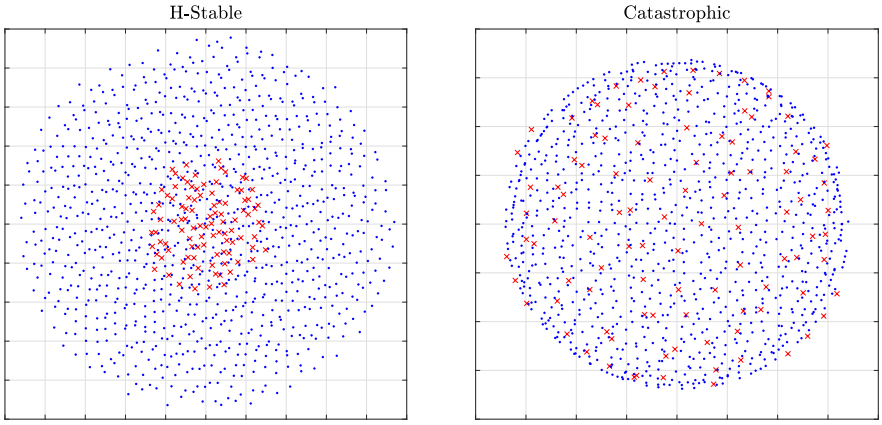

Figure 1.3: **Example steady states of 1st order IBMs.** For each type H-Stable and 'catastrophic' the red x's are a simulation of 100 individuals and the blue dots are 1000 individuals. In both plots, the blue dots correspond to $N = 1000$ and the red crosses correspond to $N = 100$. $Q(\boldsymbol{x})$ is given by 1.4 with $R = 1$,$A = 0.5$,$r = 1$, and $a = 1.1$ for the H-Stable and $a = 10$ for the catastrophic.

It is possible to derive the continuum equivalent of (1.3) following the work of Bodnar and Velazquez [14]. To begin we divide up the space into small intervals, with the number of individuals in an interval given by

$$\rho(y,t) = \frac{\#\{X_i \in [y-h, y+h]\}}{2h}, \tag{1.6}$$

where in the continuum limit under consideration, h satisfies

$$\delta \ll h \ll 1, \tag{1.7}$$

with δ being the average distance between individuals. We then note by assuming that in each interval the individuals are locally at equilibrium then

as $h \to 0$ the velocity of an individual depends only on its location, i.e.

$$v(x,t) = -\nabla \sum_{n=1}^{N} \left[Q(x - X_n) \right]. \tag{1.8}$$

This allows us to approximate the velocity field using integrals to give

$$v(x,t) = -\nabla \int_{\Omega} Q(x-y)\rho(y,t)dy. \tag{1.9}$$

where Ω is our domain. The evolution of the macroscopic density as $\delta, h \to 0$ is then given by the continuity equation

$$\frac{\partial \rho(x,t)}{\partial t} + \frac{\partial j}{\partial x} = 0,$$

with particle flux given by

$$j = \rho v.$$

This results in the equations

$$\frac{\partial \rho}{\partial t} + \nabla \cdot (\boldsymbol{v}\rho) = 0, \tag{1.10}$$

with

$$\boldsymbol{v} = -\nabla Q * \rho, \tag{1.11}$$

where Q is again the social potential, ρ is the density (either mass or population per unit area) of the species in question, and $*$ is the convolution operation defined as

$$Q(x) * \rho = \int_{\Omega} Q(x-y)\rho(y)dy. \tag{1.12}$$

This is known as the non-local aggregation equation, first proposed by Mogilner and Edelstein-Keshet [68] who showed the existence and stability of swarms and found travelling wave solutions. In an analogous behaviour to 1.3 min-

imising the energy 1.5, 1.10 is a gradient flow of the form

$$\frac{\partial \rho}{\partial t} + \nabla \cdot \left(\rho \nabla \left[\frac{\delta E}{\delta \rho} \right] \right) = 0, \tag{1.13}$$

that minimises an energy functional given by

$$E[\rho] = \int_{\Omega} \frac{1}{2} \rho [Q * \rho] \, dx, \tag{1.14}$$

with $\frac{\delta E}{\delta \rho}$ being the functional derivative from calculus of variations. Using the gradient flow form of 1.11 and the social potential 1.4, Bernoff and Topaz found analytic expressions for the steady states [11].

One issue that arises with the simple model is that the maximum density grows unbounded with increasing organism mass, that is as more individuals are added the maximum density of the resulting aggregation increases rather than the width (or support) of the aggregation, similar to the 'catastrophic' regime of (1.3). This issue of unbounded density can be avoided with the inclusion of non-linear local repulsion, which leads to compact and bounded solutions [97]. Accordingly, (1.11) is modified to become

$$\boldsymbol{v} = -\nabla (Q * \rho + \gamma \rho^m), \tag{1.15}$$

where $m \geq 2$. While we have presented the model a for single population, the model has been further adapted to consider multiple interacting populations [47]. In addition, while the kinematic model does not capture complex behaviours such as alignment, the steady state solutions determine the spatial shape and density of flock solutions of second order models (i.e. collective movement of individuals in the same direction) [20, 21].

In a 2012 paper, Topaz et. al. [98] used a multi-population aggregation equation to model locusts as two distinct behavioural sub-populations, solitarious and gregarious. By considering the locust-locust interactions and the transition between the two states, they were able to deduce both the criti-

cal density ratio of gregarious locusts that would cause a group to form and visualised the rapid transition once this density ratio had been reached [98]. Similarly, in our work we focus on the formation of aggregations (or groups) of gregarious locusts, visualised as a clump of gregarious locusts, rather than on the collective movement dynamics in hopper bands. For simplicity, the Topaz model focused on inter-locust interactions and ignored interactions between locusts and the environment. While there exists some continuum models of locust food interactions to investigate the effect of food on peak locust density [12] or to consider hopper band movement [13], we are not aware of any studies that consider locust-locust and locust-food interactions as well as gregarisation in a continuum setting.

The aims of this thesis are threefold. Firstly, to introduce a new mathematical model that extends the 2012 Topaz model by including both locust-food dynamics and local repulsion. The model is based on an idealised locust which has both long and short range locust interactions and only interacts with food when it comes into direct contact with it. Secondly, we use our new model to investigate how the spacial distribution of food affects the gregarisation and group formation process. Finally, we consider under what conditions being gregarious might confer an advantage compared to being solitarious in terms of access to food.

With these goals in mind, this thesis is organised as follows. Chapter 2 introduces the model of locust foraging and the concept of foraging advantage that will be used throughout this thesis. In Chapter 3, we explore a variety of numerical techniques for non-local problems first in one dimension and then in two or more dimensions (with discussions on implementing them in MATLAB in Appendix A). Next, Chapter 4 analyses the model with a variety of analytic and numerical techniques to understand 'Does food affect the required density of locusts for the formation of locust groups?', 'Does food affect the required percentage of the locust population being gregarious for the formation of locust groups?', 'Does food affect the time required for the

formation of locust groups?', 'Does food affect the density of locust groups?' and 'Does gregarisation offer some advantage while foraging?'. Chapter 5 then expands upon the last question to explore foraging in increasingly heterogeneous environments in two dimensions. Then, in Chapter 6 we expand our model to include a dimension of hunger and explore how this affects our previous results. Finally, in Chapter 7 we discuss the important results of this thesis and avenues of further exploration.

Chapter 2

Model and measures

The aims of this chapter are to introduce a new mathematical model that extends the 2012 Topaz model by including both locust-food dynamics and local repulsion. The model is based on an idealised locust which has both long and short range locust interactions and only interacts with food when it comes into direct contact with it. In addition, we will introduce the metric of foraging advantage to measure locust foraging. In Chapter 4, we use our new model and the numerical techniques developed in Chapter 3 to investigate how the spatial distribution of food affects the gregarisation and group formation process and consider under what conditions being gregarious might confer an advantage compared to being solitarious in terms of access to food.

Chapters 2 and 4 were originally published as *F. Georgiou, J. Buhl, J. E. F. Green, B. Lamichhane, and N. Thamwattana, 'Modelling locust foraging: How and why food affects group formation', PLOS Computational Biology, vol. 17, no. 7, p. e1008353, Jul. 2021, doi: 10.1371/journal.pcbi.1008353.* [45]

2.1 Model derivation

In this section we present a PDE model of locust foraging that includes both local inter-individual and food interactions and non-local inter-individual interactions. In order to simplify the model we make the following assumptions about locust behaviour:

1. Locusts can be classified as either solitarious or gregarious.
2. Locusts only interact with food resources when they come into direct contact with them and are interactions the same for solitarious and gregarious individuals.
3. Local interactions between locusts (both gregarious and solitarious) are repulsive (i.e. they avoid close physical contact).
4. Solitarious locusts experience a non-local (i.e. longer-ranged) repulsion from other locusts of either type.
5. Gregarious locusts experience a non-local long-range attraction and short-range repulsion from other locusts, which is consistent with them forming a well-spaced aggregation [15].
6. The nature (attractive or repulsive) and strengths of all interactions are constant in time.

In this model locusts are represented as a density of individuals (number per unit area) in space and time and are either solitarious, $s(\boldsymbol{x}, t)$, or gregarious $g(\boldsymbol{x}, t)$, with the total local density defined as $\rho(\boldsymbol{x}, t) = s(\boldsymbol{x}, t) + g(\boldsymbol{x}, t)$. For convenience we will also define the total mass of locusts as

$$M = \int \rho(\boldsymbol{x}, t)\, d\boldsymbol{x}, \tag{2.1}$$

and the global gregarious mass fraction as

$$\phi_g(t) = \frac{\int g(\boldsymbol{x}, t)\, d\boldsymbol{x}}{M}. \tag{2.2}$$

We assume that the time-scale of gregarisation is shorter than the life cycle of locusts, ignoring births and deaths and thus conserving the total number of locusts. We allow for a transition from solitarious to gregarious and vice-versa depending on the local population density. Hence, conservation laws give equations of the form

$$\frac{\partial g}{\partial t} + \nabla \cdot (\boldsymbol{J}_{g_{\text{local}}} + \boldsymbol{J}_{g_{\text{non-local}}}) = K(s, g), \tag{2.3a}$$

$$\frac{\partial s}{\partial t} + \nabla \cdot (\boldsymbol{J}_{s_{\text{local}}} + \boldsymbol{J}_{s_{\text{non-local}}}) = -K(s, g), \tag{2.3b}$$

where $\boldsymbol{J}_{(s,g)_{\text{local}}}$ is the flux due to local interactions, $\boldsymbol{J}_{(s,g)_{\text{non-local}}}$ is the flux due to non-local interactions, and $K(s, g)$ represents the transition between the solitarious and gregarious states.

In addition to locust densities, we include food resources in our model and let $c(\boldsymbol{x}, t)$ denote the food density (mass of edible material per unit area). We assume that locust food consumption follows the law of mass action and on the time-scale of group formation food production is negligible, giving

$$\frac{\partial c}{\partial t} = -\kappa c(\boldsymbol{x}, t)\rho(\boldsymbol{x}, t), \tag{2.4}$$

where κ is the locust's food consumption rate.

2.1.1 Local interactions

We now turn to specifying the local interaction terms in (2.3a) and (2.3b). These are captured by taking the continuum limit of a lattice model (this should, however, be only considered an asymptotic approximation [24, 69]) following the work of Painter and Sherratt [70]. We begin by considering solitarious locust movement on a one-dimensional lattice (we assume that local gregarious locust behaviour is the same resulting in a similar derivation). Let s_i^t be the number of solitarious locusts at site i at time t, and let g_i^t, ρ_i^t, and c_i^t be similarly defined.

We assume that the transition probabilities for a locust at the i^{th} site depends on the food density at that site, and the relative population density between the current site and neighbouring sites. If we let $\mathcal{T}_i^{\pm}$ be the probability at which locusts at site i move to the right, $+$, and left, $-$, during a timestep, then our transition probabilities are

$$\mathcal{T}_i^{\pm} = F(c_i)(\alpha + \beta(\tau(\rho_i) - \tau(\rho_{i\pm1}))), \tag{2.5}$$

where F is a function of food density, τ is a function related to the local locust density, and α and β are constants. Then the number of individuals in cell i at time $t + \Delta t$ is given by

$$s_i^{t+\Delta t} = s_i^t + \mathcal{T}_{i+1}^- s_{i+1}^t + \mathcal{T}_{i-1}^+ s_{i-1}^t - (\mathcal{T}_i^- + \mathcal{T}_i^+) s_i^t. \tag{2.6}$$

Substituting (2.5) into (2.6) gives

$$\begin{aligned} s_i^{t+\Delta t} =& s_i^t + F(c_{i+1})(\alpha + \beta(\tau(\rho_{i+1}) - \tau(\rho_i)))s_{i+1}^t \\ &+ F(c_{i-1})(\alpha + \beta(\tau(\rho_{i-1}) - \tau(\rho_i)))s_{i-1}^t \\ &- [F(c_i)(\alpha + \beta(\tau(\rho_i) - \tau(\rho_{i-1}))) + F(c_i)(\alpha + \beta(\tau(\rho_i) - \tau(\rho_{i+1})))]s_i^t. \end{aligned} \tag{2.7}$$

We the rearrange (2.7) to take out the common factors α and β, giving

$$\begin{aligned} s_i^{t+\Delta t} =& s_i^t + \alpha[F(c_{i+1})s_{i+1}^t + F(c_{i-1})s_{i-1}^t - 2F(c_i)s_i^t] \\ &+ \beta\left[F(c_{i+1})s_{i+1}^t(\tau(\rho_{i+1}) - \tau(\rho_i))\right. \\ &+F(c_{i-1})s_{i-1}^t(\tau(\rho_{i-1}) - \tau(\rho_i)) \\ &\left.-F(c_i)s_i^t(2\tau(\rho_i) - \tau(\rho_{i-1}) - \tau(\rho_{i+1}))\right]. \end{aligned} \tag{2.8}$$

We then Taylor expand the terms in (2.8) to obtain the equation in relation

to the site i at time t only. Beginning with,

$$s_i^{t+\Delta t} = s_i^t + \Delta t \frac{\partial s_i^t}{\partial t} + \mathcal{O}(\Delta t^2). \tag{2.9}$$

Then for the terms related to α we get

$$\begin{aligned}
\alpha[\cdot] =& \alpha \Bigg[F(c_i)s_i^t + \Delta x \frac{\partial}{\partial x}(F(c_i)s_i^t) + \frac{\Delta x^2}{2}\frac{\partial^2}{\partial x^2}(F(c_i)s_i^t) + \frac{\Delta x^3}{6}\frac{\partial^3}{\partial x^3}(F(c_i)s_i^t) \\
& F(c_i)s_i^t - \Delta x \frac{\partial}{\partial x}(F(c_i)s_i^t) + \frac{\Delta x^2}{2}\frac{\partial^2}{\partial x^2}(F(c_i)s_i^t) - \frac{\Delta x^3}{6}\frac{\partial^3}{\partial x^3}(F(c_i)s_i^t) \\
& -2F(c_i)s_i^t + \mathcal{O}(\Delta x^4)\Big] \\
=& \alpha \Delta x^2 \frac{\partial^2}{\partial x^2}(F(c_i)s_i^t) + \mathcal{O}(\Delta x^4),
\end{aligned} \tag{2.10}$$

as the $0^{th}, 1^{st},$ and $, 3^{rd}$ order terms of Δx cancel each other out. We then turn our attention to our terms involving β, as a matter of readability we will Taylor expand each multiplication individually. To begin,

$$\begin{aligned}
\mathcal{R} =& F(c_{i+1})s_{i+1}^t(\tau(\rho_{i+1}) - \tau(\rho_i)) \\
=& \left[F(c_i)s_i^t + \Delta x \frac{\partial}{\partial x}(F(c_i)s_i^t) + \frac{\Delta x^2}{2}\frac{\partial^2}{\partial x^2}(F(c_i)s_i^t) + \frac{\Delta x^3}{6}\frac{\partial^3}{\partial x^3}(F(c_i)s_i^t) \right] \\
& \cdot \left[\tau(\rho_i) - \tau(\rho_i) + \Delta x \frac{\partial}{\partial x}(\tau(\rho_i)) + \frac{\Delta x^2}{2}\frac{\partial^2}{\partial x^2}(\tau(\rho_i)) + \frac{\Delta x^3}{6}\frac{\partial^3}{\partial x^3}(\tau(\rho_i)) \right] + \mathcal{O}(\Delta x^4) \\
=& F(c_i)s_i^t \left[\Delta x \frac{\partial}{\partial x}(\tau(\rho_i)) + \frac{\Delta x^2}{2}\frac{\partial^2}{\partial x^2}(\tau(\rho_i)) + \frac{\Delta x^3}{6}\frac{\partial^3}{\partial x^3}(\tau(\rho_i)) \right] \\
& + \Delta x \frac{\partial}{\partial x}(F(c_i)s_i^t) \left[\Delta x \frac{\partial}{\partial x}(\tau(\rho_i)) + \frac{\Delta x^2}{2}\frac{\partial^2}{\partial x^2}(\tau(\rho_i)) \right] \\
& + \frac{\Delta x^2}{2}\frac{\partial^2}{\partial x^2}\left(F(c_i)s_i^t\right) \left[\Delta x \frac{\partial}{\partial x}(\tau(\rho_i)) \right] + \mathcal{O}(\Delta x^4),
\end{aligned} \tag{2.11}$$

and

$$\begin{aligned}
\mathcal{L} =& F(c_{i-1})s_{i-1}^t(\tau(\rho_{i-1}) - \tau(\rho_i)) \\
=& \left[F(c_i)s_i^t - \Delta x\frac{\partial}{\partial x}(F(c_i)s_i^t) + \frac{\Delta x^2}{2}\frac{\partial^2}{\partial x^2}(F(c_i)s_i^t) - \frac{\Delta x^3}{6}\frac{\partial^3}{\partial x^3}(F(c_i)s_i^t)\right] \\
& \cdot \left[\tau(\rho_i) - \tau(\rho_i) - \Delta x\frac{\partial}{\partial x}(\tau(\rho_i)) + \frac{\Delta x^2}{2}\frac{\partial^2}{\partial x^2}(\tau(\rho_i)) - \frac{\Delta x^3}{6}\frac{\partial^3}{\partial x^3}(\tau(\rho_i))\right] + \mathcal{O}(\Delta x^4) \\
=& F(c_i)s_i^t\left[-\Delta x\frac{\partial}{\partial x}(\tau(\rho_i)) + \frac{\Delta x^2}{2}\frac{\partial^2}{\partial x^2}(\tau(\rho_i)) - \frac{\Delta x^3}{6}\frac{\partial^3}{\partial x^3}(\tau(\rho_i))\right] \\
& - \Delta x\frac{\partial}{\partial x}(F(c_i)s_i^t)\left[-\Delta x\frac{\partial}{\partial x}(\tau(\rho_i)) + \frac{\Delta x^2}{2}\frac{\partial^2}{\partial x^2}(\tau(\rho_i))\right] \\
& + \frac{\Delta x^2}{2}\frac{\partial^2}{\partial x^2}\left(F(c_i)s_i^t\right)\left[-\Delta x\frac{\partial}{\partial x}(\tau(\rho_i))\right] + \mathcal{O}(\Delta x^4), \qquad (2.12)
\end{aligned}$$

and finally,

$$\begin{aligned}
\mathcal{C} =& - F(c_i)s_i^t(2\tau(\rho_i) - \tau(\rho_{i-1}) - \tau(\rho_{i+1})) \\
=& - F(c_i)s_i^t\left[2\tau(\rho_i) - \tau(\rho_i) + \Delta x\frac{\partial}{\partial x}(\tau(\rho_i)) - \frac{\Delta x^2}{2}\frac{\partial^2}{\partial x^2}(\tau(\rho_i)) + \frac{\Delta x^3}{6}\frac{\partial^3}{\partial x^3}(\tau(\rho_i))\right. \\
& \left. -\tau(\rho_i) - \Delta x\frac{\partial}{\partial x}(\tau(\rho_i)) - \frac{\Delta x^2}{2}\frac{\partial^2}{\partial x^2}(\tau(\rho_i)) - \frac{\Delta x^3}{6}\frac{\partial^3}{\partial x^3}(\tau(\rho_i))\right] + \mathcal{O}(\Delta x^4) \\
=& \Delta x F(c_i)s_i^t\frac{\partial^2}{\partial x^2}(\tau(\rho_i)) + \mathcal{O}(\Delta x^4). \qquad (2.13)
\end{aligned}$$

Adding (2.11), (2.12), and (2.13), gives

$$\begin{aligned}
\mathcal{L} + \mathcal{C} + \mathcal{R} =& 2\Delta x^2\left[\Delta x F(c_i)s_i^t\frac{\partial^2}{\partial x^2}(\tau(\rho_i)) + \frac{\partial}{\partial x}(F(c_i)s_i^t)\frac{\partial}{\partial x}(\tau(\rho_i))\right] + \mathcal{O}(\Delta x^4) \\
=& 2\Delta x^2\frac{\partial}{\partial x}\left(F(c_i)s_i^t\frac{\partial}{\partial x}(\tau(\rho_i))\right) + \mathcal{O}(\Delta x^4). \qquad (2.14)
\end{aligned}$$

Combining (2.9), (2.10) and 2.14 into (2.8), gives,

$$s_i^t + \Delta t\frac{\partial s_i^t}{\partial t} + \mathcal{O}(\Delta t^2) = s_i^t + \alpha\Delta x^2\frac{\partial^2}{\partial x^2}(F(c_i)s_i^t) + 2\beta\Delta x^2\frac{\partial}{\partial x}\left(F(c_i)s_i^t\frac{\partial}{\partial x}(\tau(\rho_i))\right) + \mathcal{O}(\Delta x^4),$$

which we rearrange to obtain

$$\frac{\partial s_i^t}{\partial t} = \alpha \frac{\Delta x^2}{\Delta t} \frac{\partial^2}{\partial x^2}(F(c_i)s_i^t) + 2\beta \frac{\Delta x^2}{\Delta t} \frac{\partial}{\partial x}\left(F(c_i)s_i^t \frac{\partial}{\partial x}\left(\tau(\rho_i)\right)\right) + \mathcal{O}(\Delta x^4) + \mathcal{O}(\Delta t^2). \tag{2.15}$$

We now specify our functions, $F(c_i)$ and $\tau(\rho_i)$. For $F(c_i)$, we assume that movement decreases as food availability increases and the sensitivity of this effect decreases with increasing food availability [13, 22]. i.e. when encountering abundant food locusts are unlikely to move, and adding further food does little to affect the resulting movement rate. We thus require a monotonically decreasing positive function for $c_i \geq 0$, we use

$$F(c_i) = e^{-\frac{c_i}{c_0}}, \tag{2.16}$$

where c_0 relates the effect of food on movement to its abundance. For $\tau(\rho_i)$ we assume that locusts move from areas of higher densities to lower densities proportional to the number collisions, we turn to the law of mass action to describe these resulting in,

$$\tau(\rho_i) = \rho_i^2. \tag{2.17}$$

Substituting (2.16) and (2.17) into (2.15), we obtain

$$\frac{\partial s_i^t}{\partial t} = \alpha \frac{\Delta x^2}{\Delta t} \frac{\partial^2}{\partial x^2}\left(e^{-\frac{c_i}{c_0}} s_i^t\right) + 2\beta \frac{\Delta x^2}{\Delta t} \frac{\partial}{\partial x}\left(e^{-\frac{c_i}{c_0}} s_i^t \frac{\partial}{\partial x}\left(\rho_i^2\right)\right) + \mathcal{O}(\Delta x^4) + \mathcal{O}(\Delta t^2). \tag{2.18}$$

We then take the limit as $\Delta x, \Delta t \to 0$ such that,

$$\lim_{\substack{\Delta x \to 0 \\ \Delta t \to 0}} \alpha \frac{\Delta x^2}{\Delta t} = D, \text{ and } \lim_{\substack{\Delta x \to 0 \\ \Delta t \to 0}} 2\beta \frac{\Delta x^2}{\Delta t} = \frac{D\gamma}{2},$$

which we find

$$\frac{\partial s}{\partial t} = D \frac{\partial^2}{\partial x^2}(e^{-\frac{c}{c_0}} s) + \frac{D\gamma}{2} \frac{\partial}{\partial x}\left(e^{-\frac{c}{c_0}} s \frac{\partial}{\partial x}\left(\rho^2\right)\right). \tag{2.19}$$

We then rearrange to find our flux as

$$J_{s_{\text{local}}} = -D\left[\frac{\partial}{\partial x}\left(se^{-\frac{c}{c_0}}\right) + \gamma s\rho e^{-\frac{c}{c_0}}\frac{\partial \rho}{\partial x}\right]. \tag{2.20}$$

The derivation of $J_{g_{\text{local}}}$ follows the same method. In higher dimensions, the expressions for the fluxes are

$$\boldsymbol{J}_{g_{\text{local}}} = -D\left[\nabla\left(ge^{-\frac{c}{c_0}}\right) + \gamma g\rho e^{-\frac{c}{c_0}}\nabla\rho\right], \tag{2.21a}$$

$$\boldsymbol{J}_{s_{\text{local}}} = -D\left[\nabla\left(se^{-\frac{c}{c_0}}\right) + \gamma s\rho e^{-\frac{c}{c_0}}\nabla\rho\right]. \tag{2.21b}$$

2.1.2 Non-local interactions

For our non-local interactions, we adopt the fluxes used by Topaz et. al. [98]. By considering each locust subpopulation, solitarious and gregarious, as having different social potentials, we obtain the following expressions for the non-local flux

$$\boldsymbol{J}_{g_{\text{non-local}}} = -\nabla(Q_g * \rho)g, \tag{2.22a}$$

$$\boldsymbol{J}_{s_{\text{non-local}}} = -\nabla(Q_s * \rho)s. \tag{2.22b}$$

We also adopt the functional forms of the social potentials used by Topaz et. al. [98], as they are used extensively in modelling collective behaviour and are well studied [11]. They are based on the assumption that solitarious locusts have a long range repulsive social potential and gregarious locusts have a long range attractive and a shorter range repulsive social potential. The social potentials are given by,

$$Q_s(\boldsymbol{x}) = R_s e^{\frac{-|\boldsymbol{x}|}{r_s}} \text{ and } Q_g(\boldsymbol{x}) = R_g e^{\frac{-|\boldsymbol{x}|}{r_g}} - A_g e^{\frac{-|\boldsymbol{x}|}{a_g}},$$

where R_s and r_s are the solitarious repulsion strength and sensing distance respectively. Similarly, R_g and r_g are the gregarious repulsion strength and

sensing distance. Finally, A_g and a_g are the gregarious attraction strength and sensing distance.

2.1.3 Gregarisation dynamics

For the rates at which locusts become gregarious (or solitarious) we again follow the work of Topaz et. al. [98]. We assume that solitarious locusts transition to gregarious is a function of the local locust density (and vice versa). This gives our equations for kinetics as

$$K(s, g) = -f_1(\rho)g + f_2(\rho)s, \tag{2.23}$$

where $f_1(\rho)$ and $f_2(\rho)$ are positive functions representing density dependant transition rates. To make our results more directly comparable we again use the same functional forms as Topaz et. al. [98]:

$$f_1(\rho) = \frac{\delta_1}{1 + \left(\frac{\rho}{k_1}\right)^2}, \tag{2.24a}$$

$$f_2(\rho) = \frac{\delta_2 \left(\frac{\rho}{k_2}\right)^2}{1 + \left(\frac{\rho}{k_2}\right)^2}, \tag{2.24b}$$

where $\delta_{1,2}$ are maximal phase transition rates and $k_{1,2}$ are the locust densities at which half this maximal transition rate occurs.

2.1.4 A system of equations for locust gregarisation including food interactions

By substituting our flux expressions (2.21a) - (2.22b) and kinetics term (2.23), into our conservation equations (2.3a) and (2.3b), and rearranging the equation into an advection diffusion system, we obtain the following system of

equations

$$\frac{\partial g}{\partial t} + \nabla \cdot (g\boldsymbol{v}_g) - D\nabla \cdot \left[e^{-\frac{c}{c_0}}\nabla g\right] = -f_1(\rho)g + f_2(\rho)s, \tag{2.25a}$$

$$\frac{\partial s}{\partial t} + \nabla \cdot (s\boldsymbol{v}_s) - D\nabla \cdot \left[e^{-\frac{c}{c_0}}\nabla s\right] = f_1(\rho)g - f_2(\rho)s, \tag{2.25b}$$

$$\frac{\partial c}{\partial t} = -\kappa c(\boldsymbol{x}, t)\rho(\boldsymbol{x}, t). \tag{2.25c}$$

with

$$\boldsymbol{v}_g = -\nabla(Q_g * \rho) + De^{-\frac{c}{c_0}}\left(\frac{1}{c_0}\nabla c - \gamma\rho\nabla\rho\right),$$

and

$$\boldsymbol{v}_s = -\nabla(Q_s * \rho) + De^{-\frac{c}{c_0}}\left(\frac{1}{c_0}\nabla c - \gamma\rho\nabla\rho\right),$$

where f_1, f_2, Q_s, and Q_g are previously defined.

2.1.5 Non-dimensionalisation

We non-dimensionalise (2.25a), (2.25b), and (2.25c), and the explicit expressions for f_1, f_2, Q_s, and Q_g. We rescale length so the gregarious attraction length scale is 1 and density around k_1 as this gives a measure of when the density is low enough that a gregarious locust would start to become solitarious (we expect that k_2, which is a measure of the density at which solitarious locusts become gregarious, will be larger than k_1). Finally, let the timescale be of the order $\frac{1}{\delta_2}$ as we are looking at the time scale of gregariarization and our food scale be of the order c_0. This gives the following scalings,

$$t = \frac{1}{\delta_2}\bar{t},\ \boldsymbol{x} = a_g\bar{\boldsymbol{x}},\ (\rho, s, g) = k_1(\bar{\rho}, \bar{s}, \bar{g}),\ \text{and } c = c_0\bar{c}.$$

Then, dropping the bar notation, the dimensionless governing equations are

$$\frac{\partial g}{\partial t} + \nabla \cdot (g\boldsymbol{v}_g) - D^*\nabla \cdot \left[e^{-c}\nabla g\right] = -f_1^*(\rho)g + f_2^*(\rho)s, \tag{2.26a}$$

$$\frac{\partial s}{\partial t} + \nabla \cdot (s\boldsymbol{v}_s) - D^*\nabla \cdot \left[e^{-c}\nabla s\right] = f_1^*(\rho)g - f_2^*(\rho)s, \tag{2.26b}$$

$$\frac{\partial c}{\partial t} = -\kappa^* c(x,t)\rho(x,t), \tag{2.26c}$$

where

$$\boldsymbol{v}_g = -\nabla Q_g^* * \rho + D^* e^{-c}\left(\nabla c - \gamma^*\rho\nabla\rho\right), \boldsymbol{v}_s = -\nabla Q_s^* * \rho + D^* e^{-c}\left(\nabla c - \gamma^*\rho\nabla\rho\right),$$

and

$$Q_g^* = R_g^* e^{\frac{-|\boldsymbol{x}|}{r_g^*}} - A_g^* e^{-|\boldsymbol{x}|}, \tag{2.27}$$

$$Q_s^* = R_s^* e^{\frac{-|\boldsymbol{x}|}{r_s^*}}. \tag{2.28}$$

Finally,

$$f_1^*(\rho) = \frac{\delta^*}{1+\rho^2},\ f_2^*(\rho) = \frac{(\rho k)^2}{1+(\rho k)^2}.$$

Note that we have introduced the following dimensionless parameters,

$$D^* = \frac{D}{\delta_2 a_g^2},\ k = \frac{k_1}{k_2},\ \delta^* = \frac{\delta_1}{\delta_2},\ \gamma^* = k_1^2\gamma,\ \kappa^* = \frac{\kappa k_1}{\delta_2},$$
$$R_g^* = \frac{R_g k_1}{\delta_2 a_g},\ A_g^* = \frac{A_g k_1}{\delta_2 a_g},\ R_s^* = \frac{R_s k_1}{\delta_2 a_g},\ r_g^* = \frac{r_g}{a_g},\ r_s^* = \frac{r_s}{a_g}.$$

For notational simplicity we drop the $\cdot^*$ notation in the rest of this thesis.

2.2 Measure of foraging advantage

In order to measure the foraging advantage of gregarious locust we turn to the work of Tania et. al. [95]. We first calculate the per capita contact with

food for solitarious and gregarious locusts, respectively as

$$\eta_s(t) = \frac{1}{M}\int_0^L \frac{c(x,t)s(x,t)}{(1-\phi_g(t))}dx \text{ and } \eta_g(t) = \frac{1}{M}\int_0^L \frac{c(x,t)g(x,t)}{\phi_g(t)}dx,$$

where M is given by (2.1). We then calculate the instantaneous relative advantage at time t as

$$B(t) = \frac{\eta_g(t)}{\eta_s(t)}. \tag{2.29}$$

This allows us to measure the advantage of being gregarious, when $B(t) > 1$ gregarious organisms are out-foraging their solitarious counterparts. To differentiate between the time dependent foraging advantage and the steady state foraging advantage we label the latter, B_∞.

2.2.1 Derivation of foraging advantage

We note that it is possible to derive this quantity from first principle. When considering foraging within a modelling context a common technique is to look at an individuals ability to maximise a 'currency', here the 'currency' considered is ability to extract energy from a food source [92].

The measure we look at, known as foraging efficiency, is the ratio of energy gained to energy spent and is given mathematically by Laguë et al. [60] as

$$E(t) = \frac{E_{\text{gain}}(t)}{E_{\text{loss}}(t)} = \frac{F(t)}{p_1 t + p_2 t^*}, \tag{2.30}$$

where $F(t)$ is the total energy gained by foraging for time t, p_1 is the energy cost per unit time during foraging, p_2 is the energy lost per unit time by travel between food patches for time t^*. Note that the marginal value theorem [22, 60] is a simpler version of (2.30) given by

$$R(t) = \frac{F(t)}{t + t^*}, \tag{2.31}$$

where $R(t)$ is the rate of energy gain, $F(t)$ is the total energy gained by foraging a patch of food in time t, and t^* is the time to travel between patches.

However, (2.30) is not spatially explicit, we thus need to convert our spatially explicit equations and derive a value for individual energy gain. We first do this with a more general case before substituting our equation for consumption (2.25c). To begin, let the subscript $\cdot_g$ denote gregarious locusts and $\cdot_s$ denote solitarious. Then, let $f_g(c, s, g)$ be a function describing the energy gain for gregarious locusts per unit area per unit time (the derivation for solitarious is similar and thus omitted here). We can then calculate the total instantaneous gregarious energy gain, I_g at time t as

$$I_g(t) = \int_\Omega f_g(c, s, g)\, d\boldsymbol{x}.$$

This allows us to calculate the average gregarious individual's instantaneous energy gain by dividing $I_g(t)$ by the total number of gregarious locusts,

$$A_g(t) = \frac{\int_\Omega f_g(c, s, g)\, d\boldsymbol{x}}{\phi_g(t)M},$$

where M and ϕ_g are given by (2.1) and (2.2), respectively. We can then calculate the average gregarious individuals total energy gain over the time interval, $[0, t]$, by integrating, giving rise to

$$F_g(t) = \int_0^t \frac{\int_\Omega f_g(c, s, g)\, d\boldsymbol{x}}{\phi_g(\tau)M}\, d\tau. \tag{2.32}$$

By substituting (2.26c) into (2.32) and taking into account only the gregari-

ous contribution to ρ we obtain

$$\begin{aligned} F_g(t) &= \int_0^t \frac{\int_\Omega \kappa c g \, d\boldsymbol{x}}{\phi_g M} \, d\tau \\ &= \int_0^t \kappa \eta_g(\tau) \, d\tau. \end{aligned}$$

This gives the foraging efficiency as

$$E_g(t) = \frac{\int_0^t \kappa \eta_g(\tau) \, d\tau}{p_1 t + p_2 t^*}. \tag{2.33}$$

Similarly, for solitarious locusts we obtain

$$E_s(t) = \frac{\int_0^t \kappa \eta_s(\tau) \, d\tau}{p_1 t + p_2 t^*}. \tag{2.34}$$

To compare the two foraging efficiencies, we define the cumulative relative gregarious foraging advantage as

$$b(t) = \frac{E_g}{E_s} = \frac{\int_0^t \eta_g(\tau) \, d\tau}{\int_0^t \eta_s(\tau) \, d\tau}, \tag{2.35}$$

assuming κ, t^*, p_1 and p_2 are equal for both solitarious and gregarious. If they are unequal we would end up with some scalar multiple of $b(t)$. It should be noted that this is the definition of cumulative relative advantage from Tania et al. [95].

Finally, as the proportion of the population that is gregarious is changing in time $B(t)$ becomes difficult to interpret. We instead assume that $\phi_g(t)$ is constant over the short interval $[t, t + \Delta t]$ for some $\Delta t \ll 1$, we then let $b(t)$ be the cumulative relative advantage over this interval, which we term the

instantaneous relative advantage to be in line with Tania et al. [95]. We find

$$\begin{aligned} B(t) &= \frac{\int_t^{t+\Delta t} \eta_g(\tau)\, d\tau}{\int_t^{t+\Delta t} \eta_s(\tau)\, d\tau} \\ &\approx \frac{\Delta t \eta_g(t)}{\Delta t \eta_s(t)} \\ &\approx \frac{\eta_g(t)}{\eta_s(t)}, \end{aligned} \tag{2.36}$$

which is instantaneous relative advantage defined by [95]. We thus find that an instantaneous relative advantage would lead to a cumulative relative advantage for a fixed gregarious mass fraction, and this in turn would imply a foraging advantage to being gregarious.

2.3 Chapter summary

In this chapter we have derived our model of locust foraging that includes both intra-individual and food interactions as well as the metric of foraging advantage. In Chapter 3 we will investigate some of the numerical schemes used in this thesis, before performing a series of analytic analyses and numerical experiments in Chapter 4. Then, in Chapter 5, we will investigate the concept of foraging advantage in two dimensions.

Chapter 3

Exploring numerical methods

Over the course of this study we investigated a variety of numerical methods to simulate non-local problems [41, 42, 44]. Here we present the finite volume based one dimensional scheme used in [45] with a study of error and convergence , as well as a discussion on calculating the non-local component [44]. Finally, we present finite volume based numerical scheme for an arbitrary number of dimensions and populations used in Chapter 5.

The methods presented in this chapter have been adapted from the following publications:

1. *F.Georgiou, B. Lamichhane, and N. Thamwattana. 'An Adaptive Numerical Scheme for a Partial Integro-Differential Equation'. ANZIAM Journal 60 (2018): C187–200. doi: 10.21914/anziamj.v60i0.14066.*

2. *F Georgiou, N Thamwattana, and B P Lamichhane. 'Modelling Cell Aggregation Using a Modified Swarm Model', In Elsawah, S. (ed.) MODSIM2019, 23rd International Congress on Modelling and Simulation. Modelling and Simulation Society of Australia and New Zealand, December 2019, doi: 10.36334/modsim.2019.A1.georgiou*

3. *F. Georgiou, J. Buhl, J. E. F. Green, B. Lamichhane, and N. Thamwattana, 'Modelling locust foraging: How and why food affects group for-*

mation', PLOS Computational Biology, vol. 17, no. 7, p. e1008353, Jul. 2021, doi: 10.1371/journal.pcbi.1008353.

4. *F. Georgiou, J. Buhl, J. E. F. Green, B. Lamichhane, and N. Thamwattana, 'A Numerical Scheme for Non-Local Aggregation with Non-Linear Diffusion and Approximations of Social Potential'. ANZIAM Journal 62 (2020): C242–55. doi: 10.21914/anziamj.v62.16056.*

3.1 One dimension

We now derive the numerical scheme for (2.26a) in one dimension using a finite volume method (FVM). The numerical scheme for (2.26b) is similar and thus omitted here. For the numerical scheme the terms described in Table 3.1 are used in relation to an arbitrary cell i with cell boundaries $i \pm \frac{1}{2}$.

Table 3.1: **Definitions of symbols used in one dimensional numerical scheme at arbitrary cell i.**

Symbol	Definition
Δx	spatial size of cells in the x direction
$\mathbf{x}$	vector representing the discretised spatial grid
x_i	x value of the midpoint of a grid cell
S_i, G_i, C_i	Approximate function values of s, g, and c
$\mathbf{S}, \mathbf{G}$	vectors representing the discretised functions s and g
$\mathscr{L}_i$	Approximate value of the local component of the $\mathbf{v}_g$
$\mathscr{N}_i$	Approximate value of the non-local component of $\mathbf{v}_g$
$\mathscr{A}_i$	Approximate value of the advective component of the equation
$\mathscr{D}_i$	Approximate value of the diffusive component of the equation
$\mathscr{K}_i$	Approximate value of the kinetic component of the equation

Advection. Beginning with the local part of the velocity term (denoted $\mathscr{L}$)

$$\mathscr{L} = De^{-c}\left(\frac{\partial c}{\partial x} - \gamma\rho\frac{\partial \rho}{\partial x}\right),$$

we approximate both derivatives using central differencing schemes, giving

$$\mathscr{L}_i \approx De^{-C_i}\left(\frac{C_{i+1} - C_{i-1}}{2\Delta x} - \gamma(S_i + G_i)\frac{S_{i+1} + G_{i+1} - S_{i-1} - G_{i-1}}{2\Delta x}\right),$$

at an arbitrary cell i. Then, for the non-local component of the velocity term (denoted $\mathscr{N}$), we approximate this at a grid cell by $\mathscr{N}_i$. We discuss the various methods of finding $\mathscr{N}_i$ in Section 3.1.1. By combining the local and non-local components and letting

$$F_i = (\mathscr{L}_i + \mathscr{N}_i)G_i,$$

we can approximate the wavespeed at a cell boundary, $i - \frac{1}{2}$, as

$$P_{i-\frac{1}{2}} = \begin{cases} \frac{F_i - F_{i-1}}{G_i - G_{i-1}} & G_i \neq G_{i-1}, \\ \frac{F_i - F_{i-1}}{\Delta x} & G_i = G_{i-1}, \end{cases} \tag{3.1}$$

and the wave size as

$$W_{i-\frac{1}{2}} = G_i - G_{i-1}. \tag{3.2}$$

From this we can approximate the advection component using an upwinding scheme, giving

$$\mathscr{A}_i = \frac{1}{\Delta x}\left(\max\{P_{i-\frac{1}{2}}, 0\}W_{i-\frac{1}{2}} + \min\{P_{i+\frac{1}{2}}, 0\}W_{i+\frac{1}{2}}\right).$$

It is worth noting that as we multiply $P_{i-\frac{1}{2}}$ with $W_{i-\frac{1}{2}}$ the denominator of the fraction used to calculate $P_{i-\frac{1}{2}}$ is cancelled out and the only information

that is used is the sign of $G_i - G_{i-1}$, we therefore simplify (3.1) and (3.2) to

$$\hat{S}_{i-\frac{1}{2}} = (F_i - F_{i-1})\text{sign}(G_i - G_{i-1}),$$

and

$$\hat{W}_{i-\frac{1}{2}} = \text{sign}(G_i - G_{i-1}),$$

where

$$\text{sign}(x) = \begin{cases} -1 & x < 0, \\ 0 & x = 0, \\ 1 & x > 0, \end{cases}$$

giving the upwinding scheme for the advection component as

$$\mathscr{A}_i = \frac{1}{\Delta x}\left(\max\{\hat{S}_{i-\frac{1}{2}}, 0\}\hat{W}_{i-\frac{1}{2}} + \min\{\hat{S}_{i+\frac{1}{2}}, 0\}\hat{W}_{i+\frac{1}{2}}\right).$$

Diffusion. Next, for the diffusion term, $\mathscr{D}$

$$\mathscr{D} = D\frac{\partial}{\partial x}\left[e^{-c}\frac{\partial g}{\partial x}\right].$$

We can approximate this using FVM as

$$\mathscr{D}_i \approx \frac{D}{\Delta x^2}\left(e^{-\frac{C_{i-1}+C_i}{2}}(G_i - G_{i-1}) - e^{-\frac{C_{i+1}+C_i}{2}}(G_{i+1} - G_i)\right).$$

Then the kinetic component is given by

$$\mathscr{K}_i = -f_1(S_i + G_i)G_i + f_2(S_i + G_i)S_i.$$

Combining all the terms we obtain,

$$G_i^{t+\Delta t} = G_i^t - \Delta t(\mathscr{A}_i + \mathscr{D}_i - \mathscr{K}_i).$$

Finally, for we use an adaptive Dormand-Prince method [35] for the time component.

3.1.1 Solving the non-local component

Returning to the non-local component of the advection term, given by

$$\mathscr{N} = -\nabla(Q_g * \rho).$$

We can use the following property of convolutions

$$\frac{\partial}{\partial x}(f * g) = \left(\left(\frac{\partial}{\partial x} f\right) * g\right) = \left(f * \left(\frac{\partial}{\partial x} g\right)\right),$$

to turn the convolution component of the advection term into

$$\mathscr{N} = \left[-\frac{\partial}{\partial x} Q_g\right] * \rho.$$

We can then find approximations to $\mathscr{N}$ using a variety of techniques, the first being direct calculation.

Direct calculation. It is possible to directly calculate the convolution using classic numerical integration techniques. For example using the midpoint rectangle rule we find

$$\mathscr{N} \approx \mathscr{N}_i = \sum_{k=1}^{N} \dot{Q}_g(x_i - x_k)(S_k + G_k)\Delta x, \tag{3.3}$$

where N is the number of grid cells and

$$\dot{Q}_g(x) = \begin{cases} 0 & \text{if } x = 0, \\ \frac{A_g}{a_g} e^{-\frac{|x|}{a_g}} - \frac{R_g}{r_g} e^{-\frac{|x|}{r_g}} & \text{if } x > 0, \\ -\frac{A_g}{a_g} e^{-\frac{|x|}{a_g}} + \frac{R_g}{r_g} e^{-\frac{|x|}{r_g}} & \text{if } x < 0. \end{cases} \tag{3.4}$$

However, this method requires a considerable amount of computing power and even with the inclusion of optimisation techniques such as gradient based grid refinements (which we explored in a related problem in [42]) the computation time can be prohibitively expensive for high resolution simulations. It was found that the use of Fourier transforms (and specifically the fast Fourier transform algorithm) could reduce the computation requirement by up to 1000 times [41]. Specifically, by moving from direct calculations with complexity $O(n^2)$ (every doubling of points leads to an approximately four-fold increase in computation time), to the fast Fourier transform with complexity $O(n \log n)$ (every doubling of points leads to marginally more than a doubling of computation time) we are able to greatly reduce computation time.

Fourier transforms. The key to using Fourier transforms is the convolution theorem, which states that under suitable conditions the Fourier transform of a convolution of two functions is equal to the point-wise product of their individual Fourier transforms, i.e.,

$$\mathscr{F}\{f * g\} = \mathscr{F}\{f\} \cdot \mathscr{F}\{g\},$$

where $\mathscr{F}$ represents the Fourier transform (we also denote the inverse Fourier transform as $\mathscr{F}^{-1}$). This allows us to turn the convolution component of the advection term into

$$\mathscr{N} = \mathscr{F}^{-1}\left\{\mathscr{F}\left\{-\frac{\partial}{\partial x}Q_g\right\} \cdot \mathscr{F}\left\{\rho\right\}\right\}.$$

We can then approximate the convolution as

$$\mathscr{N} \approx \text{real}\left\{\text{ifft}\left\{\text{DFT}\left\{-\frac{\partial}{\partial x}Q_g(\mathbf{x})\right\} \cdot \text{fft}\left\{\mathbf{S} + \mathbf{G}\right\}\right\}\right\},$$

where fft and ifft represent the fast Fourier transform and inverse fast Fourier transform respectively, and DFT represents the discrete Fourier transform. We take only the real component of the ifft as any imaginary value will simply be due to error. We also require $Q_g(x)$ to be periodic on the domain $x \in [0, L]$. We therefore need a method of finding $\mathscr{F}\left\{-\frac{\partial}{\partial x}Q_g\right\}$.

The two methods we explore are the discrete time Fourier transform (DTFT) derived by [98]:

$$\text{DTFT}\left\{-\frac{\partial}{\partial x}e^{-\frac{|x|}{r}}\right\} = -\frac{i\Delta x \sin(\Delta x q)}{r\left(\cosh(\Delta x/r) - \cos(\Delta x q)\right)}, \tag{3.5}$$

where q is our frequency domain. DTFTs are the discrete analog of Fourier transforms in that they take an infinite sum of discrete points in space and produce a continuous function in the frequency domain. In contrast DFTs take a finite sum of points in space and produce a finite set of points in the frequency domain. With this in mind we can approximate the above DTFT using the method given by [43],

$$\frac{\partial}{\partial x}e^{\frac{-|x|}{r}} = \begin{cases} 0 & \text{if } x = 0, \\ \frac{1}{r}\left(-e^{-\frac{|x|}{r}} + e^{-\frac{|(L+\Delta x)-x|}{r}}\right) & \text{if } x > 0. \end{cases} \tag{3.6}$$

which is then converted to the frequency domain using a DFT. We will term (3.5) the exact DTFT and (3.6) the approximate.

3.1.2 Error and computation time

In order to test our numerical scheme of (2.26a) with the social potential (2.27), we ran a series of simulations with 64, 128, 256, 512, 1024, and 2048 grid cells, and only gregarious locusts. The initial density is given by $g(x, 0) = \max(2 + \mu, 0)$ where μ is some normally distributed noise with mean 0 and standard deviation 1. In addition, one set of initial conditions was created at the lowest resolution and interpolated up to higher resolutions

to ensure all simulations had the same initial conditions. The spatial domain was $x \in [0, 20]$ with periodic boundary conditions (i.e. $g(0, t) = g(20, t)$) and time was run to the pseudo steady state $t = 500$. We then took both the exact DTFT and approximate transform (given by (3.5) and (3.6), respectively). The constants were set as $D = 0.01$,$\gamma = 0.6$,$R_g = 0.25$,$A_g = 1$, and $r_g = 0.5$. We also let $c(x, t) = 0$. Finally, we let the 2048 grid cells with exact DTFT be our reference solution; a snapshot at times $t = 0,\ 0.72,\ 4.80,$ and 500 can be seen in Figure 3.1.

The error and computation time can be seen in Figure 3.2, a) and b) respectively. In order to calculate the error, we interpolated our reference solution down to each lower resolution (denoted $\mathbf{G}_{\text{ref}}$), then for each number of grid cells (64, 128, 256, 512, and 1024) and each social potential (approximate and exact DTFT) we calculated our total error, ϵ, as

$$\epsilon = ||\mathbf{G}_{\text{ref}} - \mathbf{G}||,$$

where $||\cdot||$ represents the standard L_2 norm. Error is calculated at the pseudo steady state of $t = 500$. From this we estimated the average convergence rate as greater than 1.8 for both the exact DTFT and approximate social potentials (1.8829 and 1.9114 respectively), however the approximated social potential has a non-uniform convergence. Computation time was comparable for both approximated and exact DTFT social potentials. The most startling aspect of this numerical experiment is that for the majority of grid cells the approximation is closer to the reference solution than the exact DTFT.

To test whether the approximation continues to be more accurate than the exact DTFT, we ran simulations with a different set of constants. The constants in (2.27) were changed to $R_g = 1$, $A_g = 1$, and $r_g = 0.1$ with everything else set as before. The error and computation time can be seen in Figure 3.3, a) and b) respectively. It can again be seen that at certain resolutions the approximation outperforms the exact DTFT. This time the average convergence rate is greater than 1.7 for both the exact DFT and

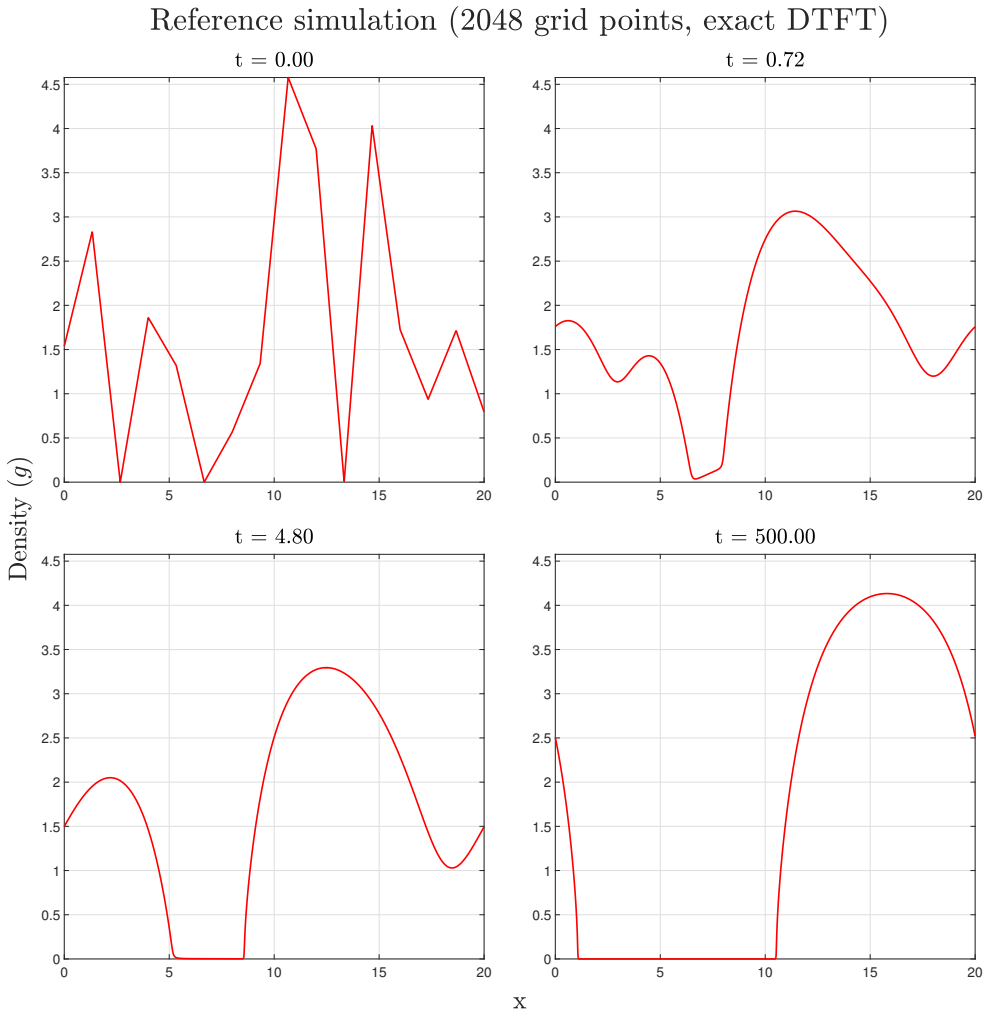

Figure 3.1: **One dimensional reference solution.** Reference solution of (2.26a) with social potential given by (2.27) with $D = 0.01$, $\gamma = 0.6$, $R_g = 0.25$, $A_g = 1$, and $r_g = 0.5$ on the periodic domain $x \in [0, 20]$. We also let $c(x, t) = 0$. The reference solution uses the exact DTFT given by (3.5) and 2048 grid cells.

approximate social potentials (1.7512 and 1.8684 respectively).

In order to better understand this, we turned back to our original values and looked at the relative error between the high resolution (2048 grid cells)

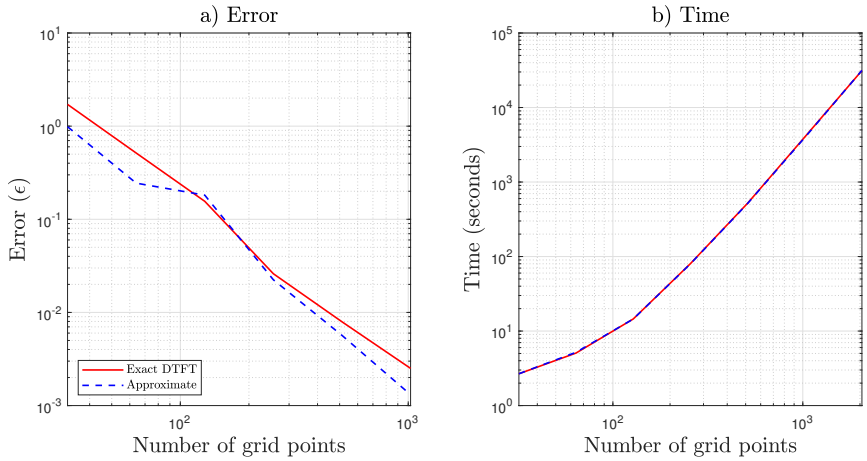

Figure 3.2: **One dimensional error and computation time.** Numerical error estimates (ϵ) and computation time for 64, 128, 256, 512, and 1024 grid cells at time $t = 500$ for both the exact DTFT and approximated social potentials with $D = 0.01$, $\gamma = 0.6$, $R_g = 0.25$, $A_g = 1$, and $r_g = 0.5$.

exact DTFT of the social potential and the lower resolution exact DTFT and approximate social potentials. We then defined the relative error between social potentials as,

$$\epsilon_{\text{rel}} = \frac{||\mathbf{Q}_{\text{ref}} - \mathbf{Q}_{\text{app}}||}{||\mathbf{Q}_{\text{ref}} - \mathbf{Q}_{\text{ext}}||},$$

where $\mathbf{Q}_{\text{ref}}$ is high resolution exact DTFT, $\mathbf{Q}_{\text{app}}$ is the approximation, and $\mathbf{Q}_{\text{ext}}$ is the lower resolution exact DTFT (we also calculate the relative error between simulations in a similar manner). $\mathbf{Q}_{\text{ref}}$ and $\mathbf{Q}_{\text{ext}}$ have been converted back to the spatial domain using a DFT. The results can be seen in Figure 3.4 (blue line, left axis), with $\epsilon_{\text{rel}} < 1$ showing that the estimate is more accurate than the exact DFT for each resolution. While the approximation is closer to the reference social potential at each resolution it is not a good predictor of the relative error between simulations (red dashed line, right axis).

While this numerical scheme worked fantastically for one dimension, we ran into some problems adapting the scheme into higher dimensions. Due to limits with computation power we needed to derive scheme that could be

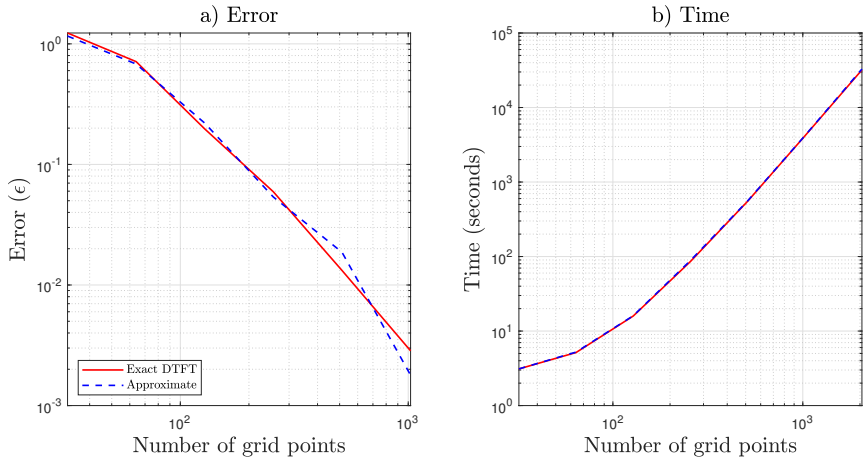

Figure 3.3: **Alternate one dimensional error and computation time.** Numerical error estimates (ϵ) and computation time for 64, 128, 256, 512, and 1024 grid cells at time $t = 500$ for both the exact DTFT and approximated social potentials with $D = 0.01$, $\gamma = 0.6$, $R_g = 1$, $A_g = 1$, and $r_g = 0.1$.

implemented on a graphics processing unit.

3.2 *d*-dimensions

Here we derive a more general numerical scheme used for the 2D simulations shown in Chapter 5, we derive it for N interacting populations in d dimensions. The spatial component follows the work of Burger et. al. [19]. We also adopt their notation, given in Table 3.2. It is the same as for the one dimensional case with an aribtrary cell i, however i is now a d-dimensional vector with cell boundaries $i \pm \frac{1}{2}\boldsymbol{e_l}$ where $\boldsymbol{e_l}$ d-dimensional unit vector in the direction l, i.e. $\boldsymbol{e_1} = (1, 0, ..., 0)$.

Given a system of equations of the form

$$\frac{\partial u_j}{\partial t} + \nabla \cdot (u_j V_j) = \nabla^2(\phi_j(x)u_j),$$

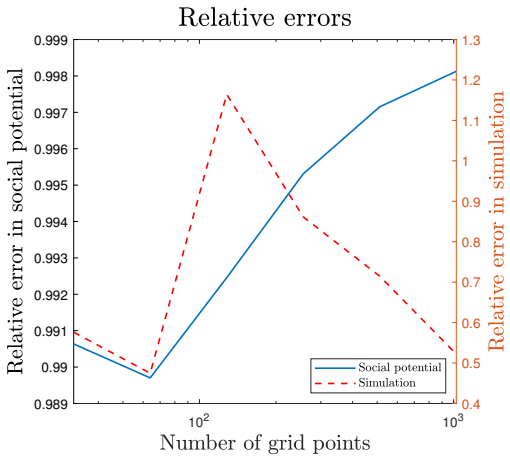

Figure 3.4: **Relative error in social potential.** $\epsilon_{\text{rel}} < 1$ indicating that the approximation is more accurate than the exact DTFT for each resolution. While the approximation is closer to the reference social potential at each resolution it is not a good predictor of the relative error between simulations (red dashed line, right axis)

where

$$V_j = \nabla \left(\sum_{k=1}^{N} Q_j * S_{j,k} u_k \right) + \phi_j(x) \gamma_j \nabla \rho^m,$$

$$\phi_j(x) = D_j e^{-c},$$

and

$$\rho = \sum_{j=1}^{N} u_j.$$

While the numerical method is designed to be two dimensional with periodic boundary conditions, it can be defined in d-dimensions. Let our domain be the d-dimensional cube,

$$\Omega := (-L_1, L_1) \times \cdots \times (-L_d, L_d).$$

To begin we can calculate ϱ_i as

Table 3.2: **Definitions of symbols used in d-dimensional numerical scheme at arbitrary cell i.**

Symbol	Description
i	d-dimensional cell index
$\boldsymbol{x_i}$	Midpoint of cell i
$\boldsymbol{e_l}$	d-dimensional unit vector in the direction l, i.e. $\boldsymbol{e_1} = (1, 0, ..., 0)$
$U_i^{(j)}$	approximation of u_j over cell i at time t
$U_{i+\frac{1}{2}\boldsymbol{e_l}}^{(j)}$	approximation of u_j at the boundary of cell i in the l direction at time t
ϱ_i	the value of ρ over cell i at time t
$V_i^{(j)}$	approximation of V_j over cell i at time t
$\tilde{V}_{i+\frac{1}{2}\boldsymbol{e_l}}^{(j)}$	approximation of the derivative of V_j at the boundary of cell i in the l direction at time t

$$\varrho_i = \sum_{k=1}^{N} U_i^{(k)}.$$

Linear diffusion discretisation. Let $\boldsymbol{D}(U^{(j)})_i$ represent the spatial discretisation of the linear diffusion, $\nabla^2(\phi(x)u_j)$, then

$$\boldsymbol{D}(U^{(j)})_i = \sum_{l=1}^{d} \frac{1}{\Delta x_l^2} \left(\phi(\boldsymbol{x}_{i+\boldsymbol{e_l}}) U_{i+\boldsymbol{e_l}}^{(j)} - 2\phi(\boldsymbol{x}_i) U_i^{(j)} + \phi(\boldsymbol{x}_{i-\boldsymbol{e_l}}) U_{i-\boldsymbol{e_l}}^{(j)} \right). \quad (3.7)$$

Advection discretisation. In order to solve the convolution component, we denote

$$\boldsymbol{N} = \sum_{k=1}^{N} Q_j * u_k.$$

Next, taking the d-dimensional Fourier transform and utilising the convolution theorem we get

$$\boldsymbol{N} = \mathscr{F}^{-1}\left\{\mathscr{F}\big\{Q(\boldsymbol{x})\big\} \cdot \mathscr{F}\left\{\sum_{k=1}^{N} Q_j * u_k\right\}\right\},$$

which can be solved efficiently using the fast Fourier transform. We can then find the gradient at the cell boundary as

$$\tilde{V}^{(j)}_{i+\frac{1}{2}\boldsymbol{e_l}} = \frac{1}{\Delta x_l}\left(N_{i+\boldsymbol{e_l}} - N_i + \frac{\phi(\boldsymbol{x}_{i-\boldsymbol{e_l}}) + \phi(\boldsymbol{x}_i)}{2}\left(\varrho^m_i - \varrho^m_{i+\boldsymbol{e_l}}\right)\right).$$

This then lets us use an upwinding scheme to find the value of $U^{(j)}$ at the cell boundary as

$$U^{(j)}_{i+\frac{1}{2}\boldsymbol{e_l}} = \begin{cases} U^{(j)}_i, \text{ if } \tilde{V}^{(j)}_{i+\frac{1}{2}\boldsymbol{e_l}} \geq 0, \\ U^{(j)}_{i+\boldsymbol{e_l}}, \text{ if } \tilde{V}^{(j)}_{i+\frac{1}{2}\boldsymbol{e_l}} < 0. \end{cases}$$

Finally this allows us to find the advection component $\boldsymbol{A}(U^{(j)})$ as

$$\boldsymbol{A}(U^{(j)})_i = -\sum_{l=1}^{d} U^{(j)}_{i+\frac{1}{2}\boldsymbol{e_l}} \tilde{V}^{(j)}_{i+\frac{1}{2}\boldsymbol{e_l}} - U^{(j)}_{i-\frac{1}{2}\boldsymbol{e_l}} \tilde{V}^{(j)}_{i-\frac{1}{2}\boldsymbol{e_l}}. \tag{3.8}$$

Combining equations (3.7) and (3.8) we get

$$\frac{dU^{(j)}_i}{dt} = \boldsymbol{A}(U^{(j)})_i + \boldsymbol{D}(U^{(j)})_i.$$

Finally, we need to derive a method of time integration that can be implemented on GPU.

Time discretisation. Here we derive an adaptive time stepping scheme that is used in two (and higher) dimensions, the error estimates were first derived by Horsea and Shampine [52]. Given an initial value problem of the

form

$$\frac{du}{dt} = f(u,t),\ u(t_0) = u_0,$$

we use the standard Runge-Kutta 4 algorithm [77], so let u_n be the approximation of u at the n^{th} time step of size Δt, then

$$\begin{aligned} u_{n+1} &= u_n + \frac{1}{6}\Delta t\left(k_1 + 2k_2 + 2k_3 + k_4\right), \\ t_{n+1} &= t_n + \Delta t, \end{aligned}$$

where

$$\begin{aligned} k_1 &= f\left(u_n, t_n\right), \\ k_2 &= f\left(u_n + \Delta t\frac{k_1}{2}, t_n + \frac{\Delta t}{2}\right), \\ k_3 &= f\left(u_n + \Delta t\frac{k_2}{2}, t_n + \frac{\Delta t}{2}\right), \\ k_4 &= f\left(u_n + \Delta t k_3, t_n + \Delta t\right). \end{aligned}$$

We then approximate the error of the scheme using the method given by [52]. Let est_n be the error estimate of the pair of steps n and $n+1$, then

$$\text{est}_n = \frac{\Delta t}{32} = (-k_1 + 2k_2 - k_3 + 3k_1^* - k_3^*), \tag{3.9}$$

where $\cdot^*$ denotes belonging to the $(n+1)^{th}$ step. This error estimate allows us to update our step size Δt every second timestep, and accept/reject time step pairs based on the error. Then if $|\text{est}_n|_\infty < \text{maxerr}$, where $|\cdot|_\infty$ is the infinity norm and maxerr is the maximum error tolerance, we take our error estimate and look at the ratio of error to max allowed error as [89],

$$\text{err}_r = 1.25\left(\frac{|\text{est}_n|_\infty}{\text{maxerr}}\right)^{1/5},$$

before updating the time-step using

$$\Delta t^* = \begin{cases} 5\Delta t, \text{ if } \mathrm{err}_r < 0.2, \\ \frac{\Delta t}{\mathrm{err}_r}, \text{ if } 0.2 < \mathrm{err}_r < 0.8, \\ \Delta t. \text{ otherwise} \end{cases}$$

If $|\mathrm{est}_n|_\infty >$ maxerr we reject the pair of time steps and let

$$\Delta t^* = \frac{\Delta t}{2}.$$

Finally if $\Delta t < \Delta t_{\min}$ (i.e. the minimum timestep) we end the simulation.

3.2.1 Error and computation time

Again, in order to test our numerical scheme of (2.26a) with the social potential (2.27), we ran a series of simulations with 16, 32 64,128,256, and 512 grid cells, and only gregarious locusts. The initial density is given by $g(x, 0) = \max(1 + \mu, 0)$ where μ is some normally distributed noise with mean 0 and standard deviation 1. In addition, one set of initial conditions was created at the lowest resolution and interpolated up to higher resolutions to ensure all simulations had the same initial conditions.

The spatial domain was $x \in [0, 10]$ with periodic boundary conditions and time was run to the pseudo steady state $t = 20$. The constants were set as $D = 0.1$, $\gamma = 1$, $R_g = 0$, $A_g = 1$, and $r_g = 0.5$ (for computational simplicity, we ignore the short range repulsion in this case). We also let $c(x, t) = 0$. Finally, we let the 512 grid cells simulation be our reference solution; a snapshot at times $t = 0,\ 0.5,\ 1.2,$ and 10 can be seen in Figure 3.5.

The error and computation time can be seen in Figure 3.6, a) and b) respectively. In order to calculate the error, we interpolated our reference solution down to each lower resolution (denoted $\mathbf{G}_{\mathrm{ref}}$), then for each number

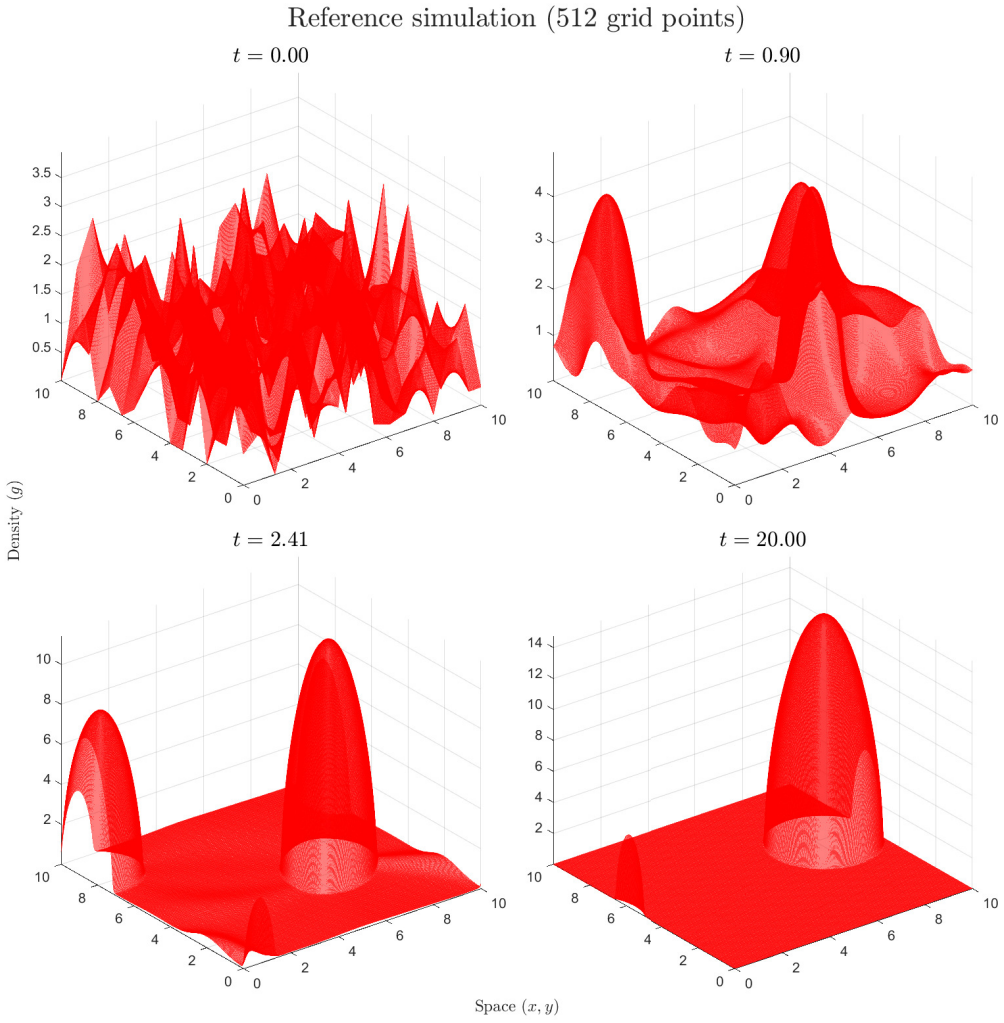

Figure 3.5: **Two dimensional reference solution.** Reference solution of (2.26a) with social potential given by (2.27) with $D = 0.1$, $\gamma = 1$, $R_g = 0$, $A_g = 1$, and $r_g = 0.5$ (we ignore the short range repulsion in this case) on the periodic domain $x \in [0, 10]$. We also let $c(x, t) = 0$.

of grid cells (16, 32, 64, 128, and 256) we calculated our total error, ϵ, as

$$\epsilon = ||\mathbf{G}_{\text{ref}} - \mathbf{G}||,$$

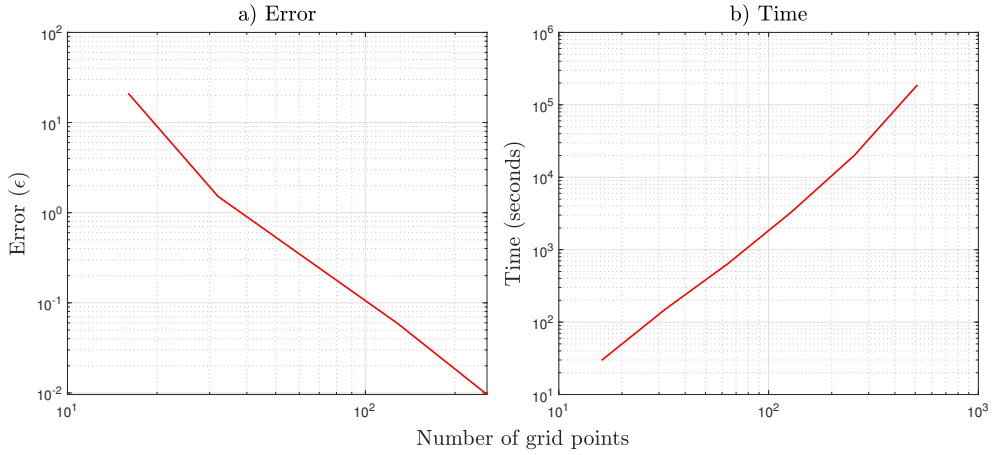

Figure 3.6: **Two dimensional error and computation time.** Numerical error estimates (ϵ) and computation time for 16, 32 64,128, and 256 grid cells at time $t = 10$ with $D = 0.1$, $\gamma = 1$, $R_g = 0$, $A_g = 1$, and $r_g = 0.5$.

where $||\cdot||$ represents the standard L_2 norm. Error is calculated at the pseudo steady state of $t = 10$. From this we estimated the average convergence rate as 2.7746, however the convergence is non-uniform.

3.3 Chapter summary

In this chapter we introduced two finite volume based numerical scheme for simulating our equations in one and two (and higher) dimensions. We also tested their accuracy and convergence using common social potentials. In addition, in the one dimensional case, we compared an exact DTFT of the social potential with a method for approximating it and found that under the tested conditions the approximation outperformed the exact DTFT. While more work needs to be done to understand why this is the case, the approximation method appears to work well and could be used for social potentials whose DTFT have no closed-form expression. For a discussion on implementing numerical schemes in MATLAB, see Appendix A.

Chapter 4

How and why food affects group formation

In this chapter we analyse the model introduced in Chapter 2. In section 4.1, we begin by analysing (2.26a) using various PDE analysis techniques under some simplifying assumptions. Then in section 4.2 we investigate how varying food distributions affect the formation of gregarious aggregations and how gregarisation affects foraging efficiency, before finally concluding this study in section 4.3.

4.1 PDE model analysis

In this section we investigate the behaviour of our model with a spatially uniform and temporally constant food density. This assumption corresponds to environments where the lengthscale of the food footprint is larger than the lengthscale over which the locusts are distributed, and where the rate of food consumption is negligible compared to the speed of locust interactions. Aside from simplifying the analysis, this assumption also provides a baseline with which to compare our later results, and hence assess the impact of a patchy food distribution. Using this and other simplifying assumptions, we

are able to calculate the maximum density and size of gregarious groups for both small and large numbers of locusts. We then consider the linear stability of the homogeneous steady states to investigate how the availability of food affects group formation, before finally investigating how the center of mass is affected by locust interactions.

4.1.1 Density of gregarious groups

Under some simplifying assumptions we can estimate the maximum density and width of gregarious locusts for both small and large numbers of locusts (i.e. as $M \to 0$ and $M \to \infty$, respectively), termed the small and large mass limits, in one dimension. To begin, we assume that c is constant and not depleting, there are minimal solitarious locusts present in the group (i.e. $\rho \approx g$), and the effect of phase transitions in the group is negligible (i.e. $f_1(\rho)s = f_2(\rho)g = 0$). Finally, while the support of g is infinite (due to the linear diffusion) the bulk of the mass is contained as a series of aggregations; consequently we approximate the support of a single aggregation as Ω. Using these assumptions we can rewrite (2.26a) as a gradient flow of the form,

$$\frac{\partial g}{\partial t} = \nabla \cdot \left(g \nabla \left[\frac{\delta E}{\delta g} \right] \right),$$

where

$$E[g] = \int_\Omega \frac{1}{2} g[Q_g * g] + \frac{De^{-c}\gamma}{6} g^3 + De^{-c}(g \log(g) - g)\, dx, \tag{4.1}$$

where $E[g]$ represents an energy functional (can be thought of as a function of a function, see [2] for more details on gradient flows) with the minimisers satisfying

$$\frac{\delta E}{\delta g} = (Q_g * g) + \frac{De^{-c}\gamma}{2} g^2 + De^{-c} \log(g) = \lambda.$$

Next, we follow the work of [12, 18, 97] and with a series of simplifying assumptions we consider both the large and small mass limit in turn. First, we note that (2.1) becomes

$$M = \int_\Omega \rho(x)\,dx = \int_\Omega g(x)\,dx.$$

To find the large mass limit, we begin with (4.1) and assume that $g(x)$ is approximately rectangular (i.e. constant within the aggregation and 0 elsewhere) and for a single aggregation that the support is far larger than the range of $e^{\frac{-|x|}{r}}$. This gives $e^{\frac{-|x|}{r}} \approx 2r\delta(x)$ (where $\delta(x)$ is the Dirac delta function) to ensure that the volume of the integration is preserved, and therefore

$$Q_g = R_g e^{\frac{-|x|}{r_g}} - A_g e^{-|x|} \approx 2\left(R_g r_g - A_g\right)\delta(x).$$

Next, as g is rectangular, we have

$$||\Omega|| = \frac{M}{g}.$$

Substituting into (4.1) we get

$$E[g] = M\left(\left(R_g r_g - A_g\right)g + \frac{De^{-c}\gamma}{6}g^2 + De^{-c}(\log(g) - 1)\right).$$

We can then find

$$\frac{dE}{dg} = M\left(\left(R_g r_g - A_g\right) + \frac{De^{-c}\gamma}{3}g + \frac{De^{-c}}{g}\right),$$

which has critical point at

$$\frac{De^{-c}\gamma}{3}g^2 + \left(R_g r_g - A_g\right)g + De^{-c} = 0.$$

Thus

$$g = \frac{3\left(-\left(R_g r_g - A_g\right) \pm \sqrt{\left(R_g r_g - A_g\right)^2 - \frac{4(De^{-c})^2\gamma}{3}}\right)}{2De^{-c}\gamma}.$$

Based on numerical simulations we take only the larger root, then as the solution is constant

$$||g||_\infty = \frac{3\left(-\left(R_g r_g - A_g\right) + \sqrt{\left(R_g r_g - A_g\right)^2 - \frac{4(De^{-c})^2\gamma}{3}}\right)}{2De^{-c}\gamma}, \tag{4.2}$$

with support

$$||\Omega|| = \frac{2MDe^{-c}\gamma}{3\left(-\left(R_g r_g - A_g\right) + \sqrt{\left(R_g r_g - A_g\right)^2 - \frac{4(De^{-c})^2\gamma}{3}}\right)}. \tag{4.3}$$

The accuracy of this approximation is illustrated by Figure 4.1. We observe that within our model as c increases so too does the maximum density of our locust formation. However, as the mass of locusts, M, increases the maximum density remains constant and the support $||\Omega||$ becomes larger. Finally, by using these derived relationships with field measurements of maximum locust densities we can estimate values of γ.

For the small mass limit, we begin with (4.1) and assume that the support of g is much smaller than the range of interaction, r. We thus approximate the social interaction potential using a Taylor expansion, $e^{\frac{-|x|}{r}} \approx 1 - \frac{|x|}{r}$, giving

$$Q_g = R_g e^{\frac{-|x|}{r_g}} - A_g e^{-|x|} \approx \left(R_g - A_g\right) - |x|\left(\frac{R_g}{r_g} - A_g\right).$$

In addition, to be able to solve the resulting equations we ignore the effect of linear diffusion within Ω. While this gives a less accurate approximation it still shows the effect of food on maximum density. Under these assumptions,

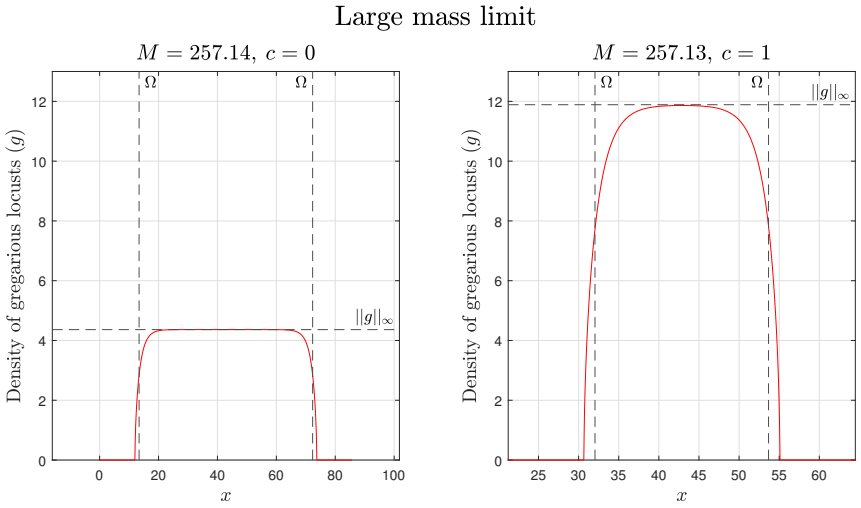

Figure 4.1: **Large mass limit with estimates for the max value and support.** The estimates of the max value and support are labelled $||g||_\infty$ and Ω respectively, with simulation results given by the red lines. For both the simulation and calculations $D = 0.01,\ \gamma = 60,\ R_g = 0.25,\ r_g = 0.5,\ A_g = 1$, and $c = 0$ and 1. We can see that as the amount of food is increased from $c = 0$ on the left to $c = 1$ on the right, the maximum density for the gregarious locusts increases.

(4.1) yields

$$E[g] = \int_\Omega \frac{1}{2} g \left(\left[(R_g - A_g) - |x| \left(\frac{R_g}{r_g} - A_g \right) \right] * g \right) + \frac{De^{-c}\gamma}{6} g^3 \, dx. \quad (4.4)$$

Based on these assumptions we can find

$$\frac{\delta E}{\delta g} = \left((R_g - A_g) - |x| \left(\frac{R_g}{r_g} - A_g \right) \right) * g + \frac{De^{-c}\gamma}{2} g^2 = \lambda,$$

which becomes

$$(R_g - A_g)M - \left(\frac{R_g}{r_g} - A_g \right) (|x| * g) + \frac{De^{-c}\gamma}{2} g^2 = \lambda.$$

We then exploit the property that $(|x|)_{xx} = 2\delta(x)$ and differentiate twice to obtain

$$-2\left(\frac{R_g}{r_g} - A_g\right) g + \frac{De^{-c}\gamma}{2}(g^2)_{xx} = 0.$$

Following [12] we place the maximum of g at the origin; this implies $g_x(0) = 0$ and $g(0) = ||g||_\infty$. We then let

$$p = \frac{g}{||g||_\infty}, \text{ and } \zeta = \frac{x}{\sqrt{||g||_\infty}}, \tag{4.5}$$

giving

$$(p^2)_{\zeta\zeta} - \frac{4\left(\frac{R_g}{r_g} - A_g\right)}{De^{-c}\gamma} p = 0, \; p(0) = 1, \; p_\zeta(0) = 0.$$

We then multiply through by $(p^2)_\zeta$ and integrate to obtain

$$2p^2(p)_\zeta^2 - \frac{8\left(\frac{R_g}{r_g} - A_g\right)}{3De^{-c}\gamma} p^3 + c = 0.$$

Then applying the conditions at $\zeta = 0$ we find

$$2p^2(p)_\zeta^2 - \frac{8\left(\frac{R_g}{r_g} - A_g\right)}{3De^{-c}\gamma}(p^3 - 1) = 0,$$

which can be simplified into

$$p_\zeta = \sqrt{\frac{4\left(A_g - \frac{R_g}{r_g}\right)}{3De^{-c}\gamma}\left(\frac{1}{p^2} - p\right)}.$$

Performing a separation of variables gives

$$d\zeta = \sqrt{\frac{3De^{-c}\gamma}{4\left(A_g - \frac{R_g}{r_g}\right)}} \frac{p\, dp}{\sqrt{1 - p^3}}. \tag{4.6}$$

We can then find the implicit solution

$$\zeta = \sqrt{\frac{3De^{-c}\gamma}{4\left(A_g - \frac{R_g}{r_g}\right)}} \int_p^1 \frac{p\,dp}{\sqrt{1-p^3}}.$$

As $p \to 0$, $\zeta \to \frac{||\Omega||}{2\sqrt{||g||_\infty}}$, we find

$$\begin{aligned} ||\Omega|| &= 2\sqrt{||g||_\infty}\sqrt{\frac{3De^{-c}\gamma}{4\left(A_g - \frac{R_g}{r_g}\right)}} \int_0^1 \frac{p\,dp}{\sqrt{1-p^3}} \\ &= 2\sqrt{||g||_\infty}\sqrt{\frac{3De^{-c}\gamma}{4\left(A_g - \frac{R_g}{r_g}\right)}} \frac{1}{3} B\left(\frac{2}{3}, \frac{1}{2}\right) \\ &= \sqrt{||g||_\infty \frac{De^{-c}\gamma}{3\left(A_g - \frac{R_g}{r_g}\right)}} B\left(\frac{2}{3}, \frac{1}{2}\right), \end{aligned} \tag{4.7}$$

where B is the β-function (for definition see [102], page 207). Next using the mass constraint,

$$M = 2\int_0^{\frac{||\Omega||}{2}} g(x)\,dx = 2\int_{-\frac{||\Omega||}{2}}^0 g(x)\,dx,$$

and substituting (4.5) we obtain

$$M = 2||g||_\infty^{\frac{3}{2}} \int_{-\frac{||\Omega||}{2\sqrt{||g||_\infty}}}^0 p(\zeta)\,d\zeta,$$

which using (4.6) becomes,

$$\begin{aligned} M &= ||g||_{\infty}^{\frac{3}{2}} \sqrt{\frac{3De^{-c}\gamma}{\left(A_g - \frac{R_g}{r_g}\right)}} \int_0^1 \frac{p^2\, dp}{\sqrt{1-p^3}} \\ &= ||g||_{\infty}^{\frac{3}{2}} \sqrt{\frac{4De^{-c}\gamma}{3\left(A_g - \frac{R_g}{r_g}\right)}}. \end{aligned} \tag{4.8}$$

Then using (4.7) and (4.8) we can find $||\Omega||$ and $||g||_\infty$ in terms of M, giving

$$||g||_{\infty} = \sqrt[3]{\frac{3M^2\left(A_g - \frac{R_g}{r_g}\right)}{4De^{-c}\gamma}}, \tag{4.9}$$

and

$$||\Omega|| = B\left(\frac{2}{3}, \frac{1}{2}\right) \sqrt[3]{\frac{MDe^{-c}\gamma}{6\left(A_g - \frac{R_g}{r_g}\right)}}. \tag{4.10}$$

The results of these approximations can be seen in Figure 4.2. While less accurate than those of the large mass limit, they illustrate that as the amount of food increases, so too does the maximum locust density. However, the effect is less pronounced than in the large mass case. It also demonstrates how the maximum locust density and support both increase with an increase in locust mass.

The accuracy of both the small and large mass approximations and the transition between the two can be seen in Figure 4.3 for both the maximum group density and support. In the simulations, we estimate the finite support, Ω, as the region where $g > 0.01$. While the maximum density approaches the approximation,there does exist errors in the small mass limit and in estimates of the support. A likely source of these discrepancies is the linear diffusion term, in that for calculating the small mass limit it was ignored and in numerically estimating the support it creates long tails at the edges of an aggregation. It is worth noting that the results for large and small mass

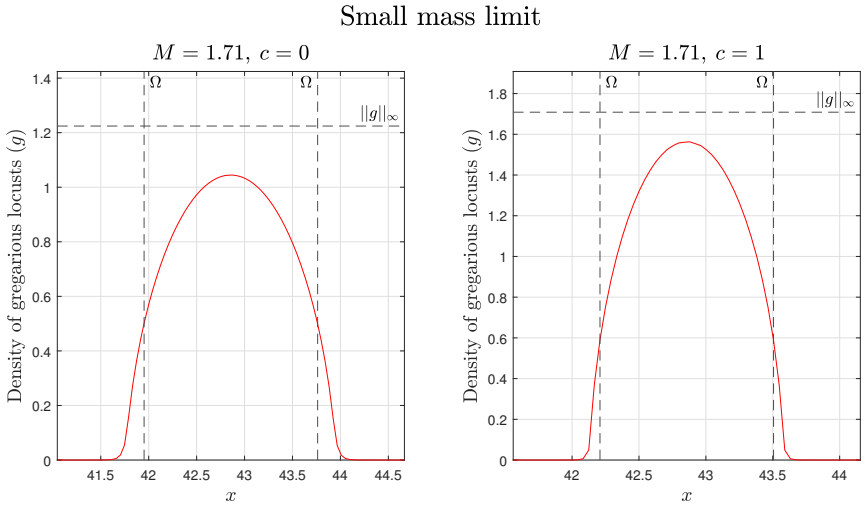

Figure 4.2: **Small mass limit with estimates for the max value and support.** The estimates of the max value and support are labelled $||g||_\infty$ and Ω respectively, with simulation results given by the red lines. For both the simulation and calculations $D = 0.01,\ \gamma = 60,\ R_g = 0.25,\ r_g = 0.5,\ A_g = 1$, and $c = 0$ and 1.

limits likely apply to locust hopper bands and not just gregarious groups [20, 21].

4.1.2 Linear stability analysis of homogeneous steady states

In order to gain insights into the conditions under which groups can form, we investigate the stability of spatially-homogeneous steady states. In this analysis we perturb the homogeneous steady states by adding a small amount of noise. We then find under what conditions the small perturbations grow and are likely to lead to gregarious aggregations.

We begin by defining the homogeneous steady states of s, g, and c, as $\bar{s}$, $\bar{g}$, and $\bar{c}$, with the total density given as $\bar{\rho} = \bar{s} + \bar{g}$. We again assume that c does not deplete (i.e. $\kappa = 0$). As we assume either an infinite or periodic

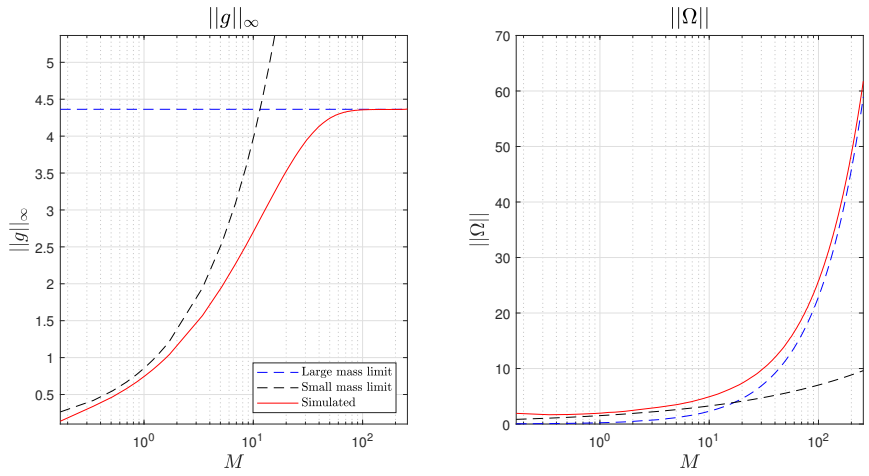

Figure 4.3: **Small and Large mass limit estimates and simulated results for both the maximum group density (left) and support (right).** In the simulations we estimate the finite support, Ω, as the region where $g > 0.01$.

domain with spatially homogeneous locust densities, we must redefine the global gregarious mass fraction, (2.2), as

$$\phi_g(t) = \frac{g(t)}{\rho(t)}. \tag{4.11}$$

Thus, in the case of spatially-homogeneous steady states $\phi_g = \frac{\bar{g}}{\bar{\rho}}$. Let

$$s = \bar{s} + \epsilon\tilde{s}, \ g = \bar{g} + \epsilon\tilde{g}, \text{ and } c = \bar{c} + \epsilon\tilde{c},$$

where $0 < \epsilon \ll 1$, $\bar{\cdot}$ represents a homogeneous steady state and $\epsilon\tilde{\cdot}$ represents a small perturbation. Naturally,

$$\rho = \bar{\rho} + \epsilon\tilde{\rho} = \bar{s} + \bar{g} + \epsilon(\tilde{s} + \tilde{g}).$$

Substituting this into (2.26a), (2.26b), and (2.26c), performing a Taylor ex-

pansion on $f_1(\bar{\rho}+\epsilon\tilde{\rho})$, $f_2(\bar{\rho}+\epsilon\tilde{\rho})$ and $De^{-(\bar{c}+\epsilon\tilde{c})}$, neglecting terms of $O(\epsilon^2)$ and higher, and for notational convenience letting $\hat{D} = De^{-\bar{c}}$, gives

$$\frac{\partial}{\partial t}\begin{bmatrix}\tilde{s}\\ \tilde{g}\\ \tilde{c}\end{bmatrix} = \begin{bmatrix}-\bar{s}\left[-Q_s * \nabla^2(\tilde{s}+\tilde{g}) + \hat{D}\left(\nabla^2\tilde{c} - \gamma\bar{\rho}\nabla^2(\tilde{s}+\tilde{g})\right)\right] + \hat{D}\Delta(\tilde{s}) - \tilde{s}A + \tilde{g}B\\ -\bar{g}\left[-Q_g * \nabla^2(\tilde{s}+\tilde{g}) + \hat{D}\left(\nabla^2\tilde{c} - \gamma\bar{\rho}\nabla^2(\tilde{s}+\tilde{g})\right)\right] + \hat{D}\Delta(\tilde{g}) + \tilde{s}A - \tilde{g}B\\ 0\end{bmatrix},$$

where

$$A = f_2(\bar{\rho}) + f_2'(\bar{\rho})\bar{s} - f_1'(\bar{\rho})\bar{g},$$
$$B = f_1(\bar{\rho}) - f_2'(\bar{\rho})\bar{s} + f_1'(\bar{\rho})\bar{g}.$$

We then perform a Fourier series expansion of $\tilde{s}$, $\tilde{g}$, and $\tilde{c}$,

$$\tilde{s} = \sum_{\hat{k}} S_{\hat{k}}(t)e^{i\hat{k}x},\ \tilde{g} = \sum_{\hat{k}} G_{\hat{k}}(t)e^{i\hat{k}x},\ \text{and}\ \tilde{c} = \sum_{\hat{k}} C_{\hat{k}}(t)e^{i\hat{k}x},$$

as well as taking the Fourier transform of Q_s and Q_g denoted as $\hat{Q}_s$ and $\hat{Q}_g$. This gives

$$\frac{\partial}{\partial t}\begin{bmatrix}S_{\hat{k}}\\ G_{\hat{k}}\\ C_{\hat{k}}\end{bmatrix} = \begin{bmatrix}-\bar{s}\hat{k}^2\left(\hat{Q}_s+\gamma\hat{D}\right) - \hat{k}^2\hat{D} - A & -\bar{s}\hat{k}^2\left(\hat{Q}_s+\gamma\bar{\rho}\hat{D}\right) + B & \hat{D}\bar{s}\hat{k}^2\\ -\bar{g}\hat{k}^2\left(\hat{Q}_g+\gamma\hat{D}\right) + A & -\bar{g}\hat{k}^2\left(\hat{Q}_g+\gamma\bar{\rho}\hat{D}\right) - \hat{k}^2\hat{D} - B & \hat{D}\bar{g}\hat{k}^2\\ 0 & 0 & 0\end{bmatrix}\begin{bmatrix}S_{\hat{k}}\\ G_{\hat{k}}\\ C_{\hat{k}}\end{bmatrix}.$$

We find the eigenvalues of the coefficient matrix as

$$\lambda_1 = -\hat{D}\hat{k}^2 - f_1(\bar{\rho}) - f_2(\bar{\rho}),\ \lambda_2 = -\hat{D}\hat{k}^2 - \bar{g}\hat{k}^2(\hat{D}\bar{\rho}\gamma + \hat{Q}_g) - \bar{s}\hat{k}^2(\hat{D}\bar{\rho}\gamma + \hat{Q}_s),\ \text{and}\ \lambda_3 = 0.$$

To determine the conditions under which the homogeneous steady state is unstable to small perturbations and thus likely to lead to aggregations, we need to find a $\hat{k}$ such that λ_1, λ_2 or λ_3 is greater than 0. As $f_1(\rho), f_2(\rho)$ are

positive functions, $\lambda_1 < 0 \,\forall\, \hat{k}$ and $\lambda_3 = 0$. For λ_2, we need,

$$-\hat{D}\hat{k}^2 - \bar{g}\hat{k}^2(\hat{D}\bar{\rho}\gamma + \hat{Q}_g) - \bar{s}\hat{k}^2(\hat{D}\bar{\rho}\gamma + \hat{Q}_s) > 0,$$
$$-\bar{g}(\hat{D}\bar{\rho}\gamma + \hat{Q}_g) - \bar{s}(\hat{D}\bar{\rho}\gamma + \hat{Q}_s) > \hat{D}.$$

Then by rewriting $\bar{s}$ and $\bar{g}$ in terms of the global gregarious mass fraction (4.11) and the total density $\bar{\rho}$ [98],

$$\bar{g} = \phi_g\bar{\rho}, \text{ and } \bar{s} = (1-\phi_g)\bar{\rho}.$$

This gives

$$-\phi_g\bar{\rho}(\hat{D}\bar{\rho}\gamma + \hat{Q}_g) - (1-\phi_g)\bar{\rho}(\hat{D}\bar{\rho}\gamma + \hat{Q}_s) > \hat{D},$$

where by taking $-\bar{\rho}$ as a common factor gives,

$$-\bar{\rho}\left[\phi_g(\hat{D}\bar{\rho}\gamma + \hat{Q}_g) + (1-\phi_g)(\hat{D}\bar{\rho}\gamma + \hat{Q}_s)\right] > \hat{D}.$$

Next, we re-arrange to make ϕ_g the object of the inequality to give

$$\phi_g > \bar{\phi_g} = \frac{\frac{\hat{D}}{\bar{\rho}} + \hat{D}\bar{\rho}\gamma + \hat{Q}_s}{\hat{Q}_s - \hat{Q}_g}. \tag{4.12}$$

From this, it can be seen that as $\bar{\rho}$ increases above (or decreases below) $\sqrt{\frac{1}{\gamma}}$ the gregarious fraction required for group formation increases. This effect is diminished as the amount of available food increases.

For our specific functions $Q_g = R_g e^{-\frac{|x|}{r_g}} - A_g e^{-|x|}$ and $Q_s = R_s e^{-\frac{|x|}{r_s}}$, we begin by taking the one dimensional Fourier transforms of Q_s and Q_g using the following definition,

$$\hat{f}(\hat{k}) = \int_{\mathbb{R}^n} f(\boldsymbol{x}) e^{-i\hat{k}\cdot\boldsymbol{x}}\, d\boldsymbol{x},$$

to get

$$\hat{Q}_g = \frac{2R_g r_g}{1 + r_g^2 \hat{k}^2} - \frac{2A_g}{1 + \hat{k}^2}, \quad \hat{Q}_s = \frac{2R_s r_s}{1 + r_s^2 \hat{k}^2}.$$

As Q_s and $-Q_g$ have a maximum value at $\hat{k} = 0$, we let $\hat{k} = 0$ and substitute into (4.12), which gives,

$$\phi_g > \bar{\phi_g} = \frac{\frac{\hat{D}}{\bar{\rho}} + \hat{D}\bar{\rho}\gamma + 2R_s r_s}{2A_g - 2R_g r_g + 2R_s r_s}. \tag{4.13}$$

Interestingly, (4.12) suggests that there is also an upper limit on locust density for group formation. This is likely to correspond with an environment so thick with locusts that there is insufficient room for aggregations to form. We can find this density by taking (4.13) and substituting $\bar{\phi_g} = 1$ and solving for $\bar{\rho}$ as

$$\bar{\rho} = \frac{(A_g - R_g r_g) + \sqrt{(A_g - R_g r_g)^2 - (De^{-\bar{c}})^2 \gamma}}{De^{-\bar{c}}\gamma} \approx \frac{2}{3}||g||_\infty,$$

where $||g||_\infty$ is maximum density for the large mass limit given in (4.2).

Finally, we calculate if it is possible for a particular homogeneous density of locusts to become unstable (and thus form a gregarious aggregation). By calculating the homogeneous steady state gregarious mass fraction as

$$\phi_g = \frac{f_2(\bar{\rho})}{f_1(\bar{\rho}) + f_2(\bar{\rho})},$$

and combining with (4.13) we obtain an implicit condition for group formation as

$$\frac{f_2(\bar{\rho})}{f_1(\bar{\rho}) + f_2(\bar{\rho})} > \frac{\frac{De^{-\bar{c}}}{\bar{\rho}} + De^{-\bar{c}}\bar{\rho}\gamma + 2R_s r_s}{2A_g - 2R_g r_g + 2R_s r_s}. \tag{4.14}$$

In (4.14), if the values on the left are not greater than those on the right then it is not possible for a great enough fraction of locusts to become gregarious and for instabilities to occur. As the value of the right hand side decreases

as the amount of food increases, we can deduce that the presence of food lowers the required density for group formation.

4.1.3 Time until group formation with homogeneous locust densities

Continuing with homogeneous locust densities and a constant c, we also calculate the time until group formation. By assuming that s and g are homogeneous we can ignore the spatial components of (2.26a) and (2.26b). We again denote the combined homogeneous locust density as $\bar{\rho}$, however now $\bar{\rho} = s(t) + g(t)$. Finally, assuming that $g(0) = 0$, we find that the homogeneous density of gregarious locusts as a function of time is given by

$$g(t) = \frac{\bar{\rho} f_2(\bar{\rho})}{f_1(\bar{\rho}) + f_2(\bar{\rho})} \left(1 - e^{-[f_1(\bar{\rho}) + f_2(\bar{\rho})]t}\right),$$

which we then solve for t^* such that $g(t^*) = \bar{\phi_g}\bar{\rho}$, where $\bar{\phi_g}$ is given by (4.12). This gives an estimation for time of group formation (i.e. the time required for the homogeneous densities to become unstable) as

$$t^* = \frac{-\ln\left(1 - \frac{\bar{\phi_g}(f_1(\bar{\rho}) + f_2(\bar{\rho}))}{f_2(\bar{\rho})}\right)}{f_1(\bar{\rho}) + f_2(\bar{\rho})}. \tag{4.15}$$

Thus, as increasing food decreases the gregarious mass fraction ($\bar{\phi_g}$) required for group formation it follows that it also decreases the time required for group formation.

4.1.4 Conservation properties

Another aspect of the model we investigate is what properties of locust densities the model conserves. By construction, our model preserves the mass of locusts, i.e. (2.1) is constant in time. In addition, using a similar method

to [97] we show that in $\mathbb{R}^n$ and with a constant food source, i.e. $c(\boldsymbol{x}, t)$ is constant in space and time, the center of mass is also preserved. We assume that our domain is $\Omega' = \mathbb{R}^n$ with $\rho(\boldsymbol{x}, t) \to 0$ at infinity and a bounded mass M. Finally, Q_s and Q_g are symmetric. To begin, we add (2.26a) and (2.26b), and let $\hat{D} = De^{-c}$, to obtain,

$$\frac{\partial(g+s)}{\partial t} + \nabla \cdot (g\boldsymbol{v}_g + s\boldsymbol{v}_s) - \hat{D}\nabla \cdot [\nabla(g+s)] = 0,$$

where

$$\boldsymbol{v}_g = -\nabla(Q_g * \rho) + \hat{D}\left(\nabla c - \gamma\rho\nabla\rho\right),$$

and

$$\boldsymbol{v}_s = -\nabla(Q_s * \rho) + \hat{D}\left(\nabla c - \gamma\rho\nabla\rho\right).$$

Then rewriting the equations in terms of the local gregarious mass fraction,

$$\psi_g(\boldsymbol{x}, t) = \frac{g(\boldsymbol{x}, t)}{\rho(\boldsymbol{x}, t)}, \tag{4.16}$$

we obtain

$$\frac{\partial\rho}{\partial t} + \nabla \cdot ((\boldsymbol{v}_g(1-\psi_g) + \boldsymbol{v}_s\psi_g)\rho) - \hat{D}\nabla \cdot [\nabla\rho] = 0.$$

Next, we expand $\boldsymbol{v}_g$ and $\boldsymbol{v}_s$ to get

$$\frac{\partial\rho}{\partial t} = -\nabla\cdot\Big[-\nabla(Q_s * \rho)\rho + \nabla(Q_s * \rho)\psi_g\rho - \nabla(Q_g * \rho)\psi_g\rho - \gamma\hat{D}\rho^2\nabla\rho - \hat{D}\nabla\rho\Big].$$

We now look at the behaviour of the center of mass. For notational simplicity we let

$$\langle a, b\rangle = \int_{\Omega'} ab\, d\boldsymbol{x}.$$

Then, (2.1) can be written as

$$M = \langle\rho, 1\rangle,$$

and the center of mass, C, of ρ, can be found as

$$C = \frac{1}{M}\langle \rho, \boldsymbol{x} \rangle.$$

To see if the center of mass is conserved, we evaluate

$$\begin{aligned}
M\frac{\partial C}{\partial t} &= \left\langle \frac{\partial \rho}{\partial t}, \boldsymbol{x} \right\rangle \\
&= \langle -\nabla \cdot [-\nabla(Q_s * \rho)\rho + \nabla(Q_s * \rho)\psi_g\rho - \nabla(Q_g * \rho)\psi_g\rho \\
&\quad -\gamma\hat{D}\rho^2\nabla\rho - \hat{D}\nabla\rho\Big], \boldsymbol{x} \Big\rangle \\
&= \langle -\nabla(Q_s * \rho)\rho + \nabla(Q_s * \rho)\psi_g\rho - \nabla(Q_g * \rho)\psi_g\rho \\
&\quad -\gamma\hat{D}\rho^2\nabla\rho - \hat{D}\nabla\rho, 1 \Big\rangle \\
&= \langle -\nabla(Q_s * \rho), \rho\rangle + \langle \nabla(Q_s * \rho), \psi_g\rho\rangle - \langle \nabla(Q_g * \rho), \psi_g\rho\rangle \\
&\quad - \left\langle \gamma\hat{D}\rho^2\nabla\rho, 1 \right\rangle - \left\langle \hat{D}\nabla\rho, 1 \right\rangle.
\end{aligned}$$

Starting with the diffusion terms, we get

$$\begin{aligned}
-\left\langle \hat{D}\nabla\rho, 1 \right\rangle - \left\langle \gamma\hat{D}\rho^2\nabla\rho, 1 \right\rangle &= -\left\langle \hat{D}\nabla\rho, 1 \right\rangle - \left\langle \frac{\gamma\hat{D}}{3}\nabla\rho^3, 1 \right\rangle \\
&= -\left\langle \frac{\gamma\hat{D}}{3}\rho^3, 0 \right\rangle - \left\langle \hat{D}\rho, 0 \right\rangle \\
&= 0.
\end{aligned}$$

This gives

$$M\frac{\partial C}{\partial t} = \langle -\nabla(Q_s * \rho), \rho\rangle + \langle \nabla(Q_s * \rho), \psi_g\rho\rangle - \langle \nabla(Q_g * \rho), \psi_g\rho\rangle.$$

Then using integration by parts, we find

$$M\frac{\partial C}{\partial t} = \langle Q_s * \rho, \nabla(\rho)\rangle - \langle Q_s * \rho, \nabla(\psi_g\rho)\rangle + \langle Q_g * \rho, \nabla(\psi_g\rho)\rangle. \qquad (4.17)$$

However, using properties of convolutions, specifically $\nabla(Q_s * \rho) = \nabla(Q_s) * \rho = Q_s * \nabla(\rho)$ and the assumption Q_s and Q_g are symmetric, we find

$$\begin{aligned} M\frac{\partial C}{\partial t} &= -\langle \nabla(Q_s * \rho), \rho\rangle + \langle \nabla(Q_s * \rho), \psi_g\rho\rangle - \langle \nabla(Q_g * \rho), \psi_g\rho\rangle \\ &= -\langle (\nabla Q_s) * \rho), \rho\rangle + \langle (\nabla Q_s) * \rho, \psi_g\rho\rangle - \langle (\nabla Q_g) * \rho, \psi_g\rho\rangle \\ &= -\langle \rho, (\nabla Q_s) * \rho\rangle + \langle \rho, (\nabla Q_s) * \psi_g\rho\rangle - \langle \rho, (\nabla Q_g) * \psi_g\rho\rangle \\ &= -\langle \rho, Q_s * \nabla(\rho)\rangle + \langle \rho, Q_s * \nabla(\psi_g\rho)\rangle - \langle \rho, Q_g * \nabla(\psi_g\rho)\rangle \\ &= -\langle Q_s * \rho, \nabla(\rho)\rangle + \langle Q_s * \rho, \nabla(\psi_g\rho)\rangle - \langle Q_g * \rho, \nabla(\psi_g\rho)\rangle . \end{aligned} \tag{4.18}$$

Summing (4.17) and (4.18) we get

$$\begin{aligned} 2M\frac{\partial C}{\partial t} = &\langle Q_s * \rho, \nabla(\rho)\rangle - \langle Q_s * \rho, \nabla(\psi_g\rho)\rangle + \langle Q_g * \rho, \nabla(\psi_g\rho)\rangle \\ &- \langle Q_s * \rho, \nabla(\rho)\rangle + \langle Q_s * \rho, \nabla(\psi_g\rho)\rangle - \langle Q_g * \rho, \nabla(\psi_g\rho)\rangle . \end{aligned}$$

Thus,

$$\frac{\partial C}{\partial t} = 0.$$

From this we can conclude that prior to group formation the locust's center of mass is only moved due to non-uniformities in the food source.

4.2 Numerical results

We now investigate both the effect of food on locust group formation and the effect of gregarisation on locust foraging efficiency in one dimension. The numerical method used can be found in Section 3.1

4.2.1 Parameter selection and initial conditions

The bulk of the parameters, $R_s, r_s, R_g, r_g, A_g, k$, and δ, have been adapted from [98] to our non-dimensionalised system of equations. We explore two

parameter sets that we term symmetric and asymmetric based on the time frame of gregarisation vs solitarisation. In the symmetric parameter set ($\delta = 1, k = 0.681$), gregarisation and solitarisation take the same amount of time and the density of locusts for half the maximal transition rate is lower for solitarisation. This is the default parameter set from Topaz et. al. [98] with an adjusted k_1 term that is calculated using (4.14) and the upper range for the onset of collective behaviour as ≈ 65 locusts/m^2 [10, 98]. This behaviour is characteristic of the Desert locust (*S gregaria*) [71].

In the asymmetric parameter set ($\delta = 1.778, k = 0.1$), solitarisation takes an order of magnitude longer than gregarisation, and the density of locusts for half the maximal transition rate is lower for solitarisation. This is the alternative set from Topaz et. al. [98]. The Australia plague locust (*Chortoicetes terminifera*) potentially follows this behaviour taking as little as 6 hours to gregarise but up to 72 hours to solitarise [28, 29]. The complete selection of parameters can be seen in Table 4.1.

At the densities we are investigating we assume that the majority of movement is due to locust-locust interactions rather than random motion. So we set our dimensional linear diffusion term to be of the order 10^{-2}, giving our non-dimensional linear diffusion as $D = 2.041$ for both symmetric and asymmetric parametrisation. Next, we estimate the maximum locust density as ≈ 1000 locusts/m^2 [17] and adapt this to our one dimensional simulation as $||g||_\infty \approx 10\sqrt{10}$ locusts/m. Then using (4.2) we find $\gamma = 431.87$ for the symmetric parameters and $\gamma = 294.44$ for the asymmetric parameters.

To estimate κ we begin with (2.26c) and set the nondimensionalised density of locusts to 1 ($\rho = 1$) (and $\rho = 0.5$ for the asymmetric parameters). We then assume that the locusts consume approximately 70% of the food over the course of the simulation (i.e., c transitions from $c = 1$ to $c = 0.30$). Solving for κ we find $\kappa \approx 0.09$ (and $\kappa \approx 0.18$ for the asymmetric parameters).

Our spatial domain is the interval $x = [0, L]$, where $L = 3/0.14$ (this comes from non dimensionalising the domain used by [98]), with periodic

boundary conditions (i.e., $s(0,t) = s(L,t)$). Our time interval is 12.5 units of time (in dimensional terms this is a 3m domain for a simulated 50 hours).

The initial locusts densities are given by

$$s(x,0) = \frac{\rho_{\text{amb}}}{16.6}(16.6 + \mu) \text{ and } g(x,0) = 0, \tag{4.19}$$

where ρ_{amb} is a ambient locust density and μ is some normally distributed noise, $\mu \sim \mathcal{N}(0,1)$. To ensure that simulations are comparable, we set-up three locust initial conditions and rescale them for each given ambient locust density. Finally, the initial condition for food is given by a smoothed step function of the form,

$$c(x,0) = \frac{F_M}{2\zeta}\left[\tanh\left(\alpha\left[x - \left(x_0 - \frac{\zeta}{2}\right)\right]\right) - \tanh\left(\alpha\left[x - \left(x_0 + \frac{\zeta}{2}\right)\right]\right)\right], \tag{4.20}$$

with $\alpha = 7$, $x_0 = L/2$, F_M being the food mass and ζ being the initial food footprint. We also introduce $\omega = 100\zeta/L$ which expresses the size of the food footprint as a percentage of the domain. Examples of the food distributions generated can be seen in Figure 4.4.

4.2.2 The effect of food on group formation

To investigate the effect that food has on locust group formation, we run a series of numerical simulations in which the total number of locusts and the size of food footprint are varied, while the total mass of food remains constant. The food footprint ranges from covering 2.5% of the domain to 50% of the domain ($\omega = 2.5\%$ to $\omega = 50\%$). For the symmetric parameters four food masses are tested, $F_M = 1.5, 2, 2.5$ and 3, and for the asymmetric variables two food masses are tested, $F_M = 1.5$ and 3. As a control, we also perform simulations with both no food present and a homogeneous food source, represented by $\omega = 0\%$ and $\omega = 100\%$ respectively, for each ambient locust density.

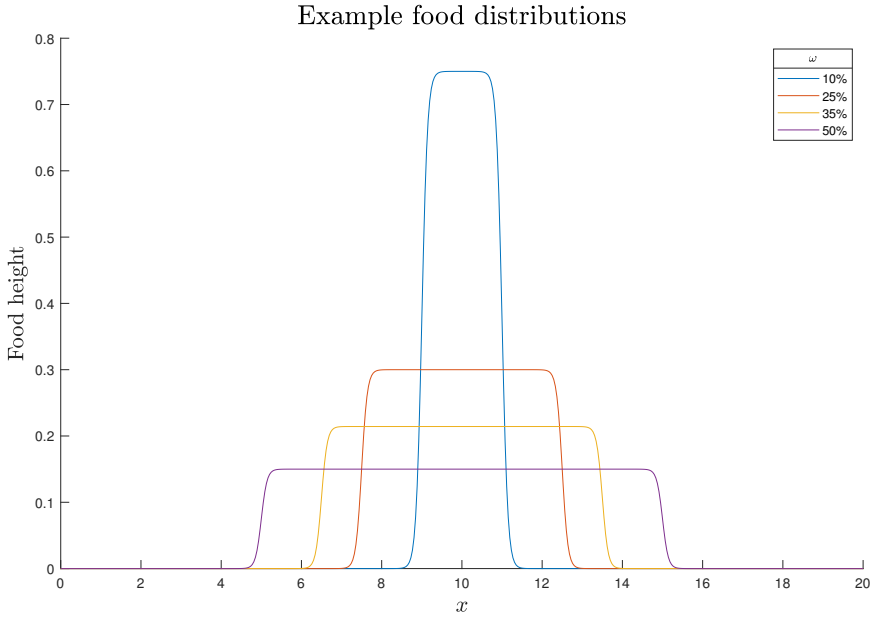

Figure 4.4: **Example food distributions.** Example food distributions generated by (4.20) with $F_M = 1.5$, $\alpha = 7$, and $\omega = 10\%$, 25%, 35%, and 50% on the domain $x = [0, 20]$.

We vary the ambient locust density ranging from $\rho_{\text{amb}} = 0.8$ to $\rho_{\text{amb}} = 1.4$ for the symmetric parameters. This range is selected based on (4.14) so that in the absence of food, group formation would not occur. In each simulation, the solitarious and gregarious populations very quickly tend to an almost smooth and symmetric distribution around the food, however a small quantity of noise persists across the population and this breaks the symmetry leading to group formation. As, in certain cases, the initial noise has an effect on whether a group will form, we run three simulations for each combination of $\rho_{\text{amb}}, \omega$, and F_M with varied initial noise and take the maximum peak density across the three simulations.

For the asymmetric variables we vary ρ_{amb} from $\rho_{\text{amb}} = 0.3$ to $\rho_{\text{amb}} = 0.55$, to test the effect food has on the time frame of group formation. From (4.14)

in the absence of food there should be group formation in the upper half of this density range. However (4.15), suggests that this only occurs outside or right at the end of our simulated time frame. We ran a single simulations for each combination of $\rho_{\text{amb}}, \omega$, and F_M.

The results for the symmetric parameter experiments are displayed in Figure 4.5. The plots show the peak gregarious density of the three simulations for each of the varying food footprint sizes and ambient locust densities. In the blue regions there was no group formation, whilst in the green regions indicate successful group formation. It can be seen in the plots that as the food mass is increased the minimum required locust density for group formation decreases. This effect is more pronounced within an optimal food width and this optimal width increases as the amount of food increases.

The results for the asymmetric parameter experiments are displayed in Figure 4.6. Again, green indicates successful group formation and blue indicates no group formation. It can be seen in these plots that with no food present a group failed to form within the simulated time. From this we can infer that food also decreases the required time for group formation, again there is an optimal food width for this effect.

We can delve deeper into the results by looking at a representative sample of simulations in Figure 4.7. In these simulations $\rho_{amb} = 1.2$, $\kappa = 0.09$, and $F_M = 1.5$, with food footprints $\omega = 7.5\%,\ 10\%$, and 12.5% as well as with no food present. In the simulations in which food is present, prior to group formation gregarious locusts aggregate at the center of the food. If the food source is too narrow ($\omega = 7.5\%,\ t = 3$) there is an attempt at group formation but the gregarious mass is too small and the food source has not been sufficiently depleted so a large portion remains within the food source, thus the group does not persist. If the food is too wide ($\omega = 12.5\%$) the gregarious locusts simply cluster in the center of the food and do not attempt group formation. However, if the food width is optimal ($\omega = 10\%$) there is a successful group formed, this is seen as clump or aggregation of

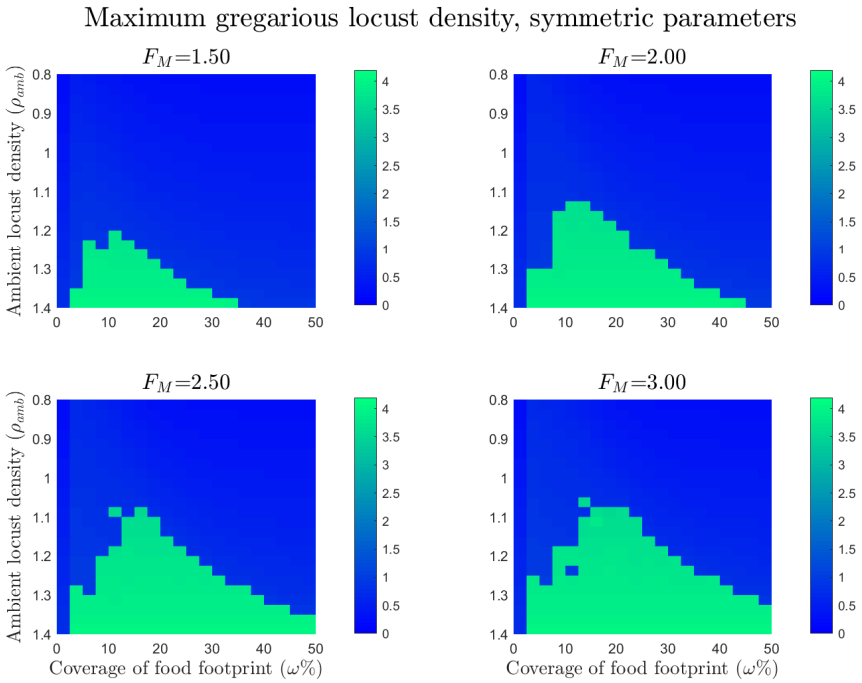

Figure 4.5: **Maximum gregarious locust density for the symmetric gregarisation parameters with varying food footprint sizes and initial ambient locust densities.** For the simulations, $x = [0, 3/0.14]$ with periodic boundary conditions and $t = [0, 12.5]$. The initial condition for locust densities is given by (4.19) and food initial conditions are given by (4.20). Ambient locust density ranges from $\rho_{\text{amb}} = 0.8$ to $\rho_{\text{amb}} = 1.4$, food footprint ranges from $\omega = 0\%$ to $\omega = 50\%$, the food mass $F_M = 1.5, 2, 2.5$ and 3, and the consumption rate $\kappa = 0.09$. The plots show the maximum peak gregarious density for the varying food footprint sizes and ambient locust densities, in the blue regions there was no group formation and in the green regions there was successful group formation. From this we can deduce that food lowers the required locust density for group formation and this is more pronounced within an optimal food width.

gregarious locusts in the final plot.

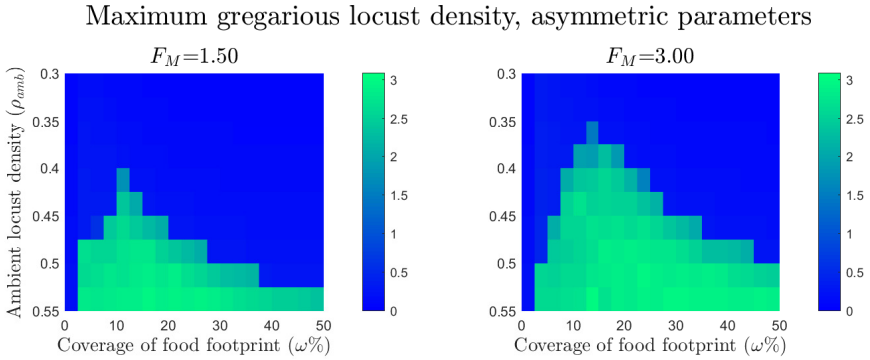

Figure 4.6: **Maximum gregarious locust density for the asymmetric gregarisation parameters with varying food footprint sizes and initial ambient locust densities.** For the simulations, $x = [0, 3/0.14]$ with periodic boundary conditions and $t = [0, 12.5]$. The initial condition for locust densities is given by (4.19) and food initial conditions are given by (4.20). Ambient locust density ranges from $\rho_{\text{amb}} = 0.3$ to $\rho_{\text{amb}} = 0.55$, food footprint ranges from $\omega = 0\%$ to $\omega = 50\%$, the food mass $F_M = 1.5$ and 3, and the consumption rate $\kappa = 0.18$. The plots show the maximum peak gregarious density for the varying food footprint sizes and ambient locust densities. In the blue regions there was no group formation and in the green regions there was successful group formation. From this we can deduce that food lowers the required time forgroup formation and again this is more pronounced within an optimal food width.

4.2.3 The effect of gregarisation on foraging efficiency

It is also possible to investigate the effect of gregarisation on foraging efficiency. Using the technique outlined in Section 2.2, we select a range of food footprints, $\omega\%$, and two food masses, F_M, for a fixed ambient density of locusts, $\rho_{amb} = 0.95$, from the previous simulations. We record the gregarious mass fraction and instantaneous relative advantage as functions of time and plot these against each other in Figure 4.8. By looking at the instantaneous relative advantage versus the global gregarious mass fraction prior to group formation in Figure 4.8, it can be seen that as the gregarious mass fraction increases so too does the foraging advantage of being gregarious. Thus, as

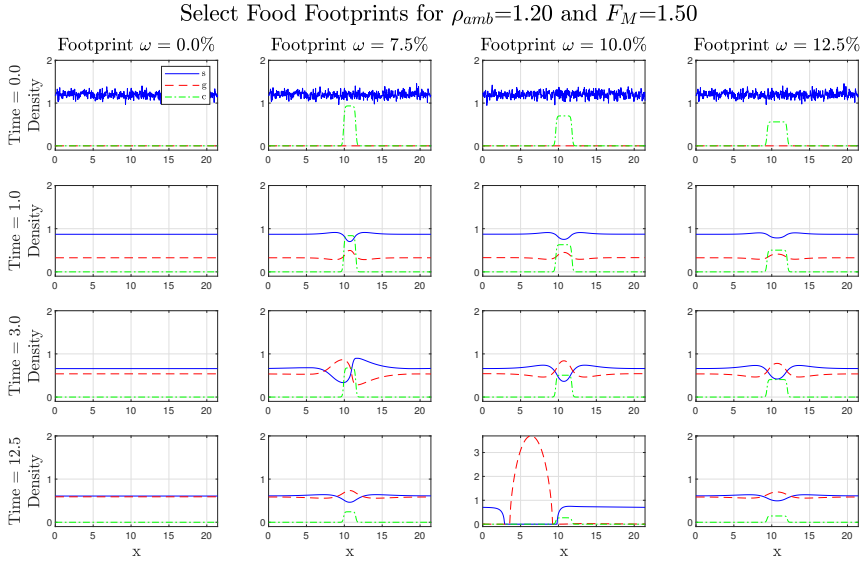

Figure 4.7: **A selection of plots showing the effect of food distribution on gregarisation and locust group formation with symmetric parameters.** In these simulations $\rho_{amb} = 1.2$, $\kappa = 0.09$, and $F_M = 1.5$ with $\omega = 7.5\%$, 10%, and 12.5%, as well as with no food present (labelled $\omega = 0\%$). In the plots, blue is solitarious, red is gregarious, and green is food. If the food source is too narrow ($\omega = 7.5\%$, $t = 3$) there is an attempt at group formation but the gregarious mass is too small and a large portion remains within the food source, thus the group does not persist. If the food is too wide ($\omega = 12.5\%$) the gregarious locusts simply cluster in the center of the food and do not attempt group formation. Finally, if the food width is optimal ($\omega = 10\%$) there is a successful group formed, this is seen as clump or aggregation of gregarious locusts in the final plot.

a greater proportion of locusts become gregarised it is more advantageous to be gregarious. This effect is increased by the mass of food present but is diminished by the size of the food footprint to the point where no advantage is conferred when the food source is homogeneous. This effect is visualised in Figure 4.7, as prior to group formation gregarious locusts aggregate in the center of the food mass and displace their solitarious counterparts.

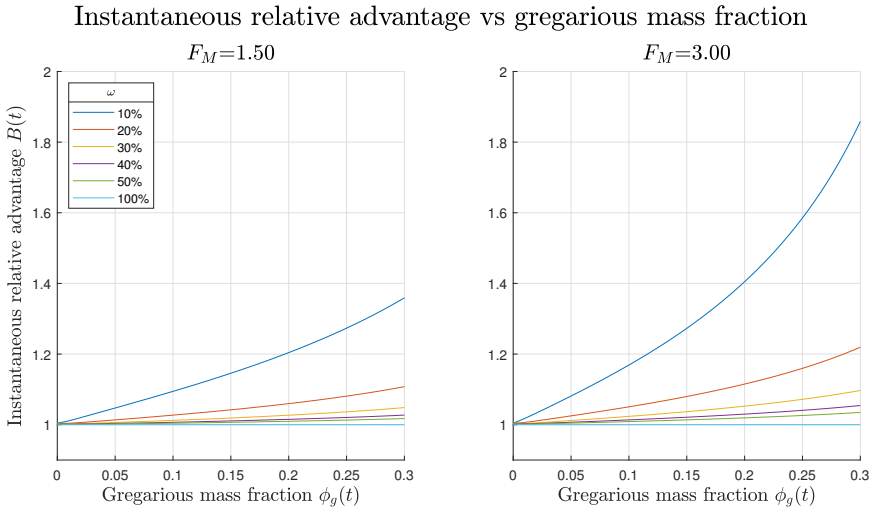

Figure 4.8: **Instantaneous relative advantage of gregarious locusts vs gregarious mass fraction at various food footprints and food masses**. In these simulations $\rho_{amb} = 0.95$ and $\kappa = 0.09$, with the symmetric parameter set. The homogeneous food source is labelled $\omega = 100\%$. It can be seen that as the gregarious mass fraction increases so too does the foraging advantage of being gregarious, this effect is increased by the mass of food present but is diminished by the size of the food footprint.

4.3 Chapter summary

Analytical investigations of our model shows that a spatially uniform and temporally constant food source has a variety of effects on locust behaviour. Firstly, by considering a purely gregarious population we found that the maximum locust density is affected by the amount of food present, in that increasing food leads to increased maximum density. Then, by performing a linear stability analysis we found the gregarious mass fraction required for group formation depends on both the ambient locust density and the amount of food present, with increasing food decreasing the required gregarious mass fraction. Using this relationship we then found that the presence of food lowers both the required time and density of locusts for group formation, and

interestingly that our model also has a theoretical maximum locust density for group formation. Finally, we have also shown that the center of mass of locusts is not dependent on the locust interactions we explored, so prior to group formation the movement of the center of mass is driven by food. In simulations this was seen when prior to group formation gregarious locusts aggregated at the center of the food source.

Then using numerical simulation techniques we confirmed in our model that similar to previous studies highly clumped food sources lead to a greater likelihood of gregarisation [31]. However, we found that there may exist an optimal width for these food clumps for group formation. Similar to our analytic investigations, food was shown to lower the required density for group formation via the symmetric parameters and the required time via the asymmetric parameters. We also found that the optimal width is dependent on the amount of food present relative to the locust population. This effect appears to be brought about by the depletion of the food source. If the food source is not sufficiently depleted, then a gregarious group will fail to form because a portion of the gregarious population will remain on the food. In addition, by looking at the relative foraging advantage of gregarious locusts in our simulations we found that as the gregarious mass fraction increases so too does the foraging advantage of being gregarious. This effect is increased by the mass of food present but is diminished by the size of the food footprint to the point where no advantage is offered with a homogeneous food source.

In the next chapter (Chapter 5) we further investigate this relationship between density dependant phase polyphenism and foraging.

Variable	Description	Symmetric Value	Asymmetric Value	Source
k	Ratio of density of maximal phase transition rates	0.681	0.1	(4.14) [16] [98] [71] [29]
δ	Ratio of maximal phase transition rates	1	1.778	[98] [71] [29]
D	Linear diffusion coefficient	2.041	2.041	
γ	Non-linear diffusion coefficient	431.87	294.44	(4.2) [17]
R_s	Strength of non-local solitarious repulsion	1063.5	878.1	[98]
r_s	Range of non-local solitarious repulsion	1	1	[98][16]
R_g	Strength of non-local gregarious repulsion	940.5	775.6	[98]
r_g	Range of non-local gregarious repulsion	0.2857	0.2857	[98][16]
A_g	Strength of non-local gregarious attraction	2008.7	1658.6	[98]
κ	Food consumption rate	0.09	0.18	(2.26c)

Table 4.1: **Dimensionless parameters used in numerical simulations for both symmetric and asymmetric gregarisation-solitarisation.**

Chapter 5

Foraging in increasingly complex environments

The mechanisms of gregarisation are becoming increasingly understood [6, 87], leaving the question of what advantages gregarisation offers [4]. In insects, a combination of modelling and experiments has shown that the gregarious state offers greater predator avoidance on the individual level [84]. In insects with aposematic colouration, the group display has a greater effect of predator deterrence [40]. In addition, the resulting aggregations may act as a means of countering disease outbreaks by limiting disease transmission between aggregations [101]. Interestingly, density dependant phase polyphenism evolved independently in the various species of locusts [71] and is not unique to locusts; for example, the African army worm exhibits similar behaviour [49, 55, 85].

This raises the question, if being gregarious offers such advantages why transition back to solitarious [4]? One possibility is that at lower densities it may be more advantageous to adopt a solitarious behaviour in order to avoid predators. This reasoning leads to the predator percolation hypothesis suggesting phase polyphenism and the resulting gregarious aggregations evolved as a means of disrupting the connectivity of predator food-patch networks

[1]. However, the predator percolation hypothesis fails to account for the collective motion phenomenon [4]. Another hypothesis which also accounts for the collective motion suggests that the behavioural change seen in density dependent phase polyphenism minimises the risk associated with cannibalistic interactions [48]. In that, at low densities it is better to avoid other individuals and at high densities it is better to simultaneously chase fleeing individuals while fleeing from pursuing individuals [48]. An older hypothesis links phase polyphenism to foraging by postulating that phase polyphenism might have arisen as an offensive trait due to the interactions between insects and plant defence mechanisms [74]. At low densities foragers avoid each other in order to not trigger a plants defences, however once a high enough density is reached to trigger these defences the strategy of overwhelming the plant via a mass attack (i.e. an aggregation) is adopted.

The relationship between foraging and gregarisation has been noted as far back as 1957 by Ellis and Ashall. They found that dense but patchy vegetation promoted the aggregation of juvenile locusts and that sparse uniform plant cover promoted their dispersal [36]. More recent investigations into this behaviour have shown that changes in resource distributions at both small and large spatial scales have an effect on locust gregarisation [25, 31, 32, 33]. With food and gregarisation being intrinsically linked, Lihoreau et al. used an agent based model to investigate how social interactions affect foraging in increasingly patchy environments, finding that social groups offer an advantage in this context [62]. This foraging advantage was also partly explored using a continuum model in one dimension in Chapter 4. Here we aim to use our model to further explore the interactions between gregarisation and foraging in two dimensions. In Chapter 4 we used a smoothed step function to represent the food distribution with the percentage of the domain covered representing patchiness. In this chapter we look at more complex food distributions and determine a way of measuring the heterogeneity (or patchiness) of the food.

The two main tools for measuring the spatial heterogeneity of an environment are; fractal dimension, based on the work of Mandelbrot [66], and entropy, borrowed from information theory [73, 83]. While there are inconsistencies with the use of term entropy and the original thermodynamic interpretation, it does serve as a measure of spatial heterogeneity [54]. In addition, there exists an equivalence relationship between normalised entropy and normalised fractal dimension [23]. As we only compare between generated food sources we therefore use normalised entropy to compare the spatial heterogeneity of our generated food distributions.

In this chapter we first explore a two dimensional simulation in which gregarisation occurs as a result of local organism density, and how this affects foraging in a highly heterogeneous environment. We then fix the proportion of the population that is gregarious and investigate the steady state foraging advantage in relation to food heterogeneity. Finally, we perform a parameter sensitivity analysis to see which model parameters have the greatest effect on foraging efficiency. Across the three experiments we find that prior to gregarious aggregations, in increasingly heterogeneous food environments there is a foraging advantage to being gregarious. Over the course of this chapter, we will assume that the movement is on a much shorter time-frame than consumption and thus work with static non-depleting food sources.

The chapter is organised as follows. In Section 5.1 we describe the simplification of the social potential presented in Section 2.1.2 and the method used to generate food distributions. Then, in Section 5.2 we give the results of three numerical experiments relating foraging and gregarisation. Finally, in Section 5.3 we summarise the key findings and offer avenues of future exploration.

This chapter has been accepted for publication as *Georgiou, F., Buhl, J., Green, J.E.F., Lamichhane, B., and Thamwattana, N. (2022). Modelling foraging competition between solitarious and gregarious organisms in increasingly heterogeneous environments. Journal of Insect Physiology.*

5.1 Model and methods

In this section we begin by looking at an overview of the foraging PDE model. Then, in Section 5.1.2, we look at generating, and measuring the heterogeneity of food distributions.

5.1.1 PDE foraging model

In our previous study (Chapters 2 and 4) we developed a PDE model of locust foraging that divides up locust behaviour into local and non-local components of movement and gregarsation dynamics (equations (2.26a), (2.26b), and (2.26c)). In this chapter, we use the same basic modelling framework to investigate the behaviour of an idealised density dependent phase polyphenic organism. The only change being that we adopt simpler assumptions for the gregarious social potential. Here, we assume that organisms experience a non-local (i.e. longer-ranged) interaction with organisms of either type and that the magnitude of that interaction is equal but opposite for solitarious and gregarious organisms (i.e. gregarious organisms have only long range attraction and solitarious organisms have only a long range repulsion). We obtain the following expressions for the social potentials

$$Q_g = -Ae^{-\frac{|\boldsymbol{x}|}{r}} = -Q_s, \tag{5.1}$$

where A is the strength of attraction (or in the case of solitarious, repulsion) and r is the sensing distance. In addition, we use the following scalings

$$t = \frac{1}{T}\bar{t},\ \boldsymbol{x} = r\bar{\boldsymbol{x}},\ (\rho, s, g) = k_1(\bar{\rho}, \bar{s}, \bar{g}),\ \text{and } c = c_0\bar{c}.$$

Then, dropping the bar notation, our model can be written as the following system of dimensionless equations:

$$\frac{\partial g}{\partial t} + \nabla \cdot (g\boldsymbol{v}_g) - D^*\nabla \cdot \left[e^{-c}\nabla g\right] = -f_1^*(\rho)g + f_2^*(\rho)s, \tag{5.2a}$$

$$\frac{\partial s}{\partial t} + \nabla \cdot (s\boldsymbol{v}_s) - D^*\nabla \cdot \left[e^{-c}\nabla s\right] = f_1^*(\rho)g - f_2^*(\rho)s, \tag{5.2b}$$

$$\frac{\partial c}{\partial t} = -\kappa^* c(x,t)\rho(x,t), \tag{5.2c}$$

where

$$\boldsymbol{v}_g = -\nabla Q_g^* * \rho + D^* e^{-c}\left(\nabla c - \gamma^*\rho\nabla\rho\right), \boldsymbol{v}_s = -\nabla Q_s^* * \rho + D^* e^{-c}\left(\nabla c - \gamma^*\rho\nabla\rho\right),$$

and

$$Q_g^* = -A^* e^{-|\boldsymbol{x}|} - A_g^* = -Q_s,\ f_1^*(\rho) = \frac{\delta_1^*}{1+\rho^2},\ f_2^*(\rho) = \frac{\delta_2^*(\rho k)^2}{1+(\rho k)^2},$$

where $k = \frac{k_1}{k_2}$ is the ratio of densities at which maximal phase transition rates occur. Note that we have also introduced the following dimensionless parameters,

$$D^* = \frac{D}{Ta_g^2},\ \delta_1^* = \frac{\delta_1}{T},\ \delta_2^* = \frac{\delta_2}{T},\ \gamma^* = k_1^2\gamma,\ \kappa^* = \frac{\kappa k_1}{T},\ A^* = \frac{Ak_1}{Tr}.$$

In addition, we use the parameter T to rescale the dimensionless parameters for the parameter sensitivity analysis. Finally, for notational simplicity we drop the $\cdot^*$ notation in the rest of this chapter.

5.1.2 Generating food distributions

In order to create food distributions of increasing spatial heterogeneity that are continuous at the spatial scale under consideration, we use the following method. We begin by creating a low resolution matrix of normally distributed

noise with mean 0 and variance 1 (in the case of these simulations, a 5×5 matrix). We then append the first row and first column to the end of the matrix to make it periodic. Using MATLAB's natural interpolation we upscale our noise matrix to the simulation resolution. We denote the upscaled noise matrix, N. Finally, we generate increasingly heterogeneous food distributions, denoted F_α (where $\alpha \in [0, 1]$ is a parameter), according to the formula,

$$F_\alpha = \frac{1 + \alpha \frac{N}{|N|_\infty}}{\left| 1 + \frac{N}{|N|_\infty} \right|_\infty}, \ \alpha = [0, 1], \tag{5.3}$$

where $|\cdot|_\infty$ is the infinity norm, i.e. $|N|_\infty$ is the largest absolute value in the matrix N.

In order to calculate the entropy, E, of a food distribution and thus measure its spatial heterogeneity, we divide up the interval of possible values for food density, $c \in [0, 1]$, into $n = 256$ bins (this selection of n comes from image processing) [46]. We then calculate the number of grid squares in our generated distribution in each bin, and divide this by the total number of squares to obtain the probability of a square being in a particular bin, labelled P_i. We then use the definition of Shannon entropy [83] given by

$$E = -\sum_{i=1}^{n} P_i \log_2 P_i,$$

to calculate the entropy of a food distribution. We then normalise this entropy by the maximum entropy obtained for a particular noise matrix N - i.e., if we label the entropy of a particular food distribution, F_α, as E_α, we can then calculate the normalised entropy, $\hat{E}_\alpha$, as

$$\hat{E}_\alpha = \frac{E_\alpha}{\max\limits_{\alpha \in [0,1]} (E_\alpha)},$$

where $\max\limits_{\alpha \in [0,1]} (E_\alpha)$ gives the maximum entropy across all $\alpha = [0, 1]$.

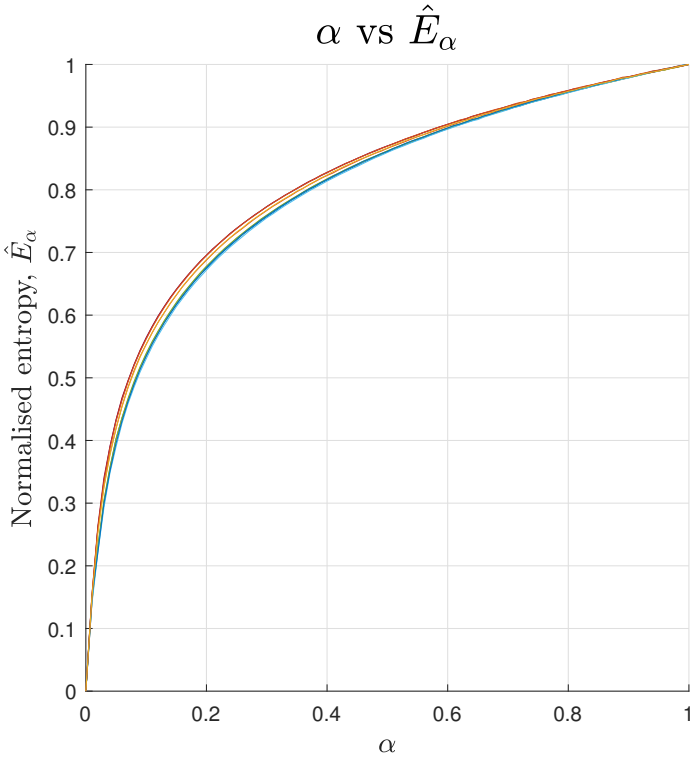

Figure 5.1: **Relationship between α and normalised entropy.** Relationship between α and normalised entropy, $\hat{E}_\alpha$, for 10 different random food distributions with each coloured line representing a different food distribution. It can be seen that the method presented in Section 5.1.2 results in monotonically increasing $\hat{E}_\alpha$ with increasing α.

We investigate the relationship between α and the entropy of the initial food distribution by calculating F_α for different values of α using ten different noise matrices, N. As shown in Figure 5.1, the entropy, $\hat{E}_\alpha$, (and thus spatial heterogeneity) increases monotonically with increasing α, and almost independent of the particular matrix N used. We then selected at random a single noise matrix for use in this chapter; two examples of a generated food distribution can be seen in Figure 5.2.

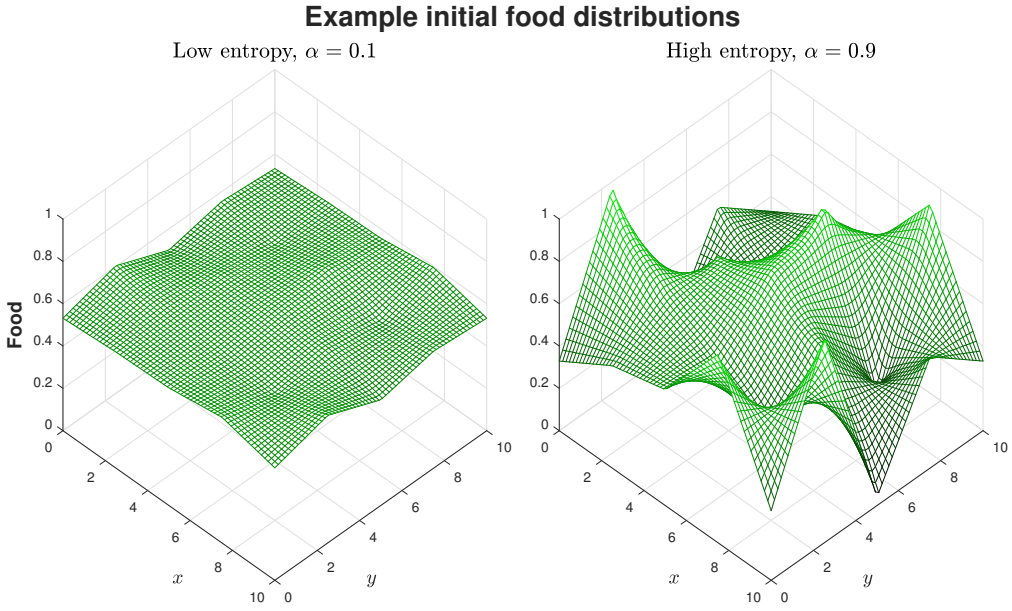

Figure 5.2: **Two example food distributions.** The food distributions are made using the method presented in Section 5.1.2. The left food distribution has a low α value and thus a low spatial heterogeneity. The right food distribution has a high spatial heterogeneity.

5.2 Results

In order to simulate the system of equations in two dimensions we developed a first order finite volume based numerical scheme for the spatial component based on the work of Burger et.al. [19] with an adaptive Runge-Kutta scheme for the time component using the work of Horsea and Shampine [52]. This combination of methods allows us to solve the equations numerically and obtain a close approximation to the analytic solutions without needing to exactly solve the governing equations. For the derivation see Chapter 3 and for the MATLAB implementation see Appendix A.2.

5.2.1 Parameter selection and initial conditions

Over the course of the numerical experiments we test a wide variety of parameter combinations, with the full selection of values given in Table 5.1. For our initial single simulation we select parameters such that organism movement and gregarisation occur on roughly the same timescales (the column labelled 'Single'). Then for our foraging advantage section simulations we scale the parameters to reduce numerical complexity, the parameters used are in the 'Bulk' column. Finally, for our parameter sensitivity analysis we sample a wide range of parameters, given in the 'PSA' column. Over the course of the simulations we use a static or non-depleting food source, i.e. from (5.2c), $\kappa = 0$.

Variable	Description	Single	Bulk	PSA
k	Ratio of densities at which maximal phase transition rates occur	1	N/A	N/A
δ_1	Rate of maximal phase transition for solitarious to gregarious	0.5	N/A	N/A
δ_2	Rate of maximal phase transition for gregarious to solitarious	0.5	N/A	N/A
D	Linear diffusion coefficient	0.2	0.01	$[0, 1]$
γ	Non-linear diffusion coefficient	10	10	$[0, 100]$
A	Strength of non-local interactions	10	1	$[0, 10]$
ϕ	Gregarious mass fraction, (2.2)	Variable	$[0, 0.3]$	$[0, 0.3]$
α	Heterogeneity of the food	1	$[0, 1]$	$[0, 1]$
ρ_{amb}	Ambient organism density	1	$[0.1, 0.5]$	0.1

Table 5.1: **Dimensionless parameters used in numerical simulations.** The 'Single' values are used in the single example simulation with gregarisation. The 'Bulk' values are used in foraging advantage section. Finally, 'PSA' values are used in the parameter sensitivity section. Here $[a, b]$ represents the closed interval from a to b.

All simulations have a spatial domain given by the two dimensional square with sides $0 < x < 10$ and $0 < y < 10$ divided up into a 64×64 grid.

In addition, we use periodic boundary conditions (i.e. if something leaves through the left it returns through the right, and similarly with the top and bottom boundaries). For the single simulation we run the simulation to $t = 10$. For both the bulk simulations and the simulations in the parameter sensitivity analysis we run each simulation to pseudo steady state of $t = 100$ at which there is be minimal movement of the organisms.

5.2.2 Simulation with gregarisation

To illustrate the behaviour of the model we run a two-dimensional simulation with the density dependent gregarisation kinetics. We use an initial solitarious density of $\rho_{\text{amb}} \approx 1$ with parameter values given in the 'single' column of Table 5.1. The results can be seen in Figure 5.3. In the first row, showing the early time dynamics, we can see the solitarious organisms transition to gregarious in a fairly spatially homogeneous manner with small peaks forming within the food peaks. Then, in the second row, we see the gregarious peaks within the food peaks continue to grow as they attract the other gregarious organisms before forming discrete aggregations which combine. It is at this point that the aggregations reach a stationary steady state even if no food is present, highlighting the need for collective movement (such as alignment and marching) or a mechanism for dispersal. An animation of this simulation is located in the supplementary material.

It is also possible to gain insight into the mechanism by which gregarious organisms out-forage their solitarious counterparts. Prior to aggregation both solitarious and gregarious organisms are drawn towards the food and so congregate where the food density is highest. However, since solitarious individuals are repelled from others they are pushed out of the peaks by the gregarious individuals who can tolerate the crowding. This is highlighted in Figure 5.4, by plotting the gregarious foraging advantage against the gregarious mass fraction prior to aggregation formation. It can be seen that as the gregarious mass fraction increases so too does the foraging advantage.

5.2.3 Foraging advantage

In order to further explore the foraging advantage of gregarisation we switch off the ability of individuals to change from solitarious to gregarious or vice versa (i.e. $f_1(\rho) = f_2(\rho) = 0$), giving a fixed gregarious mass fraction. We investigate the combined effect of population density, gregarious fraction and food heterogeneity by running simulations with $0.1 < \rho_{\text{amb}} < 0.5$, $0.03 < \phi < 0.3$, and $0 < \alpha < 1$. We simulate every combination of parameters to the pseudo steady state, $t = 100$, and then measure the final foraging advantage, B_∞ (given by (2.29)). The results of these numerical experiments can be seen in Figure 5.5.

In Figure 5.5 we can see that as α increases the foraging advantage of being gregarious increases, this effect occurs to a lesser extent by increasing gregarious mass fraction ϕ. However, this does not appear to be greatly affected by increasing the mass of organisms (over the range of masses and variable combination we tested). We can thus further explore the results by looking at a larger range of ϕ for a given mass. The results of this are seen in Figure 5.6. Once again we see that foraging advantage increases both with increasing α and ϕ. We note that in every simulation in the area labelled "aggregation region" a aggregation of gregarious individuals formed similar to that seen in Figure 5.3. This highlights the need for a mechanism of collective movement or dispersal as once the aggregation has formed, depending on the heterogeneity of the landscape, it ends up being a disadvantage to be gregarious.

5.2.4 Parameter sensitivity analysis

A key advantage of using the PDE model is the ability to perform a parameter sensitivity analysis. This method attempts to quantify the relative importance of the input factors in determining the output of a model [79, 88]. In this case, the effect of the coefficients, D, γ, and A, gregarious mass

fraction, ϕ, and landscape heterogeneity, α, on the steady state gregarious foraging advantage, B_∞. This is done by writing the model output (in this case B_∞) as a function of the input (D,γ,A,ϕ, and α) in the form

$$B_\infty = f(D, \gamma, A, \phi, \alpha).$$

We then measure the effect of the inputs on the variance of the output to find the relative importance of the inputs. The relative importance is measured as two distinct indices (known as Sobol indices) normalised by the output variance. The first describes "first order" effects, labelled S_i (where i refers to the input parameter), or the effect of varying a single parameter (and fixing all others) on the model output. The second index gives the "total" effects, labelled S_{Ti}, or the interaction between all model parameters and their effect on the output. A recent example of the use of a parameter sensitivity analysis in the context locust hopper bands is given by Bernoff et al. [13], and a detailed description of parameter sensitivity analyses given by Saltelli et al. [80]. In addition a brief guide on parameter sensitivity analyses as well as the use of T can be found in Appendix B.

To perform the parameter sensitivity analysis over the range of values given in the 'PSA' column of Table 5.1, we use a Sobol quasirandom sequence and Radial sampling to sample the parameter space [81]. In total, we create 8750 different combinations of D, γ, A, ϕ, and α. The results of the parameter sensitivity analysis can be found in Figure 5.7. It can be seen that in relation to the first order effects, S_i, the greatest effect on gregarious foraging advantage is given by the strength of non-local interactions, A, the gregarious mass fraction, ϕ, and the heterogeneity of the landscape, α. However once we get into the total order effects, S_{Ti}, α has by far the most influence on foraging advantage.

The effect of α on foraging advantage is perhaps best seen by looking at the scatter plot of foraging advantage against α of all simulations, depicted in Figure 5.8. Included in the plot is the red dot-dashed line at $B = 1$, and a

quadratic line of best fit show as a yellow dashed line. We can see that as α increases so too does foraging advantage almost regardless to the parameter combinations used, this suggests that the foraging advantage is intrinsic to the solitarious/gregarious behavioural dynamic. In the four outliers where $B < 1$ an aggregation formed.

5.3 Chapter summary

In this chapter we have further explored our model and the concept of foraging advantage in two dimensions. We did this by developing a simple algorithm to make food distributions of increasing heterogeneity and then using these distributions to see the effect of gregarisation on foraging in increasingly heterogeneous environments. Through a series of numerical experiments, we have further found that prior to mass aggregations, in increasingly heterogeneous food environments it is better to be gregarious than solitarious. However, once an aggregation is fully formed this advantage can be quickly lost, highlighting the need to evolve a migration/collective movement mechanism for the gregarious phase to remain viable over time. In addition, the advantage is also lost in homogeneous environments. Finally, through the parameter sensitivity analysis, we have shown that the foraging advantage is intrinsic to the solitarious/gregarious behavioural dynamic as it occurs almost regardless of the parameters selected.

The question that now arises is 'does this relationship occur in more detailed models?', we begin an exploration into this in Chapter 6 where we modify our original model to include a component of hunger.

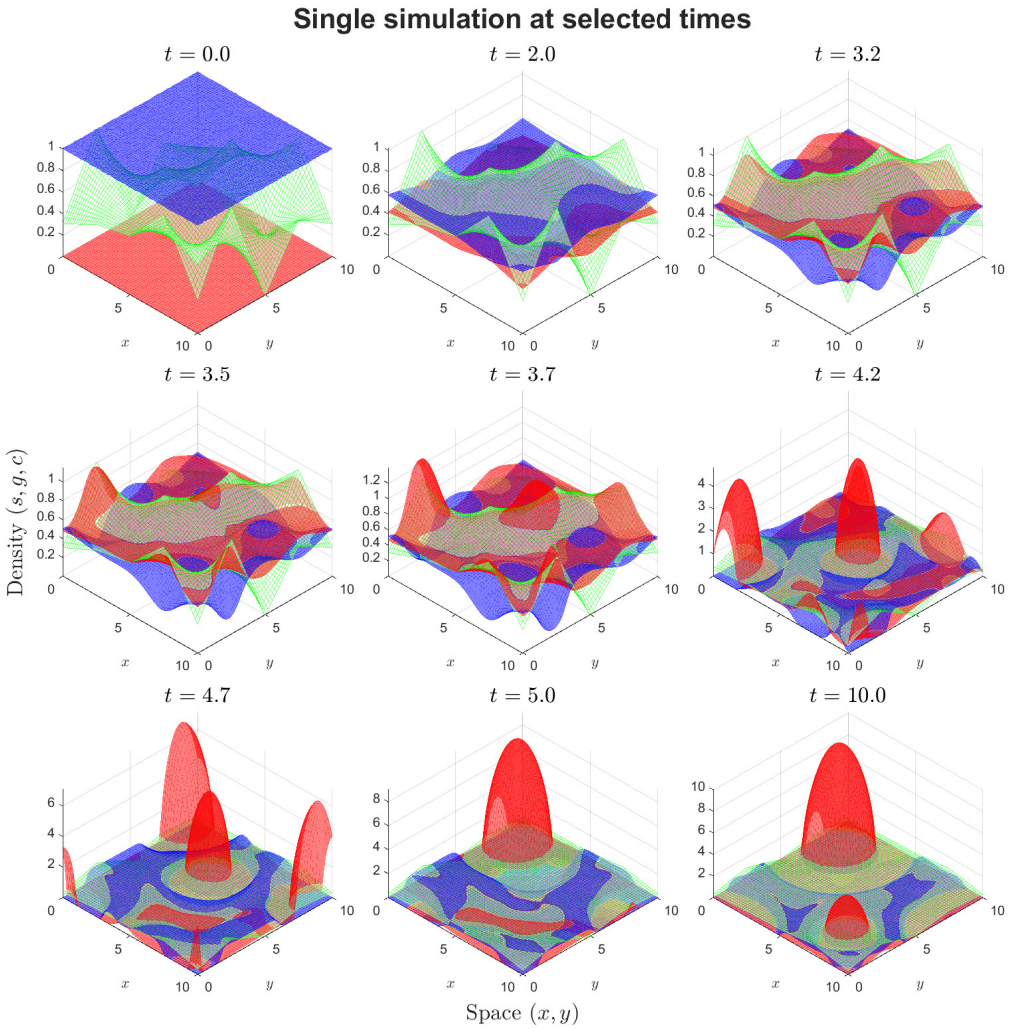

Figure 5.3: **Single simulation with $\alpha = 1$ and organism kinetics.** The blue surface in the plots is solitarious organism density (initially $s(x, 0) \approx 1$), red is gregarious organism density (initially $g(x, 0) = 0$), and green represents food. We see the solitarious organisms transition to gregarious until a critical ratio is reached after which the gregarious organisms form a massive aggregation.

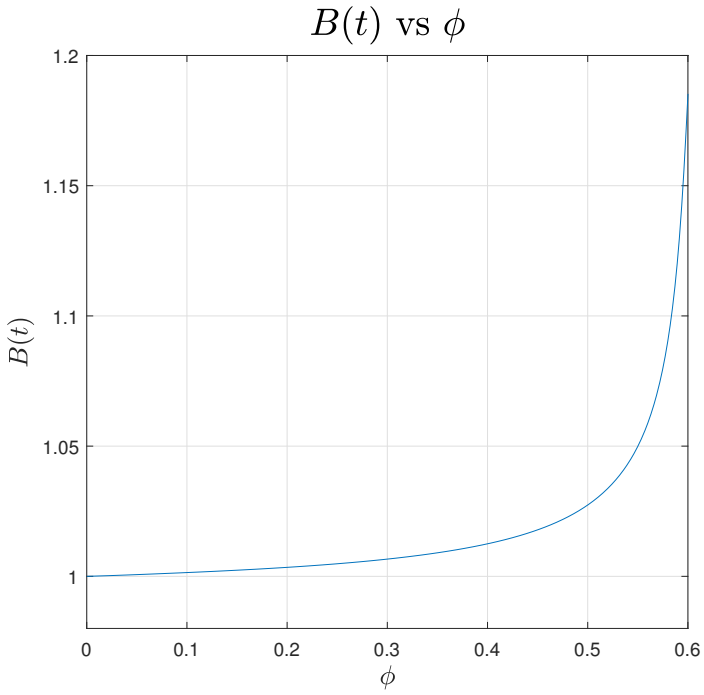

Figure 5.4: **Foraging advantage versus gregarious mass fraction from 2D simulation with gregarisation.** It can be seen that as the gregarious mass fraction increases so too does the foraging advantage.

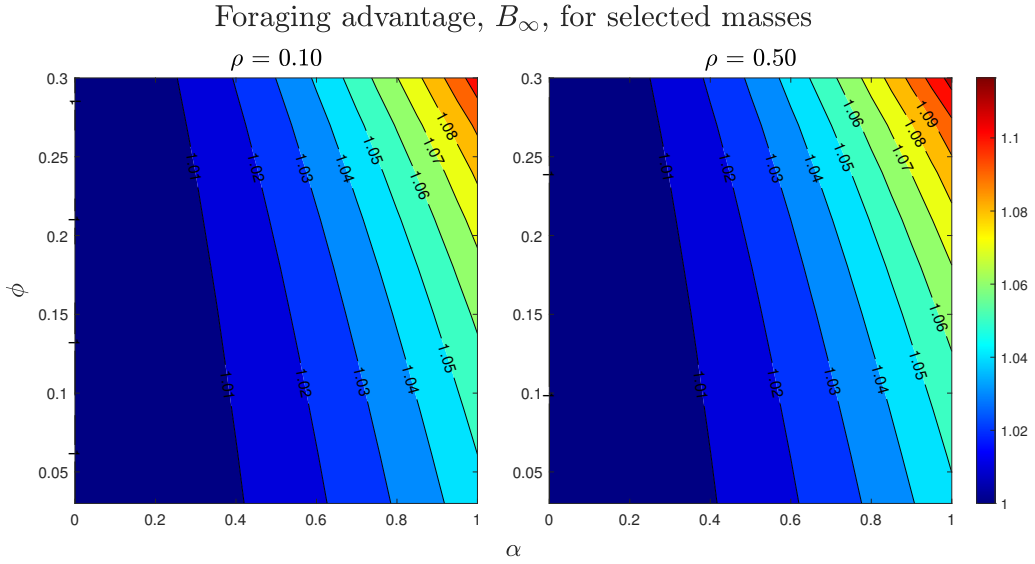

Figure 5.5: **Gregarious foraging advantage for selected ambient densities.** For each ambient density the gregarious mass fraction, ϕ was varied from $\phi = 0.03$ to $\phi = 0.3$ in 0.03 step increments. In addition, the heterogeneity of the food, α, was varied from $\alpha = 0$ to $\alpha = 1$ in 0.05 increments. It can be seen that as α increases the foraging advantage of being gregarious increases, this effect occurs to a lesser extent by increasing gregarious mass fraction ϕ. However, this does not appear to be greatly affected by increasing the mass of organisms.

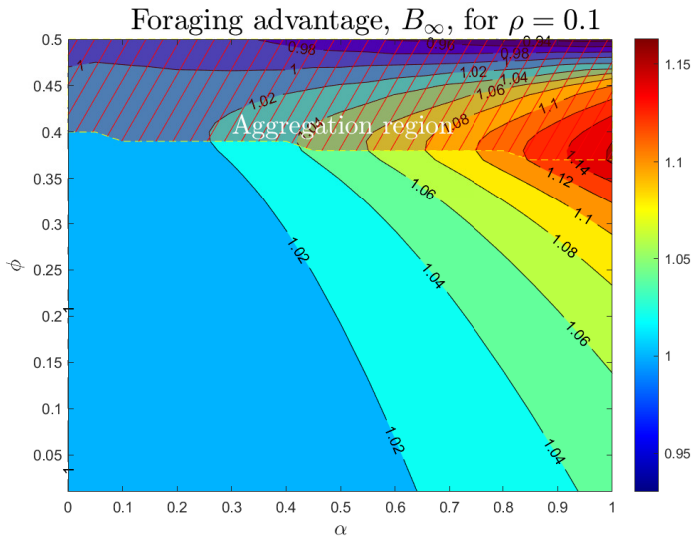

Figure 5.6: **Gregarious foraging advantage for the gregarious mass fraction range, $\phi = 0.03$ to $\phi = 0.5$.** It can be seen that as α increases the foraging advantage of being gregarious increases, this is further compounded by increasing gregarious mass fraction ϕ.

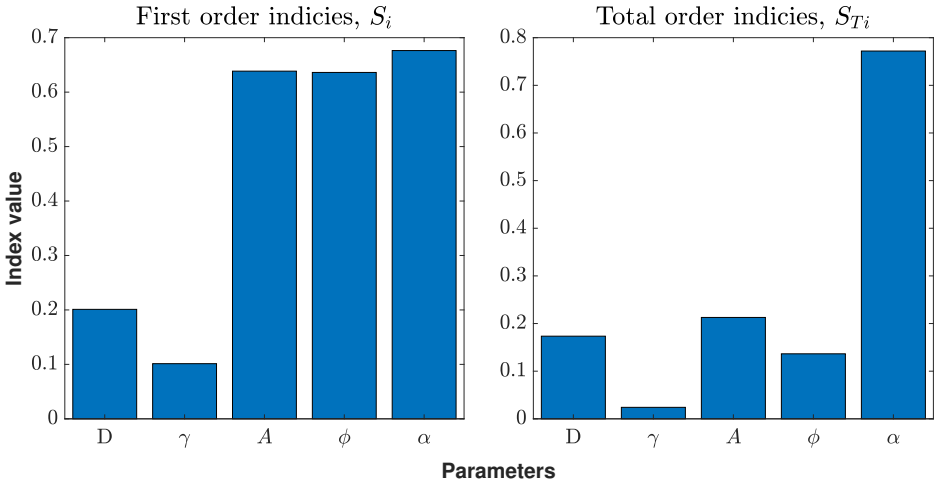

Figure 5.7: **Results of the parameter sensitivity analysis.** It can be seen that in relation to the first order effects, S_i, the greatest effect on gregarious foraging advantage is given by the strength of non-local interactions, A, the gregarious mass fraction, ϕ, and the heterogeneity of the landscape, α. However once we get into the total order effects, S_{Ti}, α is by far the greater determiner of foraging advantage.

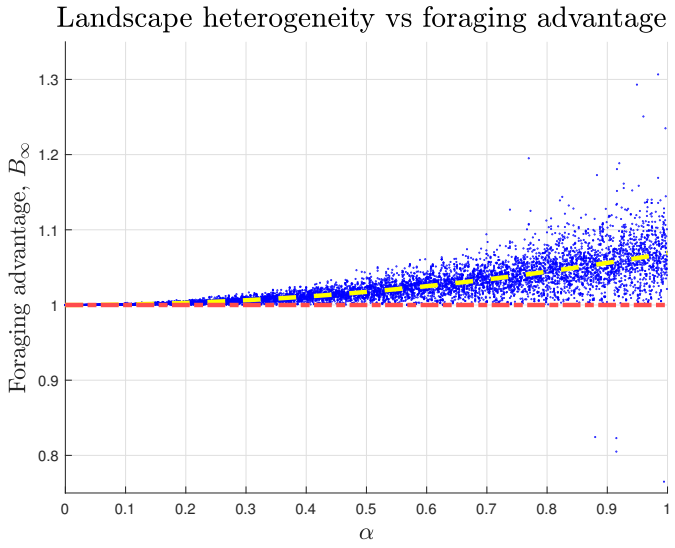

Figure 5.8: **The effect of α on foraging advantage.** Included in the plot is the red dot-dashed line at $B_\infty = 1$, and a quadratic line of best fit show as a yellow dashed line. We can see that as α increases so too does foraging advantage almost regardless of the other parameter values. In the four outliers where $B_\infty < 1$ an aggregation formed.

Chapter 6

Increasing model complexity with hunger

Throughout this thesis we have explored a model of locust foraging that includes non-local locust interactions, local locust and food interactions, and gregarisation dynamics to better understand the interaction between foraging and gregarisation. However, in order to keep the model computationally tractable we have had to make a variety of simplifying assumptions, which does impact the direct biological relevance. The assumptions are:

1. Locusts can be classified as either solitarious or gregarious.
2. Locusts only interact with food resources when they come into direct contact with them.
3. Local interactions between locusts (both gregarious and solitarious) are repulsive (i.e. they avoid close physical contact).
4. Solitarious locusts experience a non-local (i.e. longer-ranged) repulsion from other locusts of either type.
5. Gregarious locusts experience a non-local long-range attraction and short-range repulsion from other locusts, which is consistent with them forming a well-spaced aggregation [15].

6. The nature (attractive or repulsive) and strengths of all interactions are constant in time.

Regarding assumption 6, we note that the nature of locusts movement is dependent on many factors. These include weather conditions [100], internal body temperature [65], time of day [94], and level of hunger [34, 72]. Each of which may effect our results, and the last being perhaps the most fitting to our study. The effect of hunger on locust movement can be considerable, with a 1996 study by Raubenheimer and Gäde finding that food deprivation can triple the amount of time spent moving by a locust [72]. With this in mind, in this chapter we look at expanding our model by having our local locust interactions depend on their levels of hunger, i.e. we alter our original assumption 6 to be:

6. The nature (attractive or repulsive) and strengths of non-local interactions are constant in time, and the strength of local interactions depend on the hunger levels of individual locusts.

We begin by expanding our model to include a dimension of hunger and introduce a new metric of foraging in Section 6.1. Then in Section 6.2 we repeat the analysis of Section 4.1 with our modified model. Finally, we perform a series of numerical experiments in Section 6.3 to investigate the relationship between food, hunger, and gregarisation.

6.1 Model and methods

In earlier chapters, our model locusts are represented as a density of individuals (number per unit area) with dimensions of space, $\boldsymbol{x}$, time, t. We now introduce a dimension of hunger, $n = [0, 1]$, where $n = 0$ is hungry and $n = 1$ is completely satiated. Again, locusts are either solitarious, $s(\boldsymbol{x}, n, t)$,

or gregarious $g(\boldsymbol{x}, n, t)$, with the total local density defined as

$$\rho(\boldsymbol{x}, t) = \int_0^1 s(\boldsymbol{x}, n, t) + g(\boldsymbol{x}, n, t) dn.$$

For later convenience we will also define the total mass of locusts as

$$M = \int \rho(\boldsymbol{x}, t)\, d\boldsymbol{x}, \tag{6.1}$$

and the global gregarious mass fraction as

$$\phi_g(t) = \frac{\int g(\boldsymbol{x}, n, t)\, d\boldsymbol{x} dn}{M}. \tag{6.2}$$

We assume that the time-scale of gregarisation is shorter than the life cycle of locusts, ignoring births and deaths and thus conserving the total number of locusts. We allow for a transition from solitarious to gregarious and vice-versa depending on the local population density. We also allow for locusts to change their hunger levels. Hence, conservation laws give equations of the form

$$\frac{\partial g}{\partial t} + \nabla \cdot (\boldsymbol{J}_{g_{\text{local}}} + \boldsymbol{J}_{g_{\text{non-local}}}) + \frac{\partial}{\partial n}(g n_g) = K(s, g), \tag{6.3a}$$

$$\frac{\partial s}{\partial t} + \nabla \cdot (\boldsymbol{J}_{s_{\text{local}}} + \boldsymbol{J}_{s_{\text{non-local}}}) + \frac{\partial}{\partial n}(s n_s) = -K(s, g), \tag{6.3b}$$

where $\boldsymbol{J}_{(s,g)_{\text{local}}}$ is the flux due to local interactions, $\boldsymbol{J}_{(s,g)_{\text{non-local}}}$ is the flux due to non-local interactions, $n_{(s,g)}$ are functions that describe the change in locust hunger levels, and $K(s, g)$ represents the transition between the solitarious and gregarious states.

In addition to locust densities, we again include food resources in our model and let $c(\boldsymbol{x}, t)$ denote the food density (mass of edible material per unit area). We assume that locust food consumption is based on their contact with food and their hunger levels and on the time-scale of group formation

food production is negligible, giving

$$\frac{\partial c}{\partial t} = -c(\boldsymbol{x}, t) \int_0^1 \psi(n)(s(\boldsymbol{x}, n, t) + g(s(\boldsymbol{x}, n, t))dn, \tag{6.4}$$

where $\psi(n)$ is a function relating the locust's hunger and food consumption rate.

6.1.1 Local interactions

Similar to the model derived in Chapter 2 we derive the local interactions as the limit of a lattice model, following the work of Painter and Sherratt [70]. We begin here by considering solitarious locust movement on a two-dimensional lattice one dimension of space and one of hunger with movement restricted to the spatial dimension (we assume that local gregarious locust behaviour is the same resulting in a similar derivation). Let $s_{i,j}^t$ be the number of solitarious locusts at site i with hunger level n_j at time t, and let $g_{i,j}^t$, and c_i^t be similarly defined. In addition let,

$$\rho_i^t = \sum_{j=1}^{N} s_{i,j}^t + g_{i,j}^t,$$

where N is the number of hunger levels, i.e. ρ_i^t is the total number of locusts at spatial site i and time t regardless of hunger.

We assume that the transition probabilities for a locust at the $(i,j)^{th}$ site depends on the food density at that site, the hunger of the locust, and the relative population density between the current site and neighbouring sites. If we let $\mathcal{T}_{i,j}^{\pm}$ be the probability at which locusts at site (i,j) move to the right, $+$, and left, $-$, during a timestep, then our transition probabilities are

$$\mathcal{T}_{i,j}^{\pm} = F(n_j, c_i)(\alpha + \beta(\tau(\rho_i) - \tau(\rho_{i\pm1}))), \tag{6.5}$$

where F is a function of food density and hunger, τ is a function related to the local locust density, and α and β are constants. Then the number of individuals at site (i, j) at time $t + \Delta t$ is given by

$$s_{i,j}^{t+\Delta t} = s_{i,j}^t + \mathcal{T}_{i+1,j}^- s_{i+1,j}^t + \mathcal{T}_{i-1,j}^+ s_{i-1,j}^t - (\mathcal{T}_{i,j}^- + \mathcal{T}_{i,j}^+) s_{i,j}^t. \tag{6.6}$$

Substituting (6.5) into (6.6) gives

$$\begin{aligned} s_{i,j}^{t+\Delta t} =& s_{i,j}^t + F(n_j, c_{i+1})(\alpha + \beta(\tau(\rho_{i+1}) - \tau(\rho_i)))s_{i+1,j}^t \\ &+ F(n_j, c_{i-1})(\alpha + \beta(\tau(\rho_{i-1}) - \tau(\rho_i)))s_{i-1,j}^t \\ &- [F(n_j, c_i)(\alpha + \beta(\tau(\rho_i) - \tau(\rho_{i-1}))) + F(n_j, c_i)(\alpha + \beta(\tau(\rho_i) - \tau(\rho_{i+1})))]s_{i,j}^t. \end{aligned} \tag{6.7}$$

Which following the derivation in Section 2.1.1 gives our flux as

$$J_{s_{\text{local}}} = -D\left[\frac{\partial}{\partial x}\left(sf(n)e^{-\frac{c}{c_0}}\right) + \gamma s\rho f(n)e^{-\frac{c}{c_0}}\frac{\partial \rho}{\partial x}\right], \tag{6.8}$$

where $f(n)$ is a function relating locust hunger to the strength of local interactions, we assume that $f(n)$ increases as $n \to 0$. The derivation of $J_{g_{\text{local}}}$ follows the same method.

6.1.2 Hunger levels

We assume that locusts become hungrier based on energy lost due to metabolism and movement, and that locusts become satiated by eating at a rate proportional to their hunger. These assumptions give,

$$\begin{aligned} n_s &= -\kappa_1 n - \kappa_2 |V_s|^2 + \lambda(n)c(\boldsymbol{x}, t), \\ n_g &= -\kappa_1 n - \kappa_2 |V_g|^2 + \lambda(n)c(\boldsymbol{x}, t), \end{aligned}$$

where $\lambda(n)$ describes how fast the locusts eat based on hunger, κ_1 is the energy lost due to metabolism, κ_2 is the energy lost due to movement, and $V_{s,g}$ are the advective velocities of the locusts.

6.1.3 System of equations

Our non-local flux and locust kinetics remain the same as in the previous iteration of the model, Sections 2.1.2 and 2.1.3, respectively. In addition, we use the previous scalings,

$$t = \frac{1}{\delta_2}\bar{t},\ \boldsymbol{x} = a_g\bar{\boldsymbol{x}},\ (\rho, s, g) = k_1(\bar{\rho}, \bar{s}, \bar{g}),\ \text{and } c = c_0\bar{c}.$$

Thus we update our equations from Chapter 2 to become

$$\frac{\partial g}{\partial t} + \nabla\cdot(g\boldsymbol{v}_g) + \frac{\partial}{\partial n}(gn_g) = D\nabla\cdot\left[f(n)e^{-c}\nabla g\right] - \frac{\delta}{1+\rho^2}g + \frac{(\rho k)^2 s}{1+(\rho k)^2}, \tag{6.9a}$$

$$\frac{\partial s}{\partial t} + \nabla\cdot(s\boldsymbol{v}_s) + \frac{\partial}{\partial n}(sn_s) = D\nabla\cdot\left[f(n)e^{-c}\nabla s\right] + \frac{\delta}{1+\rho^2}g - \frac{(\rho k)^2 s}{1+(\rho k)^2}, \tag{6.9b}$$

$$\frac{\partial c}{\partial t} = -c(\boldsymbol{x}, t)\int_0^1 \psi(n)(s(\boldsymbol{x}, n, t) + g(s(\boldsymbol{x}, n, t))dn, \tag{6.9c}$$

with

$$\boldsymbol{v}_g = -\nabla\left(\int_\Omega\left[R_g e^{\frac{-|\boldsymbol{x}-\boldsymbol{x'}|}{r_g}} - A_g e^{-|\boldsymbol{x}-\boldsymbol{x'}|}\right]\rho\left(\boldsymbol{x'}\right)d\boldsymbol{x'}\right) + Df(n)e^{-c}\left(\nabla c - \gamma\rho\nabla\rho\right),$$

$$\boldsymbol{v}_s = -\nabla\left(\int_\Omega R_s e^{\frac{-|\boldsymbol{x}-\boldsymbol{x'}|}{r_s}}\rho\left(\boldsymbol{x'}\right)d\boldsymbol{x'}\right) + Df(n)e^{-c}\left(\nabla c - \gamma\rho\nabla\rho\right),$$

and

$$n_s = -\kappa_1 n - \kappa_2 |V_s|^2 + \lambda(n)c(\boldsymbol{x}, t),$$
$$n_g = -\kappa_1 n - \kappa_2 |V_g|^2 + \lambda(n)c(\boldsymbol{x}, t),$$

where,Ω is our domain, $\lambda(n)$ describes how fast the locusts eat based on hunger, $\psi(n)$ is how fast food is consumed based on hunger, κ_1 is the energy lost due to metabolism and κ_2 is the energy lost due to movement.

6.1.4 Satisfaction

As we now model the hunger levels of the locusts, we can compare this between solitarious and gregarious locusts to get an alternate measure of foraging advantage. We begin by defining the instantaneous satisfaction at time t as S_g for gregarious locusts and S_s for solitarious, given by the average satiation as

$$S_g(t) = \frac{\int_0^1 \int_\Omega n g(\boldsymbol{x}, n, t)\, d\boldsymbol{x} dn}{\int_0^1 \int_\Omega g(\boldsymbol{x}, n, t)\, d\boldsymbol{x} dn}, \tag{6.10}$$

$$S_s(t) = \frac{\int_0^1 \int_\Omega n s(\boldsymbol{x}, n, t)\, d\boldsymbol{x} dn}{\int_0^1 \int_\Omega s(\boldsymbol{x}, n, t)\, d\boldsymbol{x} dn}. \tag{6.11}$$

We can then calculate the average net gregarious satisfaction over an interval $[0, T]$ as

$$S = \frac{1}{T} \int_0^T S_g(t) - S_s(t)\, dt. \tag{6.12}$$

Then if (6.12) is greater than 0 the gregarious locusts out forage their solitarious counterparts and vice versa if less than 0.

6.2 Analytic results

In this section we investigate the behaviour of our model with a spatially uniform and temporally constant food density. Similar to Chapter 4, this assumption corresponds to environments where the length scale of the food footprint is larger than the length scale over which the locusts are distributed, and where the rate of food consumption is negligible compared to the speed of locust interactions. This not only simplifies the analysis, but also provides a baseline with which to compare our later results, and hence assess the impact of a patchy food distribution.

By simply noting that (6.9a) differs from (2.26a) in that $D \to Df(n)$, we can quickly derive the results from Section 4.1 for our modified system of equations.

6.2.1 Density of gregarious groups

Again, under a few simplifying assumptions we estimate the maximum density and width of gregarious locusts at both the large and small mass limits in one dimension. To begin, our assumptions are c is constant and not depleting, there are minimal solitarious locusts present in the swarm (i.e. $\rho \approx g$), the effect of phase transitions in the swarm is negligible (i.e. $f_1(\rho)s = f_2(\rho)g = 0$), and all the locusts have the same level of hunger. Finally, we will label the support of an single aggregation of g as Ω. These assumptions give our large mass limit as,

$$||g||_\infty = \frac{3\left(-\left(R_g r_g - A_g\right) + \sqrt{\left(R_g r_g - A_g\right)^2 - \frac{4(Df(n)e^{-c})^2\gamma}{3}}\right)}{2Df(n)e^{-c}\gamma}, \qquad (6.13)$$

with support

$$||\Omega|| = \frac{2MDf(n)e^{-c}\gamma}{3\left(-\left(R_g r_g - A_g\right) + \sqrt{\left(R_g r_g - A_g\right)^2 - \frac{4(Df(n)e^{-c})^2\gamma}{3}}\right)}. \tag{6.14}$$

And the small mass limit as

$$||g||_\infty = \sqrt[3]{\frac{3M^2\left(A_g - \frac{R_g}{r_g}\right)}{4Df(n)e^{-c}\gamma}}, \tag{6.15}$$

and

$$||\Omega|| = B\left(\frac{2}{3}, \frac{1}{2}\right)\sqrt[3]{\frac{MDf(n)e^{-c}\gamma}{6\left(A_g - \frac{R_g}{r_g}\right)}}. \tag{6.16}$$

The accuracy of these approximations is illustrated by Figure 6.1. These results indicate that increasing hunger (corresponding to increasing $f(n)$) leads to a decreasing maximum group density and an increase in the size of the support. Similar to Section 4.1.1 the small mass limit overestimates the maximum density (and underestimates the support) due to ignoring the linear diffusion component of the equations.

6.2.2 Linear stability analysis

We again gain insights into the conditions under which groups can form by investigating the stability of spatially-homogeneous steady states. In this analysis we perturb the homogeneous steady states by adding a small amount of noise. We then find under what conditions the small perturbations grow and are likely to lead to gregarious aggregations. We begin by assuming that c does not deplete (i.e. $\psi(n) = 0$) and that all solitarious (gregarious) locusts are at the same level of hunger, m_s (m_g). We then rewrite equations (6.9b)

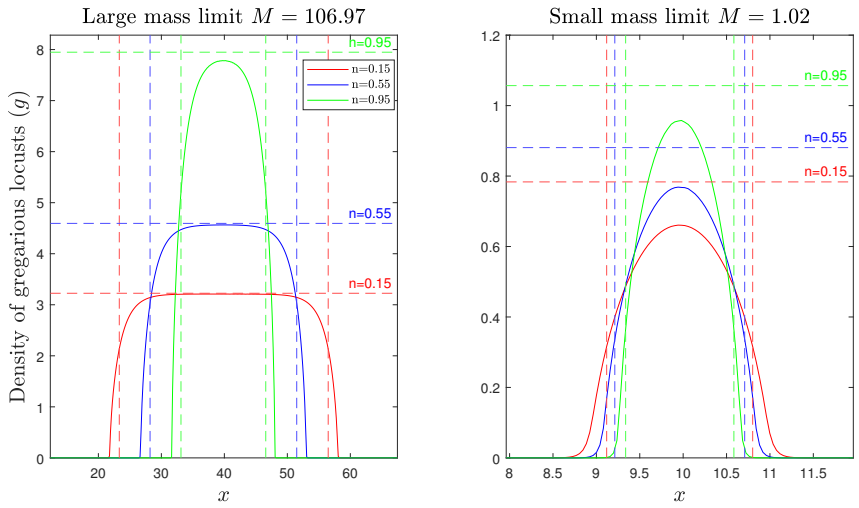

Figure 6.1: **Large and small mass limits with estimates for the max value and support.** The estimates of the max values are given by the horizontal dotted lines and the support given by the vertical dotted lines, with simulation results given by the solid lines. Each colour corresponds to a different value of n, with $n = 0.15, 0.55, 0.95$ given by red, blue, and green respectively. For both the simulation and calculations $D = 0.01$, $\gamma = 60$, $R_g = 0.25$, $r_g = 0.5$, $A_g = 1$, and $f(n) = (1.5 - n)$. We can see that decreasing n leads to a decrease in locust density and a corresponding increase in support size.

and (6.9a) in terms of the gregarious mass fraction (6.2), giving

$$\phi_g \frac{\partial \rho}{\partial t} + \phi_g \nabla \cdot (\boldsymbol{v}_g \rho) = \phi_g D \nabla \cdot \left[D f(m_g) e^{-c} \nabla \rho \right], \quad (6.17)$$

$$(1 - \phi_g) \frac{\partial \rho}{\partial t} + (1 - \phi_g) \nabla \cdot (\boldsymbol{v}_s \rho) = (1 - \phi_g) D \nabla \cdot \left[D f(m_s) e^{-c} \nabla \rho \right], \quad (6.18)$$

with

$$\boldsymbol{v}_{s,g} = -\nabla (Q_{s,g} * \rho) + D f(n_{s,g}) e^{-c} \left(\nabla c - \gamma \rho \nabla \rho \right).$$

We then perturb by letting $\rho = \bar{\rho} + \epsilon \tilde{\rho}$ where $\bar{\rho}$ is the homogeneous steady state and $\epsilon \tilde{\rho}$ is a small perturbation ($\epsilon \ll 1$). Substituting this into (6.17) and (6.18), removing terms of $\mathcal{O}(\epsilon^2)$, then adding (6.17) and (6.18) together

we find

$$\begin{aligned}\epsilon\frac{\partial\tilde{\rho}}{\partial t} &+ \nabla\cdot\left[\left(\phi_g\boldsymbol{v}_g + (1-\phi_g)\boldsymbol{v}_s\right)\epsilon\bar{\rho}\right] \\ &= D\nabla\cdot\left[\left(\phi_g Df(m_g)e^{-c} + (1-\phi_g)Df(m_s)e^{-c}\right)\epsilon\nabla\tilde{\rho}\right],\end{aligned}$$

with

$$\boldsymbol{v}_{s,g} = -(Q_{s,g} * \nabla\tilde{\rho}) - Df(n_{s,g})e^{-c}\gamma\nabla\left(\bar{\rho}\tilde{\rho}\right).$$

Next we take Fourier transforms in space and Laplace transforms in time of $\tilde{\rho}$, i.e. $\tilde{\rho} \propto e^{-ikx+\lambda t}$ to obtain

$$\begin{aligned}\epsilon\lambda\tilde{\rho} &+ \phi_g\left[k^2(\hat{Q}_g\tilde{\rho}) - Dk^2Df(m_g)e^{-c}\gamma\bar{\rho}\tilde{\rho}\right]\epsilon\bar{\rho} \\ &+ (1-\phi_g)\left[k^2(\hat{Q}_s\tilde{\rho}) - Dk^2Df(m_s)e^{-c}\gamma\bar{\rho}\tilde{\rho}\right]\epsilon\bar{\rho} \\ &= -Dk^2\left[\left(\phi_g Df(m_g)e^{-c} + (1-\phi_g)Df(m_g)e^{-c}\right)\epsilon\tilde{\rho}\right],\end{aligned}$$

where $\hat{Q}_{s,g}$ is the Fourier transform of $Q_{s,g}$. Then, dividing through by $\epsilon\tilde{\rho}$ we get

$$\begin{aligned}\lambda = &-\phi_g\left[k^2\hat{Q}_g - Dk^2Df(m_g)e^{-c}\gamma\bar{\rho}\right]\bar{\rho} \\ &-(1-\phi_g)\left[k^2\hat{Q}_s - Dk^2Df(m_s)e^{-c}\gamma\bar{\rho}\right]\bar{\rho} \\ &-Dk^2\left[\phi_g Df(m_g)e^{-c} + (1-\phi_g)Df(m_s)e^{-c}\right].\end{aligned}$$

If $\lambda > 0$ then small perturbations will grow in time, we can then find the condition for instability in terms of ϕ_g as

$$\phi_g > \phi_g^* = \frac{\hat{Q}_s + Df(m_s)e^{-c}\gamma\bar{\rho} + \frac{Df(m_s)e^{-c}}{\bar{\rho}}}{\hat{Q}_s - \hat{Q}_g + D\gamma e^{-c}\bar{\rho}(f(m_s)-f(m_g)) + \frac{De^{-c}}{\bar{\rho}}(f(m_s)-f(m_g))}. \tag{6.19}$$

The numerator is only in terms of m_s, thus as the hunger of solitarious locusts increases the gregarious mass fraction required for group formation increases.

This can be offset by the difference between solitarious and gregarious hunger, i.e. the gregarious mass fraction required for group formation reduces if gregarious locusts are less hungry than solitarious ones (i.e. $m_g > m_s$).

For our specific functions $Q_g = R_g e^{-\frac{|x|}{r_g}} - A_g e^{-|x|}$ and $Q_s = R_s e^{-\frac{|x|}{r_s}}$, we get,

$$\phi_g > \bar{\phi_g} = \frac{\frac{Df(m_s)e^{-c}}{\bar{\rho}} + Df(m_s)e^{-c}\bar{\rho}\gamma + 2R_s r_s}{2A_g - 2R_g r_g + 2R_s r_s + D\gamma e^{-c}\bar{\rho}(f(m_s) - f(m_g)) + \frac{De^{-c}}{\bar{\rho}}(f(m_s) - f(m_g))}. \tag{6.20}$$

We can then find the maximum locust density at which groups will form by taking (6.20) and substituting $\bar{\phi_g} = 1$ and solving for $\bar{\rho}$ as

$$\bar{\rho} = \frac{(A_g - R_g r_g) + \sqrt{(A_g - R_g r_g)^2 - (Df(m_g)e^{-\bar{c}})^2\gamma}}{Df(m_g)e^{-\bar{c}}\gamma} \approx \frac{2}{3}||g||_\infty, \tag{6.21}$$

where $||g||_\infty$ is maximum density for the large mass limit given in (6.13). Interestingly, while (6.19) depends on the hunger of solitarious locusts, (6.21) depends only on the hunger of the gregarious locusts.

6.2.3 Time until group formation with homogeneous locust densities

Next, we estimate time until group formation with homogeneous locust densities, constant hunger and constant food. By assuming that s and g are homogeneous we can ignore the spatial components of (6.9a) and (6.9b). We again denote the combined homogeneous locust density as $\bar{\rho}$ however now $\bar{\rho} = s(n,t) + g(n,t)$. Finally, assuming that $g(0) = 0$, we find the homogeneous density of gregarious locusts as a function of time is given by

$$g(t) = \frac{\bar{\rho} f_2(\bar{\rho})}{f_1(\bar{\rho}) + f_2(\bar{\rho})} \left(1 - e^{-[f_1(\bar{\rho}) + f_2(\bar{\rho})]t}\right),$$

which we then solve for t^* such that $g(t^*) = \bar{\phi_g}\bar{\rho}$, where $\bar{\phi_g}$ is given by (6.19). This gives an estimation for time of group formation (i.e. the time required for the homogeneous densities to become unstable) as,

$$t^* = \frac{-\ln\left(1 - \frac{\bar{\phi_g}(f_1(\bar{\rho})+f_2(\bar{\rho}))}{f_2(\bar{\rho})}\right)}{f_1(\bar{\rho}) + f_2(\bar{\rho})}. \tag{6.22}$$

Thus, as increasing hunger increases the gregarious mass fraction, $\bar{\phi_g}$, required for group formation it follows that it also increases the time required for group formation.

6.2.4 Conservation properties

Another aspect of the model we investigate is what properties of locust densities the model conserves. By construction our model preserves the mass of locusts, i.e. (6.1) is constant in time. In addition, using the same reasoning as Section 4.1.4, in $\mathbb{R}^n$, with all locusts having the same level of hunger, and with a constant food source ($c(\boldsymbol{x}, t)$ is constant in space and time), the center of mass is also preserved.

6.3 Numerical results

In this section we explore the effect of hunger and food distributions on gregarious group formation and look at the effect of food footprints on net gregarious satisfaction. We follow the experimental method outlined in Section 4.2 using the numerical method from Appendix A.1. As a summary we:

1. Initialise locust densities given by (4.19), with solitarious locusts being an ambient density, ρ_{amb} plus some normally distributed noise and gregarious locusts being initially absent. In addition, we distribution the locusts uniformly over hunger.

2. Initialise food distribution of a smoothed step function covering some percentage of the domain, ω, with mass F_m, given by (4.20).

3. Run each simulation to the time $t = 12.5$ and observe if group formation has occurred and measure the net gregarious satisfaction prior to group formation.

6.3.1 Parameter estimation

In the following experiments we use the symmetric parameters found in Table 4.1. In addition, we derive the metabolism parameters and give functional forms for $\lambda(n)$, $\psi(n)$, and $f(n)$.

Metabolism parameters. In order to estimate the gregarious metabolism parameters (the same technique applies to solitarious) we begin by writing the equations only in terms of hunger to obtain,

$$\frac{\partial g}{\partial t} + \frac{\partial}{\partial n}(g n_g) = 0,$$

with

$$n_g = -\kappa_1 n - \kappa_2 |V_g|^2 + \lambda(n) c(\boldsymbol{x}, t).$$

To begin we assume there is no movement or food consumption resulting in

$$\frac{\partial g}{\partial t} - \frac{\partial}{\partial n}(g \kappa_1 n) = 0,$$

which we can solve using the method of characteristics to find n in terms of t, given by

$$n(t) = n_0 e^{-\kappa_1 t},$$

where n_0 is our starting satiation. Then, if it takes some time, t_1^*, for the satiation level to go from $1 \to n_{\min}$, we can calculate κ_1 as

$$\kappa_1 = \frac{-\ln(n_{\min})}{t_1^*}. \tag{6.23}$$

Next we can solve the more complex problem involving energy lost due to movement. To start,

$$\frac{\partial g}{\partial t} - \frac{\partial}{\partial n}\left(g\left(\kappa_1 n + \kappa_2 |V_g|^2\right)\right) = 0.$$

Then by assuming that V_g is constant in time we can again use the method of characteristics to obtain,

$$n(t) = -\frac{\kappa_2}{\kappa_1}|V_g|^2 + \left(n_0 + \frac{\kappa_2}{\kappa_1}|V_g|^2\right) e^{-\kappa_1 t}.$$

Then, if it takes some time, t_2^*, travelling at a velocity V for the satiation level to go from $1 \to n_{\min}$, we can calculate κ_2 as

$$\kappa_2 = \frac{\kappa_1\left(n_{\min} - e^{-\kappa_1 t^*}\right)}{|V|^2\left(e^{-\kappa_1 t^*} - 1\right)}. \tag{6.24}$$

Finally we solve for our consumption of food (assuming constant food and no movement while eating),

$$\frac{\partial g}{\partial t} - \frac{\partial}{\partial n}\left(g\left(\kappa_1 n - \lambda(n)c\right)\right) = 0,$$

to find

$$\frac{dn}{dt} = \lambda(n)c - \kappa_1 n.$$

We then let $\lambda(n)$ be linear in n, i.e. $\lambda(n) = an + b$ giving

$$n(t) = \left(n_{\min} + \frac{bc}{ac - \kappa_1}\right) e^{-(ac-\kappa_1)t} - \frac{bc}{ac - \kappa_1}.$$

We then set $n_{\min} = \Delta n$ (the min value of n in the simulations), $t_1^* = 12.5$ (the length of the simulations), and $t_2^* = 2$. In addition we assume $V = 100$, then, from (6.23) and (6.24), we find

$$\kappa_1 = 0.1842,\ \kappa_2 = 3.5376 \times 10^{-5}.$$

We note that as $\kappa_1 \gg \kappa_2$ most of the change in satiation will be driven by metabolism.

Function selection For simplicity, we assume that all the relationships between hunger, feeding, and movement are linear. In addition we assume that a hungry locust consumes food twice as fast as a completely satiated one, and increases its level of locomotion by up to three times [72]. In addition we assume that our value for diffusion used in Chapter 4 is at $n = 0.5$. These assumptions give rise to the functions in Table 6.1.

Function	Description
$\lambda(n) = 2 - n$	The effect of locust feeding on satiation
$\psi(n) = 0.18(2 - n)$	The amount of food consumed based on locust hunger
$f(n) = 1.5 - n$	Change in the local component of movement based on locust hunger

Table 6.1: **Descriptions of arbitrary functions used in numerical simulations.**

6.3.2 The effect of food on group formation

Here, we perform the food footprint experiments from Section 4.2 to investigate how hunger affects our previous results. The food footprint ranges from covering 2.5% of the domain to 50% of the domain ($\omega = 2.5\%$ to $\omega = 50\%$). In addition, two food masses are tested, $F_M = 1.5$, 2, 2.5, and 3. As a control,

we also perform simulations with both no food present and a homogeneous food source, represented by $\omega = 0\%$ and $\omega = 100\%$ respectively, for each ambient locust density.

We vary the ambient locust density ranging from $\rho_{\text{amb}} = 0.8$ to $\rho_{\text{amb}} = 1.6$ (this is a larger range than Section 4.2). This range is selected based on (6.20) so that in the absence of food, group formation would not occur with a hungry population. In each simulation, the solitarious and gregarious populations very quickly tend to an almost smooth and symmetric distribution around the food, however a small quantity of noise persists across the population and this breaks the symmetry leading to group formation.

The results are shown in Figure 6.2. The plots show the peak gregarious density of the simulations for each of the varying food footprint sizes and ambient locust densities. In the blue regions there was no group formation, whilst in the green regions indicate successful group formation. Similar to Section 4.2, it can be seen in the plots that as the food mass is increased the minimum required locust density for group formation decreases. This effect is more pronounced within an optimal food width and this optimal width increases as the amount of food increases. In addition, the peak of the optimal width is more pronounce than in the model without hunger. However, in contrast to our results from Chapter 4 due to the increase in diffusion brought about by hunger no groups formed in the $F_m = 1.5$ experiment.

We investigate this lower bound by looking at a representative sample of simulations in Figure 6.3. In these simulations $\rho_{amb} = 1.125$ and $F_M = 3$, with food footprints $\omega = 15\%$ 17.5%, and 20% as well as with no food present. In the simulations in which food is present, prior to group formation gregarious locusts aggregate at the center of the food. If the food source is too narrow ($\omega = 15\%$, $t = 3$) there is an attempt at group formation but the gregarious mass is too small and the food source has not been sufficiently depleted so a large portion remains within the food source, thus the group does not persist. Alternatively, if the food width is not too narrow ($\omega =$

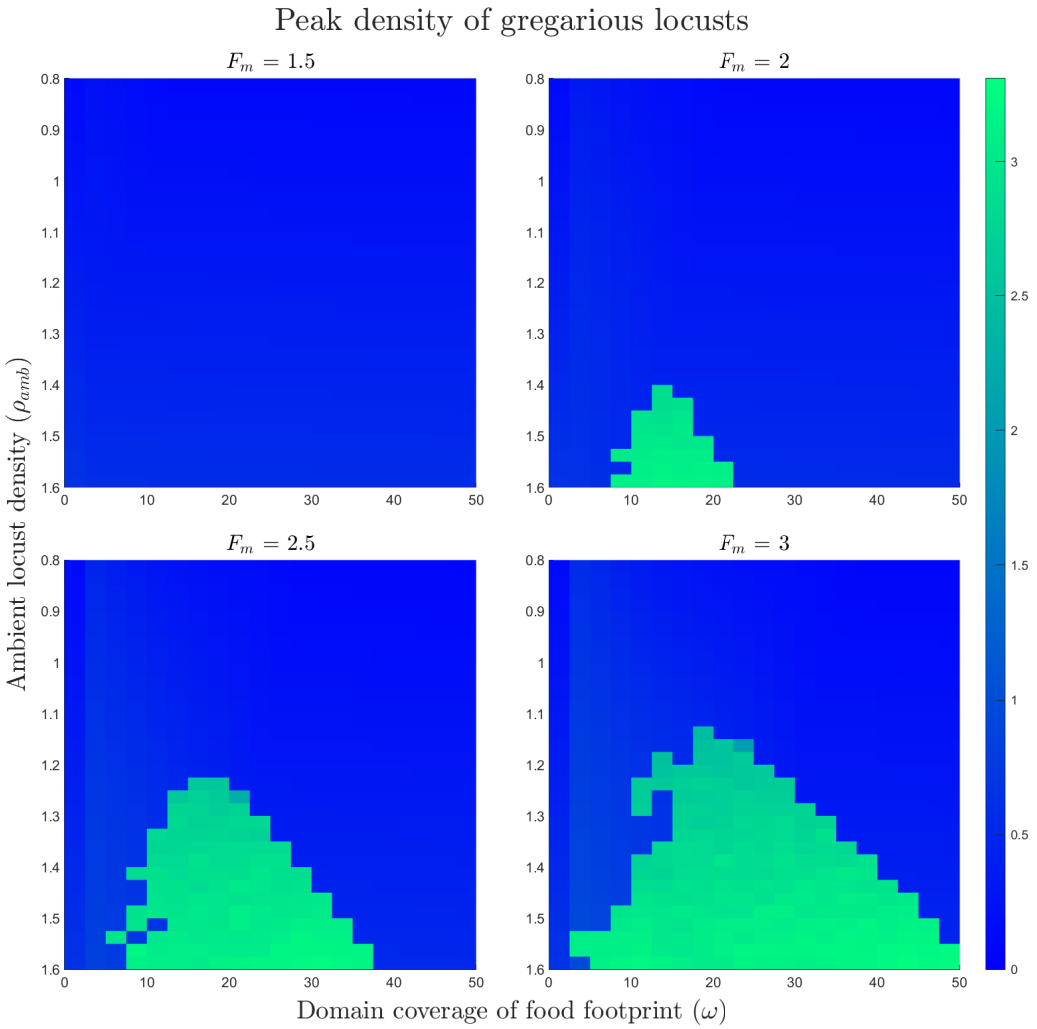

Figure 6.2: **Maximum gregarious locust density for symmetric gregarisation parameters with varying food footprint sizes and initial ambient locust densities.** For the simulations, $x = [0, 3/0.14]$ with periodic boundary conditions and $t = [0, 12.5]$. The initial condition for locust densities is given by (4.19) and food initial conditions are given by (4.20). Ambient locust density ranges from $\rho_{\text{amb}} = 0.8$ to $\rho_{\text{amb}} = 1.6$, food footprint ranges from $\omega = 0\%$ to $\omega = 50\%$, and food mass $F_M = 1.5$, 2, 2.5, and 3. Parameters are given in the symmetric parameter column in Table 4.1 and food functions given in Table 6.1. The plots show the maximum peak gregarious density for the varying food footprint sizes and ambient locust densities, in the blue regions there was no group formation and in the green regions there was successful group formation. From this we can deduce that food lowers the required locust density for group formation and this is more pronounced within an optimal food width.

17.5%) there is a successful group formed, this is seen as clump or aggregation of gregarious locusts in both the third and final plots. Once the aggregation has formed the gregarious locusts appear to move to the antipode of the food source, while interesting behaviour this is likely a mathematical artefact as gregarious aggregations engage in directed collective movement which we do not model here. Finally, if the food is too wide it is simply consumed. This is similar to our previously obtained results.

6.3.3 Net gregarious satisfaction

We then calculate the net gregarious satisfaction, prior to group formation and food depletion, for the previous simulations using (6.12). The results are shown in Figure 6.4. It can be seen that net gregarious satisfaction increases with decreasing food footprint and a decreasing ambient locust density. This supports the previous conclusion that in increasingly patchy environments gregarious locusts will out forage their solitarious counterparts.

6.4 Chapter summary

In this chapter we expanded our model of locust foraging to include hunger and its effects on locust movement. Through the use of numerical and analytic techniques we found that hunger acts to decrease the maximum density of locust groups and raises the percentage of the population that needs to be gregarious for group formation. In addition, many of the key results relating group formation and food from previous chapters persist. These include food lowering the required density for group formation around some optimal food width, and this optimal width being dependent on the amount of food present relative to the locust population. In the next Chapter we summarise our key findings and offer some avenues for further exploration.

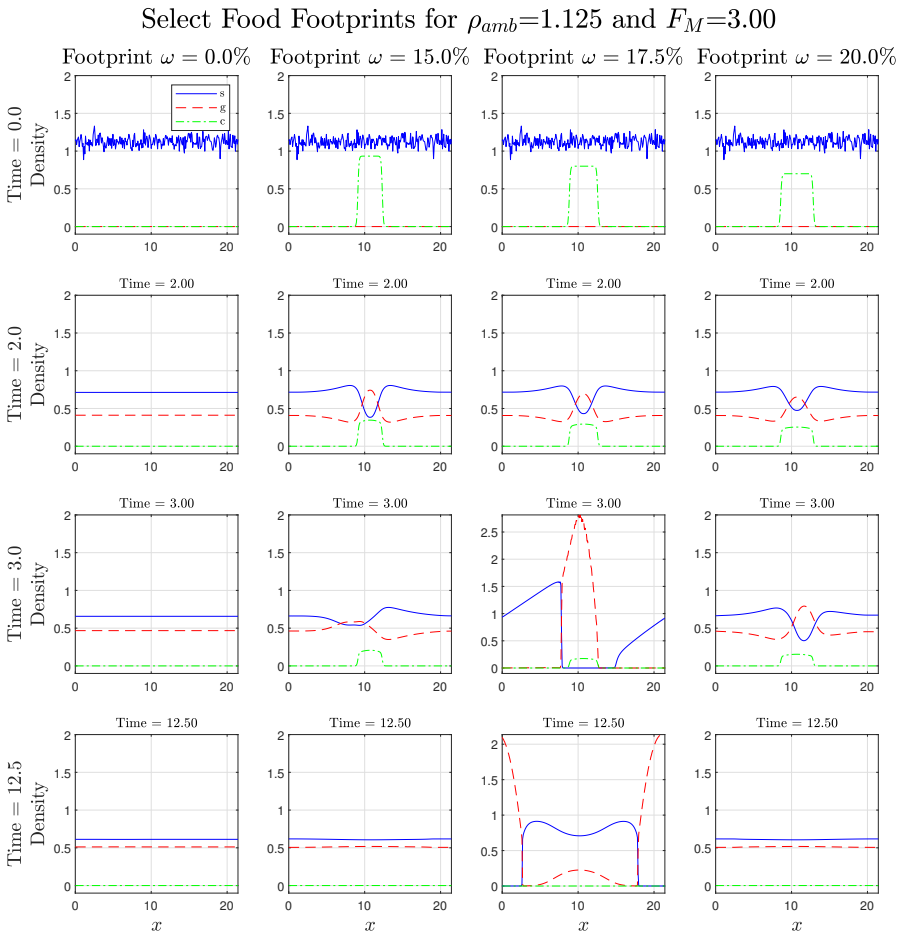

Figure 6.3: **A selection of plots showing the effect of food distribution on gregarisation and locust group formation.** In these simulations $\rho_{amb} = 1.125$ and $F_M = 3$ with $\omega = 15\%$ 17.5%, and 20% as well as with no food present (labelled $\omega = 0\%$). In the plots, blue is solitarious, red is gregarious, and green is food. If the food source is too narrow ($\omega = 15\%$, $t = 3$) there is an attempt at group formation but the gregarious mass is too small and the food source has not been sufficiently depleted so a large portion remains within the food source, thus the group does not persist. Alternatively, if the food width is not too narrow ($\omega = 17.5\%$) there is a successful group formed, this is seen as clump or aggregation of gregarious locusts in both the third and final plots. Finally, if the food is too wide it is simply consumed.

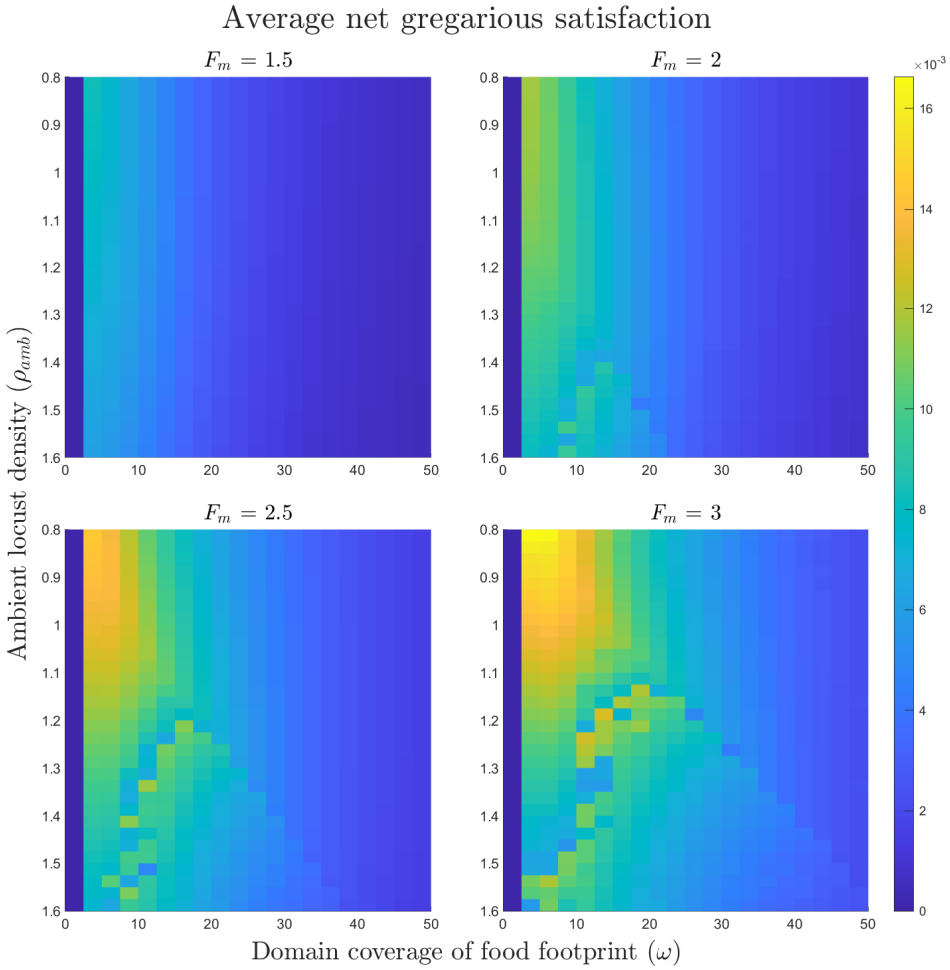

Figure 6.4: **Average net gregarious satisfaction prior to group formation, S given by** (6.12)**, for symmetric gregarisation parameters with varying food footprint sizes and initial ambient locust densities.** The plots show the average net gregarious satisfaction prior to group formation. It can be seen that net gregarious satisfaction increases with decreasing food footprint and a decreasing ambient locust density.

Chapter 7

Summary and discussions of locust foraging

Locusts continue to be a global threat to agriculture and food security, and so insights into the hopper band formation process that can help predict and control outbreaks is of great importance. In addition, while research is getting closer to unravelling the mystery of density dependent phase polyphenism, there is still an important question of what advantages it offers [4, 6, 87]. For general group living in animals [58] or specifically gregarious behaviour in insects [40, 84, 101] there exists a variety of analyses into the costs and benefits. However, there are limited explanations within the context of density dependent phase polyphenism [1, 4, 48, 74]. A relatively new area of exploration is around the advantages and disadvantages gregarisation offers in terms of foraging.

To begin, in Chapter 2 we presented a continuum model that includes non-local and local inter-individual interactions and interactions with food resources. This model extends the model of Topaz et. al. 2012 [98] for locust gregarisation to include food interactions and local repulsion. Next, in Chapter 3 we introduced and analysed two finite volume based numerical schemes that we used throughout the thesis. Then, in Chapter 4, we

analysed and simulated our new model finding that food acts to: increase maximum locust density, lower the gregarious fraction required for group formation (an important precursor to locust hopper bands), and decreases both the required density and time for group formation with this effect being more pronounced at some optimal food width. In addition, by looking at the relative foraging advantage of gregarious locusts in our simulations we found that as the gregarious mass fraction increases so too does the foraging advantage of being gregarious. This effect is increased by the mass of food present but is diminished by the size of the food footprint to the point where no advantage is offered with a homogeneous food source.

Then in Chapter 5, through a series of numerical experiments, we further found that prior to mass aggregations, in increasingly heterogeneous food environments it is better to be gregarious than solitarious. However, once an aggregation is fully formed this advantage can be quickly lost, highlighting the need to evolve a migration/collective movement mechanism for the gregarious phase to remain viable over time. In addition, the advantage is also lost in homogeneous environments. Finally, through the parameter sensitivity analysis, we showed for the first time that the foraging advantage is intrinsic to the solitarious/gregarious behavioural dynamic as it occurs almost regardless of the parameters selected. Our study, in line with previous studies about solitary and social foraging in complex environments and Ellis and Ashall observations [36], show the advantages the gregarisation offers in terms of foraging.

However, in order to keep the model computationally tractable we have had to make a variety of simplifying assumptions, which does impose a limit on the direct biological relevance at present. While our model is most applicable in the stage prior to hopper band formation and does not properly capture the movement of hopper bands, these results presented can give guidance on how higher order models might behave [20, 21]. With this in mind, there are many ways that the model could be further developed to see if this

relationship between gregarisation and foraging persists. One example that we explored in Chapter 6 was having locust behaviour dependent on hunger [34]. Other possibilities are the inclusion of a heterogeneous age structure and differing local locust-locust and locust-food interactions between solitarious and gregarious populations. Another technique to consider is using a higher order model that is able to capture collective movement mechanisms such as alignment or pursuit/escape interactions [75]. If the foraging relationship does persist with these introduced complexities, the next step would be to create an evolutionary model and investigate if it is enough to drive the evolution of density dependent phase polyphenism. If this is the case, we hypothesise that environments with highly oscillatory food sources (i.e. frequent switching between abundance and scarcity) would be the most likely for density dependent phase polyphenism to develop.

Finally, preventative methods are the key to improving locust control. This includes the ability to predict mass gregarisation according to resource distribution patterns so that the area searched for locusts is reduced and control efforts are deployed in high risk areas early on [93]. Further exploration of our results has the potential to improve predictive gregarisation models and early detection efforts by further increasing our understanding of the link between gregarisation and vegetation (resource) distribution (the latter becoming increasingly easy to quantify during field surveys, and aerial surveys including drones and satellite imagery [29, 32]). Future research could focus on developing decision support systems integrating predictive gregarisation models and GIS data from surveys.

Appendix A

Implementing numerical schemes in MATLAB

The purpose of this appendix is to give an overview of the numerical schemes implementation in MATLAB that hopefully proves useful to the reader. We begin with a vectorised implementation used in Chapter 6 before showing a 2D GPU implementation of the scheme introduced in Section 3.2 and used in Chapter 5.

In each section we divide the code up into setup, space, and time with notes and comments presented on each code snippet.

A.1 One dimension

We will begin with code for one spatial dimension and one hunger dimension.

A.1.1 Initial setup

Before simulating our system of equations we must setup all our constants, social potential, etc. as well as the constraints of the simulation such as time-frame to simulate, spatial resolution, time sample points. To make terms easier to keep track of we utilise MATLAB structures, these can be initialised in the same way as variables but with the addition of a .subvariable. For example we begin by initialising the timeframe to simulate, `tmax`, spatial resolution (keep as some 2^n for ffts to work properly), `X`, hunger resolution, `N`, boundary conditions, and time sample points and storing them in a structure

called `etc`.

```
etc.tmax = 10;
etc.X=256; %Number of spatial points
etc.N=10; %Number of hunger points

tsamplepow = 2;
tpow = nthroot(etc.tmax,tsamplepow);
t = [0:tpow/500:tpow];
etc.t = t.^tsamplepow;
```

Here, we have used a trick to do non-linear time sampling as many simulations have greater activity at the start. Next, we initialise our food related variables and functions and store them in a structure called `food`,

```
%HUNGER AND EATING
%Eating Functions
food.lambda = @(n) 1*max(2-n,0); % Eating function of locusts
food.gamma = @(n) 2*0.18*max(2-n,0); % Being eaten function of
    ↪ food
food.velocity = @(n) max(1.5-n,0); %function affecting local
    ↪ interactions
food.var = [0.1842 0.00003576]; %metabolism variables kappa1
    ↪ and kappa2
```

This shows that structures can also be used to store anonymous functions (functions not saved in a file). Next we initialise and store locust kinetics functions and variables in a `kinetics` structure,

```
%KINETICS
%Kinetic varables [delta1 delta2 densityk1 densityk2]
kinetics.var = [1 1 1 1/0.681];
kinetics.f1 = @(p) kinetics.var(1)./(1+(p/kinetics.var(3)).^2);
kinetics.f2 = @(p) kinetics.var(2)*(p*1/kinetics.var(4)).^2./(1+(p
    ↪ *1/kinetics.var(4)).^2);
```

before finally storing variables around locust movement in a structure called `move`,

```
%MOVEMENT VARIABLES
move.velocity = [1 431.87]; %advective component [c0 gamma]
move.diffusion = [2.041 2.041]; %diffusion coefficients [Ds Dg]
move.Rs = 1063.5; move.rs = 1; %Coefficients of Qs
```

```
move.Rg = 940.5; move.Ag=2008.7; move.rg=0.2857; move.ag=1; %
    ↪ Coefficients of Qg
```

We then create our spatial and hunger sample points (stored in the `etc` structure), and initialise DFT $\left\{-\frac{\partial}{\partial x}e^{-\frac{|x|}{r}}\right\}$, using the DFT derived by [98] (stored in the `move` structure),

```
xmax = 3/0.14;
%This section creates Del Qs,g
etc.dx = xmax/(etc.X-1);
etc.x = (0:etc.dx:xmax)';
etc.dn = 1/(etc.N);
etc.n= 0:etc.dn:1-etc.dn;

k = (2*pi/xmax*[0:etc.X/2-1, 0, -etc.X/2+1:-1])';
move.Qsfft = (-sqrt(-1)*move.Rs/move.rs*etc.dx).*sin(etc.dx*k)./(
    ↪ cosh(etc.dx/move.rs)-cos(etc.dx*k));
move.Qgfft = (-sqrt(-1)*move.Rg/move.rg*etc.dx).*sin(etc.dx*k)./(
    ↪ cosh(etc.dx/move.rg)-cos(etc.dx*k))-...
(-sqrt(-1)*move.Ag/move.ag*etc.dx).*sin(etc.dx*k)./(cosh(etc.dx/
    ↪ move.ag)-cos(etc.dx*k));
```

Finally we setup the initial conditions for s, g, and c as well as pointers for easier handling of variables,

```
%Setup initial conditions and pointers
y0 = zeros(1,2*etc.X*etc.N+etc.X);
pointers.slook = zeros(etc.X,etc.N);
pointers.glook = zeros(etc.X,etc.N);
pointers.clook = (2*etc.X*etc.N+1:2*etc.X*etc.N+etc.X)';

epsilon = 7;
footprint = xmax*omega/100;

FoodMass = Fm;

if footprint == 0
    c0 = zeros(etc.X,1);
elseif omega == 100
    c0 = ones(etc.X,1)*FoodMass/(2*footprint);
else
```

```
    c0 = FoodMass/(2*footprint)*(tanh(epsilon*(etc.x-(xmax/2-0.5*
        ↪ footprint)))...
    -tanh(epsilon*(etc.x-(xmax/2+0.5*footprint))));
end

y0(pointers.clook) = c0;

%Initial conditions
for i =1:etc.X
    for j=1:etc.N
        y0((i-1)*etc.N+j) = rho0/16.6*InitialS(i);
        y0(etc.X*etc.N+(i-1)*etc.N+j) = 0;

        pointers.slook(i,j) = (i-1)*etc.N+j;
        pointers.glook(i,j) = etc.X*etc.N+(i-1)*etc.N+j;
    end
end

pointers.pv = [2:etc.X 1]; pointers.mv = [etc.X 1:etc.X-1];
```

What are pointers and why use them? Pointers are basically a way of converting one set of coordinates into another, in this code we use them to keep track of indexes and allow us to embed multiple multidimensional arrays into a single one dimensional vector. For an example, if we were looking for $S_{(3,7)}$ we would look at `pnt.slook(3,7)` and that would give (for example) `268` telling us that $S_{(3,7)}$ is the 268^{th} entry in our one dimensional array. This in turn allows us to use the vector calculations instead of `for` loops to drastically speed up calculations. In addition, we use the pointers `pnt.pv` and `pnt.mv` to calculate fluxes at the positive and negative cell boundaries, respectively.

A.1.2 Spatial calculations

Here we create a function called `SpaceLocusts` that takes all our previously defined structures as inputs (`kinetics`, `move`, `food`, and `pnt`) as well as a vector, `tin`, containing the values at every grid cell. Then, the steps for the spatial calculations are:

1. Initialise output
2. Calculate locust kinetics

3. Calculate advective component
4. Calculate diffusion
5. Calculate flux due to metabolism and feeding

We begin by initialising the output vector and calculating the total density at each spatial grid cell,

```
function [tout] = SpaceLocusts(tin, kinetics, move, food, etc, pnt)
%FFTFVM Perform a single time step of locust model
%CODE STARTS HERE
% initalise output array
tout = zeros(size(tin));
%find total poopulation, the sum removes the hunger component
p = tin(pnt.slook)+tin(pnt.glook);
pflat = squeeze(sum(p,2)).*etc.dn;
```

Next, we calculate the locust kinetics using `f1` and `f2` in our `kinetics` structure, the `repmat` command takes the 1D `F1` and `F2` vectors copies them into the hunger dimension, this allows us to do an element-wise multiplication,

```
%KINETICS
%Calculate locust kinetics
F1 = kinetics.f1(pflat);
F2 = kinetics.f2(pflat);
%Change due to kinetics
tout(pnt.slook) = -tin(pnt.slook).*repmat(F2,1,etc.N)+tin(pnt.glook ).*repmat(F1,1,etc.N);
tout(pnt.glook) = tin(pnt.slook).*repmat(F2,1,etc.N)-tin(pnt.glook) .*repmat(F1,1,etc.N);
```

Next we find the fast Fourier transform of our density `pflat` and find the nonlocal and local components of our advective movement,

```
%ADVECTIVE VELOCITY CALCULATIONS
pfft = fft(pflat);
%Perform convolution operation and inverse fourier transform
VQs = real(ifft(pfft.*move.Qsfft));
VQg = real(ifft(pfft.*move.Qgfft));
```

```
%Find nonlinear diffusion component, this uses central
    ↪ difference for non
%boundary cells and left and right side approximations at
    ↪ the boundary
Ec = move.diffusion(1)*exp(-tin(pnt.clook))*food.velocity(etc.dn
    ↪ *([1:etc.N]-0.5));
W = Ec.*(1/(2*etc.dx)).*repmat( (tin(pnt.clook(pnt.pv))-tin(pnt.
    ↪ clook(pnt.mv))...
-move.velocity(2)*pflat.*(pflat(pnt.pv)-pflat(pnt.mv))), 1, etc.N )
    ↪ ;
```

Using this we calculate the flux at the cell boundaries due to advective movement

```
%Calculate Flux due to movement
Ks = (repmat(VQs,1,etc.N)+W).*tin(pnt.slook);
Kg = (repmat(VQg,1,etc.N)+W).*tin(pnt.glook);

%Set boundary fluxes
Ks(1,:)=(Ks(1,:)>0).*Ks(1,:); Ks(end,:)=(Ks(end,:)<0).*Ks(end,:);
Kg(1,:)=(Kg(1,:)>0).*Kg(1,:); Kg(end,:)=(Kg(end,:)<0).*Kg(end,:);
```

We then calculate our flux due to linear diffusion,

```
%calculate diffusion
ep = move.diffusion(1)*exp(-((tin(pnt.clook(pnt.pv))+tin(pnt.clook)
    ↪ )/(2*move.velocity(1))))*food.velocity(etc.dn*([1:etc.N]-0.5)
    ↪ );
em = move.diffusion(1)*exp(-((tin(pnt.clook)+tin(pnt.clook(pnt.mv))
    ↪ )/(2*move.velocity(1))))*food.velocity(etc.dn*([1:etc.N]-0.5)
    ↪ );
```

We can then finally calculate the change in each cell due to movement,

```
%linearised riemann approximation at cell boundaries
%Calculate wave size at cell boundaries
Wgm = sign(tin(pnt.glook)-tin(pnt.glook(pnt.mv,:)));
Wsm = sign(tin(pnt.slook)-tin(pnt.slook(pnt.mv,:)));
%Calculate wave speed
Sgm = (Kg-Kg(pnt.mv,:)).*Wgm;
Ssm = (Ks-Ks(pnt.mv,:)).*Wsm;

% Calculate the change due to movement and
```

```
tout(pnt.slook) =tout(pnt.slook)-(1/etc.dx)*(max(Ssm,0).*Wsm+min(
    ↪ Ssm(pnt.pv,:),0).*Wsm(pnt.pv,:)...
+1/etc.dx*(em.*(tin(pnt.slook)-tin(pnt.slook(pnt.mv,:)))...
-ep.*(tin(pnt.slook(pnt.pv,:))-tin(pnt.slook))));
tout(pnt.glook) =tout(pnt.glook)-(1/etc.dx)*(max(Sgm,0).*Wgm+min(
    ↪ Sgm(pnt.pv,:),0).*Wgm(pnt.pv,:)...
+1/etc.dx*(em.*(tin(pnt.glook)-tin(pnt.glook(pnt.mv,:)))...
-ep.*(tin(pnt.glook(pnt.pv,:))-tin(pnt.glook))));
```

Finally we calculate the change in each cell due to metabolism and eating,

```
%HUNGER AND FOOD CALCULATIONS
%Change in hunger calculated at the hunger boundry of cells
Ns = -food.var(1)*repmat(etc.dn*([1:etc.N]-1),etc.X,1)-food.var(2)*
    ↪ abs(Ks).^2+tin(pnt.clook)*food.lambda(etc.dn*([1:etc.N]-1));
Ng = -food.var(1)*repmat(etc.dn*([1:etc.N]-1),etc.X,1)-food.var(2)*
    ↪ abs(Ks).^2+tin(pnt.clook)*food.lambda(etc.dn*([1:etc.N]-1));

%Change in food due to feeding
Cs = sum(etc.dn*p.*repmat(food.gamma(etc.dn*([1:etc.N]-1)),etc.X,1)
    ↪ ,2);
%Flux due to hunger/feeding
sFmh = [tin(pnt.slook).*min(Ns,0)+tin(pnt.slook(:,[1 1:etc.N-1])).*
    ↪ max(Ns,0) zeros(etc.X,1)];
gFmh = [tin(pnt.glook).*min(Ng,0)+tin(pnt.glook(:,[1 1:etc.N-1])).*
    ↪ max(Ng,0) zeros(etc.X,1)];

sFmh(:,1) = 0; gFmh(:,1) = 0; %No flux boundaries

%Change due to Feeding and hunger
tout(pnt.slook) = tout(pnt.slook)-1/(etc.dn)*(-sFmh(:,1:etc.N)+sFmh
    ↪ (:,2:etc.N+1)); %Flux due to metabolism
tout(pnt.glook) = tout(pnt.glook)-1/(etc.dn)*(-gFmh(:,1:etc.N)+gFmh
    ↪ (:,2:etc.N+1));
tout(pnt.clook) = -tin(pnt.clook).*Cs; %Calculate the change in
    ↪ c
end
```

Now that we have our space component handled we can move onto time.

A.1.3 Time

As we have written our code so that the results of the space component are saved in a 1-D vector, we can use MATLABs inbuilt function `ode45`.

```
[t,y] =ode45(@(t,y) SpaceLocusts(y, kinetics, move, food, etc,
    ↪ pointers), etc.t, y0);
```

A.2 Two dimensions on GPU

The code here corresponds to the numerical scheme from Section 3.2, there are some limitations in that the social potential of all populations need to be the same. However, it is written in such a way that the addition of extra populations is as simple as adding an extra row and column to the `ATTR` and `REP` matrices and defining a new kinetics function.

A.2.1 Initial setup

We begin by defining our strength of attraction and repulsion, in this case we let solitarious locusts be population u_1 and gregarious be population u_2. The software is setup so we can have asymmetric attraction/repulsion, so `ATTR(2,1)` is the strength of attraction between gregarious locusts and solitarious locusts, and `ATTR(2,2)` is the strength of attraction between gregarious locusts and gregarious locusts (for solitarious negative `ATTR` is repulsion). The `REP` vector is the magnitude of γ, this allows for different values of γ for different populations. `KIN` are our kinetics terms, `D` is the linear diffusion coefficient, `POW` is the power of the nonlinear diffusion term. We then initialise the timeframe to simulate, `tmax`, spatial resolution (keep as some 2^n for ffts to work properly), `X`, boundary conditions, time sample points, and initialising a representation of the spatial grid.

```
ATTR = [-10 -10; 10 10];
REP = [10 10];
KIN = [0.5 1];
D=0.2; % Diffusion coefficent
POW=2; % Power of nonlinear diffusion

Us = unique(size(ATTR));
```

```
X = 64; %number of grid squares in each direction
xmax = 10; %Grid size 0->10
tmax = 5; %Time to run simulation to

tsamplepow = 1;
tpow = nthroot(tmax,tsamplepow);
t = 0:tpow/(200-1):tpow;
t = t.^tsamplepow; %Time sample points

%Setups cell coordinates
dx = xmax/(X-1);
x = 0:dx:xmax;
y = 0:dx:xmax;

xt = (-X/2:X/2-1)*dx;
yt = (-X/2:X/2-1)'*dx;
```

Next, we setup our social potential on the domain $\Omega' = [-\frac{L}{2}, \frac{L}{2}] \times [-\frac{L}{2}, \frac{L}{2}]$ and then shift it to be periodic on the domain $\Omega = [0, L] \times [0, L]$ for ffts. This is the most natural way to define the social potential as the user gives the function as its defined.

```
rs=1;
Q = -circshift(circshift(exp(-sqrt(xt.^2+yt.^2)/rs),X/2,1),X/2,2);
Qfft = gpuArray(dx^2*fft2(Q));
Q=repmat(Q,1,1,Us);
```

This loads the food distribution and precalculates De^{-c}

```
load('initFood.mat');
hrn = hrn/max(abs(hrn),[],'all');
Normval = max(abs(1+hrn),[],'all');
FOOD = max(1+alpha*hrn,0)/Normval;

DIFF = D*exp(-FOOD);

if alpha ==-1
    DIFF = D*exp(-FOOD*0);
end

DIFF = repmat(DIFF,1,1,Us);
DIFF =permute(DIFF ,[3,1,2]);
```

Finally, we define the initial conditions for s, g

```
%Initial conditions
u0 = zeros(Us,X,X);
u0(1,:,:) =rho + rho/100*rand(64,64);
```

Next, as we are using a GPU we cant use inbuilt time integration functions (like `ode45`) so we construct a new function to run the whole simulation. This function begins by setting up a series of gpu arrays for use later as well as a ndgrid. We give some forwarning, a few of the arrays get reused at multiple points as GPUs tend to have limited memory (compared to CPUs) and 2D problems require X^2 grid points and can quickly use large amounts of memory.

```
function [tout,u] = FVMRK4GPU(t, u0, Q, ATTR, REP, POW, DIFF, FUNC,
    ↪ dx)
recstep = max(size(t));
dt = 0.5*dx^2; %Starting timestep
ndt = dt; %Next time step
ermax = 10^-5; %Max error
dtmax = dx/4; %Maximum timestep
dtmin = 16*eps; %minimum timestep
usize = size(u0);

%initialise GPU arrays
u = zeros([recstep, size(u0)]);
tempNL = gpuArray(zeros(size(u0)));
tempL = gpuArray(zeros(size(u0)));
tempComplex = permute(complex(gpuArray(zeros(size(u0)))),[2,3,1]);
vxm = gpuArray(zeros(size(u0)));
vym = gpuArray(zeros(size(u0)));
rho = gpuArray(zeros(usize(2:3)));
tout = gpuArray(zeros(recstep, 1));
tout(1) = t(1);

%Real indexes
[ugrid, xgrid, ygrid] = ndgrid(gpuArray.colon(1, usize(1)),gpuArray
    ↪ .colon(1, usize(2)),gpuArray.colon(1, usize(3)));

ct = t(1);
```

```
tcounter = 2;

finished = false;

unext = gpuArray(u0);
u(1,:,:,:) = gather(u0);
```

We now move on to the spatial component.

A.2.2 Spatial calculations

We begin by setting up some functions to perform operations on a single grid cell, we then couple this with the `arrayfun` command to get the speed boost of a GPU. We do take advantage of global variables, it may be considered not the best practice and it may get a little confusing, but it worked well for our purpose. We begin with a function to calculate the non local component, with `tempNL` currently containing the densities of each type of locust, we output the sum of the non-local interactions

$$\sum_{k=1}^{N} S_{i,k} u_k$$

```
% SETUP FUNCTIONS
%Calculate the nonlocal component
function out = nonLocal(ui,xi,yi)
    out = 0;
    for i=1:usize(1)
        out = out+ATTR(ui,i)*tempNL(i,xi,yi);
    end
end
```

We then calculate the nonlinear diffusion, here `rho` contains ρ^m,

```
function out = Local(ui,xi,yi)
    out = REP(ui)*rho(xi,yi);
end
```

This function calculates the flux through the negative x boundary of the cell, at this point `tempNL` contains the value from the full convolution, `tempL` contains the local repulsion.

```
%Calculate the velocuty at the x cell boundry i-1/2
function out = velBoundX(ui,xi,yi)
    xm = xi-1;
    xm = (xm<1)*usize(2)+xm;

    out = -1/dx*( tempNL(ui,xi,yi)-tempNL(ui,xm,yi)...
    +(DIFF(ui,xi,yi)+DIFF(ui,xm,yi))/2*(tempL(ui,xi,yi)-tempL(ui,xm,
        ↪ yi)) );
end
```

This function calculates the flux through the negative y boundary of the cell,

```
%Calculate the velocuty at the y cell boundry i-1/2
function out = velBoundY(ui,xi,yi)
    ym = yi-1;
    ym = (ym<1)*usize(3)+ym;

    out = -1/dx*(tempNL(ui,xi,yi)-tempNL(ui,xi,ym)...
    +(DIFF(ui,xi,yi)+DIFF(ui,xi,ym))/2*(tempL(ui,xi,yi)-tempL(ui,xi,
        ↪ ym)) );
end
```

We can then calculate the to total change due the advective terms,

```
%Calculate the advection component
function out = advection(ui,xi,yi)
    %setup pointers
    xm = xi-1; xm = (xm<1)*usize(2)+xm;
    ym = yi-1; ym = (ym<1)*usize(3)+ym;
    xp = xi+1; xp = (xp>usize(2))*(-usize(2))+xp;
    yp = yi+1; yp = (yp>usize(3))*(-usize(3))+yp;

    %Calculate flux at cell boundries
    if (vxm(ui,xi,yi)<0), uxm = (unext(ui,xi,yi)); else, uxm = (
        ↪ unext(ui,xm,yi)); end
    if (vxm(ui,xp,yi)<0), uxp = (unext(ui,xp,yi)); else, uxp = (
        ↪ unext(ui,xi,yi)); end
    if (vym(ui,xi,yi)<0), uym = (unext(ui,xi,yi)); else, uym = (
        ↪ unext(ui,xi,ym)); end
    if (vym(ui,xi,yp)<0), uyp = (unext(ui,xi,yp)); else, uyp = (
        ↪ unext(ui,xi,yi)); end
```

```
    %Calculate total flux
    out = -1/dx*(uxp*vxm(ui,xp,yi)-uxm*vxm(ui,xi,yi)+...
    uyp*vym(ui,xi,yp)-uym*vym(ui,xi,yi));
end
```

We then calculate the diffusion terms,

```
%Calculate the diffusion component
function out = diffusion(ui,xi,yi)
    %setup pointers
    xm = xi-1; xm = (xm<1)*usize(2)+xm;
    ym = yi-1; ym = (ym<1)*usize(3)+ym;
    xp = xi+1; xp = (xp>usize(2))*(-usize(2))+xp;
    yp = yi+1; yp = (yp>usize(3))*(-usize(3))+yp;

    out = -1/(dx^2)*(4*DIFF(ui,xi,yi)*unext(ui,xi,yi)-DIFF(ui,xp,yi)
        ↪ *unext(ui,xp,yi)-DIFF(ui,xm,yi)*unext(ui,xm,yi)...
    -DIFF(ui,xi,yp)*unext(ui,xi,yp)-DIFF(ui,xi,ym)*unext(ui,xi,ym));
end
```

Finally, we calculate kinetics, `F1` and `F2` contain the outputs of $f_1(\rho)$ and $f_2(\rho)$ respectively (If you wanted to implement more populations it is this code you would have to edit).

```
%Calculate kinetics
function out = kinetics(ui,xi,yi)
    out = -F1(xi,yi)*unext(2,xi,yi)+F2(xi,yi)*unext(1,xi,yi);
    if ui == 1
        out = -out;
    end
end
```

As all our functions have been defined we can define a function to run a single timestep,

```
%Run a single step
function out = runStep()
    rho = squeeze(sum(unext,1)); %Calculate Rho
    F1 = KIN(1)./(1+rho.^2);
    F2 = (rho*KIN(2)).^2./(1+(rho*KIN(2)).^2);
```

```
    %Find LHS of convolution
    tempNL = unext;
    tempNL = arrayfun(@nonLocal, ugrid, xgrid, ygrid);

    tempComplex = fft2( permute(tempNL ,[2,3,1]) );
    tempNL = permute(real( ifft2(Q.*tempComplex) ),[3,1,2]); %
        ↪ Calculate the nonlocal convolutions

    rho = rho.^POW; %Caculate rho for the nonlinear local
        ↪ repulsion
    tempL = arrayfun(@Local, ugrid, xgrid, ygrid); %Calculate the
        ↪ local repulsion

    vxm = arrayfun(@velBoundX, ugrid, xgrid, ygrid); %calculate x
        ↪ velocity component
    vym = arrayfun(@velBoundY, ugrid, xgrid, ygrid); %calculate y
        ↪ velocity component

    %Calculate total flux
    out = arrayfun(@advection, ugrid, xgrid, ygrid)...
    +arrayfun(@diffusion, ugrid, xgrid, ygrid)...
    +arrayfun(@kinetics, ugrid, xgrid, ygrid);
end
```

Now that we have our spatial component covered we can move on to time.

A.2.3 Time

As we many of the inbuilt MATLAB functions for time integration do not support GPU arrays we have constructed our own. We went with a different numerical scheme to the more common Dormand-Prince method [35] found in `ode45` to minimise the number of arrays existing at any one point in time. This first code snippet calculates two time steps and the estimates the error using the method outlined in Section 3.2. We store the error in the array `Err`, `Vt` is used for calculating the substeps, while `Vtt` stores the total timestep.

```
while(~finished)
    accept = false;
    step = false;
    while(~accept)
```

```
    if(~step)
        uss = unext;
    end

    us = unext;

    %f0 f4
    Vt = runStep();
    Vtt = Vt;
    unext = us+dt/2*Vt;
    if(~step)
    else
        Err = Err-2*Vt;
    end

    %f1 f5
    Vt = runStep();
    Vtt = Vtt+2*Vt;
    unext = us+dt/2*Vt;
    if(~step)
        Err = -Vt;
    else
        Err = Err+3*Vt;
    end

    %f2 f6
    Vt = runStep();
    unext = us+dt*Vt;
    Vtt = Vtt+2*Vt;
    if(~step)
        Err = Err+2*Vt;
    else
    end

    %f3 f7
    Vt = runStep();
    Vtt = Vtt+Vt;
    if(~step)
        Err = Err-Vt;
    else
```

```
            Err = dt/32*(Err-Vt);
        end

        unext = us+dt/6*Vtt;
```

At the end of each pair of timesteps, we check the error estimate and if the error is too big we repeat the previous two steps with a smaller timestep (if the timestep is too small we end the simulation), and if the error is small we increase our timestep.

```
if(~step)
    step = true;
else
    est = max(abs(Err),[],'all');
    if(est <ermax)
        accept = true;
        temp = 1.25*(est/ermax)^(1/5);
        if temp > 0.2 && temp < 0.8
            ndt = dt / temp;
        elseif temp < 0.2
            ndt = 5.0*dt;
        end
        ndt = min(ndt,dtmax);
    elseif dt <= dtmin
        fprintf("WARNING: timestep has become too small and error
            ↪ margin still not met\n");
        fprintf("Ending script early\n");
    return
    else
        unext = uss; %try again
        dt =dt*0.5;
        step = false;
    end
end
end %Close accept while loop
```

Finally, if a timestep pair is accepted we check if the we should record the current state. If so the current state is copied from the GPU memory into system RAM. If the current time is greater than or equal to the requested simulation time we record the state and end the simulation.

```
%Records a particular frame
ct = ct + 2*dt;
dt=ndt;
if ct <= t(end) && ct >= t(tcounter)
tout(tcounter) = gather(ct);
uout(tcounter,:,:,:) = gather(unext);
tcounter = tcounter + 1;
end
if ct>=t(end)
finished = true;
tout(tcounter) = gather(ct);
uout(tcounter,:,:,:) = gather(unext);
end
```

Appendix B

Parameter sensitivity analyses

Parameter sensitivity analysis attempts to quantify the relative importance of the input factors in determining the output of a model [79, 88]. This guide closely follows the work of Saltelli and colleagues [81], the interested reader can find a more comprehensive treatment in [80].

To begin, given a function of the form

$$Y = f(X_1, X_2, ..., X_n),$$

we can measure the affect the inputs, $\{X_1, X_2, ..., X_n\}$, on the output, Y, to find the relative importance of the inputs. The relative importance is measured as two distinct indexes (known as Sobol indices) normalised by the output variance. The first describes "first order" effects, labelled S_i (where i refers to the input parameter), or the effect of varying a single parameter (and fixing all others) on the model output. This can be calculated using the formula

$$S_i = \frac{V_{X_i}(E_{\boldsymbol{X}_{\sim \boldsymbol{i}}}(Y|X_i))}{V(Y)}, \tag{B.1}$$

Where $V(\cdot)$ is the variance, X_i is the i-th input and $\boldsymbol{X}_{\sim \boldsymbol{i}}$ denotes the matrix of all inputs but X_i. The $E_{\boldsymbol{X}_{\sim \boldsymbol{i}}}(Y|X_i))$ term in the numerator of (B.1) can be interpreted as the mean of Y taken over all possible values of $\boldsymbol{X}_{\sim \boldsymbol{i}}$ while keeping X_i fixed, then the outer variance is taken over all possible values of X_i, which we denote as $V_{X_i}(\cdot)$ [79].

The second index gives the "total" effects, labelled S_{Ti}, or the interaction between all model parameters and their effect on the output. This can be

calculated using the formula

$$S_{Ti} = 1 - \frac{V_{\boldsymbol{X}_{\sim \boldsymbol{i}}}(E_{X_i}(Y|\boldsymbol{X}_{\sim \boldsymbol{i}}))}{V(Y)}. \tag{B.2}$$

The $E_{X_i}(Y|\boldsymbol{X}_{\sim \boldsymbol{i}})$ term in the numerator of (B.2) can be interpreted as the mean of Y taken over all possible values of X_i while keeping $\boldsymbol{X}_{\sim \boldsymbol{i}}$ fixed, then $V_{X_i}(\cdot)$ calculates the variance of this quantity over all possible values of $\boldsymbol{X}_{\sim \boldsymbol{i}}$ [79].

It is possible to estimate (B.1) and (B.2) using the method outlined by Saltelli et al. [81]. To begin let $\boldsymbol{A}$ and $\boldsymbol{B}$ be two independent sampling matrices of the inputs $\{X_1, X_2, ..., X_n\}$. They will be of size $n \times N$, where N is the number of samples. We then construct the set of matrices $\boldsymbol{A}_{\boldsymbol{B}}^{(i)}$ using radial sampling, that is $\boldsymbol{A}_{\boldsymbol{B}}^{(i)}$ is the matrix $\boldsymbol{A}$ with its ith column replaced with the ith column of the matrix $\boldsymbol{B}$. We can then estimate the numerator of (B.1) using,

$$V_{X_i}(E_{\boldsymbol{X}_{\sim \boldsymbol{i}}}(Y|X_i)) \approx \frac{1}{N} \sum_{j=1}^{N} f(\boldsymbol{B})_j \left(f(\boldsymbol{A}_{\boldsymbol{B}}^{(i)})_j - f(\boldsymbol{A})_j \right), \tag{B.3}$$

and the numerator of (B.2) using,

$$V_{\boldsymbol{X}_{\sim \boldsymbol{i}}}(E_{X_i}(Y|\boldsymbol{X}_{\sim \boldsymbol{i}})) \approx \frac{1}{2N} \sum_{j=1}^{N} \left(f(\boldsymbol{A})_j - f(\boldsymbol{A}_{\boldsymbol{B}}^{(i)})_j \right), \tag{B.4}$$

where $f(\boldsymbol{B})_j$ is the output, Y, given the jth input of the matrix $\boldsymbol{B}$ (i.e. the jth row of $\boldsymbol{B}$.

B.1 Example problem

Here, we provide code for the example problem from [81], known as Sobol's G function [3], given by

$$G = G(X_1, X_2, ..., X_n, a_1, a_2, ..., a_n) = \Pi_{i=1}^{n} g_i, \tag{B.5}$$

$$g_i = \frac{|4X_i - 2| + a_i}{1 + a_i}. \tag{B.6}$$

where a_i is a positive real number. The topology of G is driven by the dimensionality n as well as by the values of a_i. Small values of a_i, i.e. $a_i << 1$, lead to important first order effects of the corresponding X_i. Conversely large values of a_i, i.e. $a_i = 9$, lead to low first order effects [81]. If multiple a_i's are small, this leads to high total order effects for the corresponding X_i's [81].

To begin we construct the matricies using a Sobol quasi-random sequence, $\boldsymbol{A}$, $\boldsymbol{B}$, and $\boldsymbol{A}_{\boldsymbol{B}}^{(i)}$ for N samples:

```
%Setup number of tests to run
N=1000;

%Variable Ranges, this specifies the ranges
%of the variables you are testing
%You can increase the number of variables
%by adding extra entries to the vectors
%below.
Vmin = [0 0 0 0];
Vmax = [1 1 1 1];

d=size(Vmin,2);

%This section generates the input matricies,
%A, B and A_B
%(where A_B contains AB(i) for i=1..d
p=sobolset(2*d);
M=p(1:N,:);
A=repmat(Vmin, [N 1])+M(:,1:d).*repmat(Vmax-Vmin, [N 1]);
B=repmat(Vmin, [N 1])+M(:,d+1:end).*repmat(Vmax-Vmin, [N 1]);
AB=zeros(d,N,d);
for i =1:d
    AB(i,:,:)=A;
    AB(i,:,i)=B(:,i);
end
```

We then solve (B.5) for $n = 4$, using $\boldsymbol{A}$, $\boldsymbol{B}$, and $\boldsymbol{A}_{\boldsymbol{B}}^{(i)}$:

```
%% This section runs the G, with n=4
% for each a_i the smaller the value
% the greater the dependence of the
% corresponding variable X_i
Gout = zeros(d+2,N);
```

```
a1=0;a2=0;a3=9;a4=9;

FUN = @(X) (abs(4*X(1)-2)+a1)/(1+a1)*(abs(4*X(2)-2)+a2)/(1+a2)...
*(abs(4*X(3)-2)+a3)/(1+a3)*(abs(4*X(4)-2)+a4)/(1+a4);

for matrixIndex = 1:d+2
    for testIndex = 1:N
        if matrixIndex == 1
            variables = squeeze(A(testIndex,:));
        elseif matrixIndex == 2
            variables = squeeze(B(testIndex,:));
        else
            variables = squeeze(AB(matrixIndex-2,testIndex,:));
        end
    Gout(matrixIndex,testIndex) = FUN(variables);
    end
end
```

Finally, we find (B.3) and (B.4), and thus S_i and S_{Ti}:

```
%% This section runs the parameter sensitivity analysis
Exni = zeros(1,d);
Vxi = zeros(1,d);

for i = 1:d
    Exni(i) = sum((Gout(1,:)-Gout(2+i,:)).^2);
    Vxi(i) = sum(Gout(2,:).*(Gout(2+i,:)-Gout(1,:)));
end

FA = zeros((d+2)*N,1);

for i=1:d+2
    start = (i-1)*N+1;
    finish = i*N;
    FA(start:finish)=Gout(i,:);
end

Exni=1/(2*N)*Exni;
Vxi=1/N*Vxi;
Vary = var(FA);
```

```
% Find Si and Sti
Sti = Exni./Vary;
Si = Vxi./Vary;
```

B.2 Foraging advantage PSA

Using the same method as Section B.1, we construct the matricies using a Sobol quasi-random sequence, $\boldsymbol{A}$, $\boldsymbol{B}$, and $\boldsymbol{A}_{\boldsymbol{B}}^{(i)}$ for $N = 1250$ samples (for a total of 8750 simulations):

```
%Setup variables
N=1250;

%Variable Ranges [D gamma A phi alpha]
Vmin = [0 0 0 0 0];
Vmax = [1 100 10 0.3 1];

d=size(Vmin,2);

%Generate matricies
p=sobolset(2*d);
M=p(1:N,:);
A=repmat(Vmin, [N 1])+M(:,1:d).*repmat(Vmax-Vmin, [N 1]);
B=repmat(Vmin, [N 1])+M(:,d+1:end).*repmat(Vmax-Vmin, [N 1]);
AB=zeros(d,N,d);
for i =1:d
    AB(i,:,:)=A;
    AB(i,:,i)=B(:,i);
end

save('SampleVariables.mat','A','B','AB')
```

We then run a simulation for every variable combination and obtain the steady state foraging advantage and save this into a matrix `ForagingAdvantage` ↪ , we find (B.3) and (B.4), and thus S_i and S_{Ti}:

```
% Create foraging advantage vector
FA = zeros((d+2)*N,1);

for i=1:d+2
```

```
    start = (i-1)*N+1;
    finish = i*N;
    FA(start:finish)=ForagingAdvantage(i,:);
end
%Setup expected values and variances
Exni = zeros(1,d);
Vxi = zeros(1,d);

for i = 1:d
    Exni(i) = sum((ForagingAdvantage(1,:)-ForagingAdvantage(2+i,:))
        ↪ .^2);
    Vxi(i) = sum(ForagingAdvantage(2,:).*(ForagingAdvantage(2+i,:)
        ↪ ...
    -ForagingAdvantage(1,:)));
end

Exni=1/(2*N)*Exni;
Vxi=1/N*Vxi;
Vary = var(FA);

Sti = Exni./Vary;
St = Vxi./Vary;
```

Using this method we obtain the results seen in Section 5.2.4.

Appendix C

Presentations, publications, and prizes

C.1 Presentations

- 2018 Computational Techniques and Applications Conference (CTAC), *An adaptive numerical scheme for a partial integro-differential equation*
- 2018 Australia and New Zealand Industrial and Applied Mathematics New South Wales branch meeting (ANZIAM NSW), *Continuum Modelling of Bacterial Phagocytosis By Neutrophils*
- 2019 Australia and New Zealand Industrial and Applied Mathematics annual conference (ANZIAM), *Continuum modelling of phagocytosis based on cell-cell adhesion and prey-predator relationship*
- 2019 International Congress on Modelling and Simulation (MODISM), *Modelling cell aggregation using a modified swarm model*
- 2019 ANZIAM NSW, *Modelling of swarming locusts with food distributions*
- 2020 ANZIAM, *Food distributions and locust swarms*
- 2020 Annual Meeting of the Society for Mathematical Biology, Poster, *A Mathematical Model Of Locust Foraging And Its Effect On Swarm Formation*

- 2020 CTAC, *Food distributions and locust swarms*
- 2020 ANZIAM NSW, *Hungry Hungry Hoppers: Investigating the interaction of food distribution and gregarisation on the formation of locust hopper bands*
- 2020 Annual Meeting of the Australian Mathematical Society (AUSTMS), *Hungry Hungry Hoppers: Investigating the interaction of food distribution and gregarisation on the formation of locust hopper bands*
- 2021 ANZIAM, *Hungry, hungry hoppers: modelling how and why food affects locust hopper band formation*
- 2021 MODSIM, *Hungry, hungry hoppers: Multidimensinoal modelling of masticating morphs*
- 2021 ANZIAM NSW, Organiser, *Hungry, hungry hoppers: Multidimensinoal modelling of masticating morphs*
- 2022 ANZIAM, *Hungry, hungry hoppers: Multidimensinoal modelling of masticating morphs*
- 2022 ANZIAM NSW Midyear, *A state space based model of collective behaviour with a focus on locusts*

C.2 Full list of author's publications

[1] *Accepted*, Georgiou, F., Buhl, J., Green, J.E.F., Lamichhane, B., and Thamwattana, N. (2022). Modelling foraging competition between solitarious and gregarious organisms in increasingly heterogeneous environments. Journal of Insect Physiology.

[2] Georgiou, F., and Thamwattana, N. (2020). Modelling phagocytosis based on cell–cell adhesion and prey–predator relationship. Mathematics and Computers in Simulation 171, 52–64.

[3] Georgiou, F., Lamichhane, B., and Thamwattana, N. (2018). An adaptive numerical scheme for a partial integro-differential equation. ANZIAM Journal 60, C187–C200.

[4] Georgiou, F., Buhl, J., Green, J.E.F., Lamichhane, B., and Thamwattana, N. (2021). Modelling locust foraging: How and why food affects group formation. PLOS Computational Biology 17, e1008353.

[5] Georgiou, F., Thamwattana, N., and Lamichhane, B.P. (2019) Modelling cell aggregation using a modified swarm model, In Elsawah, S. (ed.) MODSIM2019, 23rd International Congress on Modelling and Simulation. Modelling and Simulation Society of Australia and New Zealand.

[6] Georgiou, F.H., Lamichhane, B., Thamwattana, N., Buhl, J., and Green, E. (2020). A numerical scheme for non-local aggregation with non-linear diffusion and approximations of social potential. ANZIAM Journal 62, C242–C255.

[7] Florio, B., Georgiou, F., Huet, O., Roberts, M.E., Tam, M., and Triadis, D. (2020). Concrush: Understanding fugitive dust production and potential emission at a recycled concrete manufacturing facility. ANZIAM Journal 62, M1–M41.

[8] Orozovic, O., Lavrinec, A., Georgiou, F., and Wensrich, C.M. (2021). A continuum mechanics derivation of the empirical expression relating slug and particle velocities. Powder Technology 380, 598–601.

[9] Shih, H.-Y., Georgiou, F., Curtis, R.A., Paterson, M.B.A., and Phillips, C.J.C. (2020a). Behavioural Evaluation of a Leash Tension Meter Which Measures Pull Direction and Force during Human–Dog On-Leash Walks. Animals 10, 1382.

[10] Shih, H.-Y., Paterson, M.B.A., Georgiou, F., Pachana, N.A., and Phillips, C.J.C. (2020b). Who Is Pulling the Leash? Effects of Human Gender and Dog Sex on Human–Dog Dyads When Walking On-Leash. Animals 10, 1894.

[11] Shih, H.-Y., Paterson, M.B.A., Georgiou, F., Mitchell, L., Pachana, N.A., and Phillips, C.J.C. (2021a). Two Ends of the Leash: Relations Between Personality of Shelter Volunteers and On-leash Walking Behavior With Shelter Dogs. Frontiers in Psychology 12.

[12] Shih, H.-Y., Paterson, M.B.A., Georgiou, F., and Phillips, C.J.C. (2021b). Do Canine Behavioural Assessments and Characteristics Predict the

Human-Dog Interaction When Walking on a Leash in a Shelter Setting? Animals 11, 26.

[13] Shih, H.-Y., Phillips, C.J.C., Mills, D.S., Yang, Y., Georgiou, F., and Paterson, M.B.A. (2021c). Dog Pulling on the Leash: Effects of Restraint by a Neck Collar vs. a Chest Harness. Frontiers in Veterinary Science 8.

C.3 Prizes

- Jul 2022, Best student talk (ANZIAM NSW)
- Feb 2022, Best student paper 2022 (Mathmatical Biology Special Intrest Group of ANZIAM)
- Nov 2021, Grant from Office of the Chief Scientist and Engineer (Sydney, NSW, AU) to host ANZIAM NSW
- Nov 2021, Best student talk - Runner up (ANZIAM NSW)
- Jul 2021, 3MT 3rd place faculty heats (School of Mathematical and Physical Sciences, University of Newcastle)
- Nov 2020, Best student talk - Runner up (ANZIAM NSW)
- Nov 2020, Industry engagement excellence award (School of Mathematical and Physical Sciences, University of Newcastle)
- Sep 2020, MoCaO prize for best student presentation CTAC2020 (Mathematics of Computation and Optimisation Special Interest Group of ANZIAM)

Bibliography

[1] Reynolds Am et al. "Predator percolation, insect outbreaks, and phase polyphenism." In: *Current Biology: CB* 19.1 (Dec. 2008), pp. 20–24. ISSN: 1879-0445. DOI: 10.1016/j.cub.2008.10.070.

[2] Luigi Ambrosio, Nicola Gigli, and Giuseppe Savare. *Gradient Flows: In Metric Spaces and in the Space of Probability Measures*. 2nd ed. Lectures in Mathematics. ETH Zürich. Birkhäuser Basel, 2008. ISBN: 978-3-7643-8721-1. URL: https://www.springer.com/gp/book/9783764387211.

[3] G. E. B. Archer, A. Saltelli, and I. M. Sobol. "Sensitivity measures,anova-like Techniques and the use of bootstrap". In: *Journal of Statistical Computation and Simulation* 58.2 (May 1997), pp. 99–120. ISSN: 0094-9655. DOI: 10.1080/00949659708811825.

[4] Gil Ariel and Amir Ayali. "Locust Collective Motion and Its Modeling". In: *PLOS Computational Biology* 11.12 (Oct. 2015), e1004522. ISSN: 1553-7358. DOI: 10.1371/journal.pcbi.1004522.

[5] Gil Ariel et al. "Individual Pause-and-Go Motion Is Instrumental to the Formation and Maintenance of Swarms of Marching Locust Nymphs". In: *PLOS ONE* 9.7 (July 2014), e101636. ISSN: 1932-6203. DOI: 10.1371/journal.pone.0101636.

[6] Amir Ayali. "The puzzle of locust density-dependent phase polyphenism". In: *Current Opinion in Insect Science*. Global change biology • Molecular Physiology 35 (Oct. 2019), pp. 41–47. ISSN: 2214-5745. DOI: 10.1016/j.cois.2019.06.008.

[7] Alethea Barbaro et al. "Discrete and continuous models of the dynamics of pelagic fish: application to the capelin". In: (Jan. 2008). URL: https://escholarship.org/uc/item/1b85v0x9.

[8] Alethea Barbaro et al. "Modelling and simulations of the migration of pelagic fish". In: *ICES Journal of Marine Science* 66.5 (June 2009), pp. 826–838. ISSN: 1054-3139. DOI: 10.1093/icesjms/fsp067.

[9] Sepideh Bazazi et al. "Collective Motion and Cannibalism in Locust Migratory Bands". In: *Current Biology* 18.10 (May 2008), pp. 735–739. ISSN: 0960-9822. DOI: 10.1016/j.cub.2008.04.035.

[10] Sepideh Bazazi et al. "Nutritional state and collective motion: from individuals to mass migration". In: *Proceedings of the Royal Society B: Biological Sciences* 278.1704 (Feb. 2011), pp. 356–363. DOI: 10.1098/rspb.2010.1447.

[11] A. Bernoff and C. Topaz. "Nonlocal Aggregation Models: A Primer of Swarm Equilibria". In: *SIAM Review* 55.4 (Jan. 2013), pp. 709–747. ISSN: 0036-1445. DOI: 10.1137/130925669.

[12] Andrew J. Bernoff and Chad M. Topaz. "Biological Aggregation Driven by Social and Environmental Factors: A Nonlocal Model and Its Degenerate Cahn–Hilliard Approximation". In: *SIAM Journal on Applied Dynamical Systems* 15.3 (Jan. 2016), pp. 1528–1562. DOI: 10.1137/15M1031151.

[13] Andrew J. Bernoff et al. "Agent-based and continuous models of hopper bands for the Australian plague locust: How resource consumption mediates pulse formation and geometry". In: *PLOS Computational Biology* 16.5 (Apr. 2020), e1007820. ISSN: 1553-7358. DOI: 10.1371/journal.pcbi.1007820.

[14] M. Bodnar and J. J. L. Velazquez. "An integro-differential equation arising as a limit of individual cell-based models". In: *Journal of Differential Equations* 222.2 (Mar. 2006), pp. 341–380. ISSN: 0022-0396. DOI: 10.1016/j.jde.2005.07.025.

[15] J. Buhl, Gregory A. Sword, and Stephen J. Simpson. "Using field data to test locust migratory band collective movement models". In: *Interface Focus* 2.6 (Dec. 2012), pp. 757–763. ISSN: 2042-8898. DOI: 10.1098/rsfs.2012.0024.

[16] J. Buhl et al. "From Disorder to Order in Marching Locusts". In: *Science* 312.5778 (June 2006), pp. 1402–1406. ISSN: 0036-8075, 1095-9203. DOI: 10.1126/science.1125142.

[17] Jerome Buhl et al. "Group structure in locust migratory bands". In: *Behavioral Ecology and Sociobiology* 65.2 (Feb. 2011), pp. 265–273. ISSN: 1432-0762. DOI: 10.1007/s00265-010-1041-x.

[18] Martin Burger, Razvan Fetecau, and Yanghong Huang. "Stationary States and Asymptotic Behavior of Aggregation Models with Nonlinear Local Repulsion". In: *SIAM Journal on Applied Dynamical Systems* 13.1 (Jan. 2014), pp. 397–424. DOI: 10.1137/130923786.

[19] Raimund Bürger et al. "Implicit-explicit methods for a class of nonlinear nonlocal gradient flow equations modelling collective behaviour". In: *Applied Numerical Mathematics* 144 (Oct. 2019), pp. 234–252. ISSN: 0168-9274. DOI: 10.1016/j.apnum.2019.04.018.

[20] J. A. Carrillo, S. Martin, and V. Panferov. "A new interaction potential for swarming models". In: *Physica D: Nonlinear Phenomena*. Emergent Behaviour in Multi-particle Systems with Non-local Interactions 260 (Oct. 2013), pp. 112–126. ISSN: 0167-2789. DOI: 10.1016/j.physd.2013.02.004.

[21] José Antonio Carrillo, Young-Pil Choi, and Maxime Hauray. "The derivation of swarming models: Mean-field limit and Wasserstein distances". In: *Collective Dynamics from Bacteria to Crowds: An Excursion Through Modeling, Analysis and Simulation*. Ed. by Adrian Muntean and Federico Toschi. CISM International Centre for Mechanical Sciences. Springer Vienna, 2014, pp. 1–46. ISBN: 978-3-7091-1785-9. DOI: 10.1007/978-3-7091-1785-9_1. URL: https://doi.org/10.1007/978-3-7091-1785-9_1.

[22] Eric L Charnov. "Optimal foraging, the marginal value theorem". In: *Theoretical population biology* 9.2 (1976), pp. 129–136.

[23] Yanguang Chen. "Equivalent relation between normalized spatial entropy and fractal dimension". In: *Physica A: Statistical Mechanics and its Applications* 553 (Sept. 2020), p. 124627. ISSN: 0378-4371. DOI: 10.1016/j.physa.2020.124627.

[24] Edward A Codling, Michael J Plank, and Simon Benhamou. "Random walk models in biology". In: *Journal of The Royal Society Interface* 5.25 (Aug. 2008), pp. 813–834. DOI: 10.1098/rsif.2008.0014.

[25] Matthew Collett et al. "Spatial scales of desert locust gregarization". In: *Proceedings of the National Academy of Sciences* 95.22 (Oct. 1998), pp. 13052–13055. ISSN: 0027-8424, 1091-6490. DOI: 10.1073/pnas.95.22.13052.

[26] Felipe Cucker and Steve Smale. "Emergent Behavior in Flocks". In: *IEEE Transactions on Automatic Control* 52.5 (May 2007), pp. 852–862. ISSN: 1558-2523. DOI: 10.1109/TAC.2007.895842.

[27] D. A. Cullen et al. "Chapter Seven - From Molecules to Management: Mechanisms and Consequences of Locust Phase Polyphenism". In: *Insect Epigenetics*. Ed. by Heleen Verlinden. Vol. 53. Advances in Insect Physiology. Academic Press, 2017, pp. 167–285. DOI: https://doi.org/10.1016/bs.aiip.2017.06.002. URL: https://www.sciencedirect.com/science/article/pii/S0065280617300231.

[28] Darron A. Cullen et al. "Behavioural phase change in the Australian plague locust, Chortoicetes terminifera, is triggered by tactile stimulation of the antennae". In: *Journal of Insect Physiology*. Locust Research in the Age of Model Organisms In honor of M.P. Pener's 80th Birthday 56.8 (Aug. 2010), pp. 937–942. ISSN: 0022-1910. DOI: 10.1016/j.jinsphys.2010.04.023.

[29] Darron A. Cullen et al. "Chapter Seven - From Molecules to Management: Mechanisms and Consequences of Locust Phase Polyphenism". In: *Advances in Insect Physiology*. Ed. by Heleen Verlinden. Vol. 53. Insect Epigenetics. Academic Press, Jan. 2017, pp. 167–285. DOI: 10.1016/bs.aiip.2017.06.002. URL: http://www.sciencedirect.com/science/article/pii/S0065280617300231.

[30] M. R. D'Orsogna et al. "Self-Propelled Particles with Soft-Core Interactions: Patterns, Stability, and Collapse". In: *Physical Review Letters* 96.10 (Mar. 2006), p. 104302. DOI: 10.1103/PhysRevLett.96.104302.

[31] E. Despland, M. Collett, and S. J. Simpson. "Small-scale processes in desert locust swarm formation: how vegetation patterns influence gregarization". In: *Oikos* 88.3 (2000), pp. 652–662. ISSN: 1600-0706. DOI: 10.1034/j.1600-0706.2000.880322.x.

[32] E. Despland and S. J. Simpson. "Small-scale vegetation patterns in the parental environment influence the phase state of hatchlings of the desert locust". In: *Physiological Entomology* 25.1 (2000), pp. 74–81. ISSN: 1365-3032. DOI: 10.1046/j.1365-3032.2000.00166.x.

[33] Emma Despland, Jane Rosenberg, and Stephen J. Simpson. "Landscape structure and locust swarming: a satellite's eye view". In: *Ecography* 27.3 (2004), pp. 381–391. ISSN: 1600-0587. DOI: 10.1111/j.0906-7590.2004.03779.x.

[34] Jamila Dkhili et al. "Effects of starvation and Vegetation Distribution on Locust Collective Motion". In: *Journal of Insect Behavior* 32.3 (May 2019), pp. 207–217. ISSN: 1572-8889. DOI: 10.1007/s10905-019-09727-8.

[35] J. R. Dormand and P. J. Prince. "A family of embedded Runge-Kutta formulae". In: *Journal of Computational and Applied Mathematics* 6.1 (Mar. 1980), pp. 19–26. ISSN: 0377-0427. DOI: 10.1016/0771-050X(80)90013-3.

[36] P. E. Ellis and C. Ashall. "Field Studies on diurnal Behaviour, Movement and Aggregation in the Desert Locust (Schistocerca gregaria Forskål)." In: *Field Studies on diurnal Behaviour, Movement and Aggregation in the Desert Locust (Schistocerca gregaria Forskål).* 25 (1957). URL: https://www.cabdirect.org/cabdirect/abstract/19570500973.

[37] The Food and Agriculture Organization of the United Nations. "FAO - News Article: Alarm over Desert Locusts increases as new generation of the destructive pests starts breeding in Horn of Africa". In: (2020). URL: http://www.fao.org/news/story/en/item/1258877/icode/.

[38] The Food and Agriculture Organization of the United Nations (2004). *Hunger in their wake: inside the battle against the desert locust.* URL: http://www.fao.org/Newsroom/en/focus/2004/51040/index.html.

[39] Zachary J. Foster. "The 1915 Locust Attack in Syria and Palestine and its Role in the Famine During the First World War". In: *Middle Eastern Studies* 51.3 (May 2015), pp. 370–394. ISSN: 0026-3206. DOI: 10.1080/00263206.2014.976624.

[40] Gabriella Gamberale and Birgitta S. Tullberg. "Aposematism and gregariousness: the combined effect of group size and coloration on signal repellence". In: *Proceedings of the Royal Society of London. Series B: Biological Sciences* 265.1399 (May 1998), pp. 889–894. DOI: 10.1098/rspb.1998.0374.

[41] F Georgiou, N Thamwattana, and B P Lamichhane. "Modelling cell aggregation using a modified swarm model". In: (), p. 6.

[42] F. Georgiou, B. P. Lamichhane, and N. Thamwattana. "An adaptive numerical scheme for a partial integro-differential equation". In: *Proceedings of the 18th Biennial Computational Techniques and Applications Conference, CTAC-2018*. Ed. by Bishnu Lamichhane, Thanh Tran, and Judith Bunder. Vol. 60. ANZIAM J. http://journal.austms.org.au/ojs/index.php/ANZIAMJ/article/view/14066 [October 9, 2019]. Oct. 2019, pp. C187–C200. DOI: 10.21914/anziamj.v60i0.14066.

[43] F. Georgiou, N. Thamwattana, and B.P. Lamichhane. "Modelling cell aggregation using a modified swarm model". In: *MODSIM2019* 6.1 (Dec. 2019). ISSN: 9780975840092. DOI: 10.36334/modsim.2019.a1.georgiou.

[44] F. Georgiou et al. "A numerical scheme for non-local aggregation with non-linear diffusion and approximations of social potential". In: *Proceedings of the 19th Biennial Computational Techniques and Applications Conference, CTAC-2020*. Ed. by William McLean, Shev Macnamara, and Judith Bunder. Vol. 62. ANZIAM J. http://journal.austms.org.au/ojs/index.php/ANZIAMJ/article/view/16056 [2022-03-07]. Mar. 2022, pp. C242–C255. DOI: 10.21914/anziamj.v62.16056.

[45] Fillipe Georgiou et al. "Modelling locust foraging: How and why food affects group formation". In: *PLOS Computational Biology* 17.7 (July 2021), e1008353. ISSN: 1553-7358. DOI: 10.1371/journal.pcbi.1008353.

[46] R. C. Gonzalez, R. E. Woods, and S. L. Eddins. *Digital Image Processing Using MATLAB*. Pearson Prentice Hall, 2004. ISBN: 978-0-13-008519-1.

[47] J. E. F. Green et al. "Non-local models for the formation of hepatocyte–stellate cell aggregates". In: *Journal of Theoretical Biology* 267.1 (Nov. 2010), pp. 106–120. ISSN: 0022-5193. DOI: 10.1016/j.jtbi.2010.08.013.

[48] Vishwesha Guttal et al. "Cannibalism can drive the evolution of behavioural phase polyphenism in locusts". In: *Ecology Letters* 15.10 (2012), pp. 1158–1166. ISSN: 1461-0248. DOI: https://doi.org/10.1111/j.1461-0248.2012.01840.x.

[49] Margaret J. Haggis. "Distribution of the African armyworm, Spodoptera exempta (walker) (Lepidoptera: Noctuidae), and the frequency of larval outbreaks in Africa and Arabia". In: *Bulletin of Entomological Research* 76.1 (Mar. 1986), pp. 151–170. ISSN: 1475-2670, 0007-4853. DOI: 10.1017/S0007485300015376.

[50] Charlotte K. Hemelrijk and Hanspeter Kunz. "Density distribution and size sorting in fish schools: an individual-based model". In: *Behavioral Ecology* 16.1 (Jan. 2005), pp. 178–187. ISSN: 1045-2249. DOI: 10.1093/beheco/arh149.

[51] H. Hildenbrandt, C. Carere, and C.K. Hemelrijk. "Self-organized aerial displays of thousands of starlings: a model". In: *Behavioral Ecology* 21.6 (Nov. 2010), pp. 1349–1359. ISSN: 1045-2249. DOI: 10.1093/beheco/arq149.

[52] M.E. Hosea and L.F. Shampine. "Estimating the error of the classic Runge–Kutta Formula". In: *Applied Mathematics and Computation* 66.2–3 (Dec. 1994), pp. 217–226. ISSN: 0096-3003. DOI: 10.1016/0096-3003(94)90117-1.

[53] Andreas Huth and Christian Wissel. "The simulation of the movement of fish schools". In: *Journal of Theoretical Biology* 156.3 (June 1992), pp. 365–385. ISSN: 0022-5193. DOI: 10.1016/S0022-5193(05)80681-2.

[54] Vranken I. et al. "A review on the use of entropy in landscape ecology: heterogeneity, unpredictability, scale dependence and their links with thermodynamics". In: *Landscape Ecology* 30 (Jan. 2015). DOI: 10.1007/s10980-014-0105-0.

[55] Matthee J.J. "A study of the phases of the army worm (Laphygma exempta Walk.)" In: *Journal of the Entomological Society of Southern Africa* 9.1 (Mar. 1946), pp. 60–77. DOI: 10.10520/AJA00128789_4393.

[56] Yael Katz et al. "Inferring the structure and dynamics of interactions in schooling fish". In: *Proceedings of the National Academy of Sciences of the United States of America* 108.46 (Nov. 2011), pp. 18720–18725. ISSN: 1091-6490. DOI: 10.1073/pnas.1107583108.

[57] Merrit Kennedy. "Why Are Swarms Of Locusts Wreaking Havoc In East Africa?" In: *NPR.org* (2020). URL: https://www.npr.org/2020/02/21/807483297/why-are-swarms-of-locusts-wreaking-havoc-in-east-africa.

[58] Jens Krause et al. *Living in Groups*. Google-Books-ID: HAoUFfVFtMcC. OUP Oxford, Oct. 2002. ISBN: 978-0-19-850818-2.

[59] Hanspeter Kunz and Charlotte K. Hemelrijk. "Artificial fish schools: collective effects of school size, body size, and body form". In: *Artificial Life* 9.3 (2003), pp. 237–253. ISSN: 1064-5462. DOI: 10.1162/106454603322392451.

[60] Marysa Laguë et al. "The effects of facilitation and competition on group foraging in patches". In: *Journal of Theoretical Biology* 310 (Oct. 2012), pp. 88–96. ISSN: 0022-5193. DOI: 10.1016/j.jtbi.2012.06.024.

[61] Yue-Xian Li, Ryan Lukeman, and Leah Edelstein-Keshet. "Minimal mechanisms for school formation in self-propelled particles". In: *Physica D: Nonlinear Phenomena* 237.5 (May 2008), pp. 699–720. ISSN: 0167-2789. DOI: 10.1016/j.physd.2007.10.009.

[62] Mathieu Lihoreau et al. "Collective foraging in spatially complex nutritional environments". In: *Philosophical Transactions of the Royal Society of London. Series B, Biological Sciences* 372.1727 (Aug. 2017). ISSN: 1471-2970. DOI: 10.1098/rstb.2016.0238.

[63] Qian Liu et al. "Climate, disasters, wars and the collapse of the Ming Dynasty". In: *Environmental Earth Sciences* 77.2 (Jan. 2018), p. 44. ISSN: 1866-6299. DOI: 10.1007/s12665-017-7194-4.

[64] Ryan Lukeman, Yue-Xian Li, and Leah Edelstein-Keshet. "A conceptual model for milling formations in biological aggregates". In: *Bulletin of Mathematical Biology* 71.2 (Feb. 2009), pp. 352–382. ISSN: 1522-9602. DOI: 10.1007/s11538-008-9365-7.

[65] Koutaro Ould Maeno et al. "A general model of the thermal constraints on the world's most destructive locust, Schistocerca gregaria". en. In: *Ecological Applications* 31.4 (2021), e02310. ISSN: 1939-5582. DOI: 10.1002/eap.2310.

[66] Benoit B Mandelbrot. *The fractal geometry of nature*. Vol. 1. WH freeman New York, 1982.

[67] A. Mogilner et al. "Mutual interactions, potentials, and individual distance in a social aggregation". en. In: *Journal of Mathematical Biology* 47.4 (Sept. 2003), pp. 353–389. ISSN: 1432-1416. DOI: 10.1007/s00285-003-0209-7.

[68] Alexander Mogilner and Leah Edelstein-Keshet. "A non-local model for a swarm". In: *Journal of Mathematical Biology* 38.6 (June 1999), pp. 534–570. ISSN: 1432-1416. DOI: 10.1007/s002850050158.

[69] Denis Mollison. "Spatial Contact Models for Ecological and Epidemic Spread". In: *Journal of the Royal Statistical Society. Series B (Methodological)* 39.3 (1977), pp. 283–326. ISSN: 0035-9246.

[70] Kevin J. Painter and Jonathan A. Sherratt. "Modelling the movement of interacting cell populations". In: *Journal of Theoretical Biology* 225.3 (Dec. 2003), pp. 327–339. ISSN: 0022-5193. DOI: 10.1016/S0022-5193(03)00258-3.

[71] Meir Paul Pener and Stephen J. Simpson. "Locust Phase Polyphenism: An Update". In: *Advances in Insect Physiology*. Vol. 36. Academic Press, Jan. 2009, pp. 1–272. DOI: 10.1016/S0065-2806(08)36001-9. URL: http://www.sciencedirect.com/science/article/pii/S0065280608360019.

[72] David Raubenheimer and Gerd Gäde. "Separating food and water deprivation in locusts: effects on the patterns of consumption, locomotion and growth". en. In: *Physiological Entomology* 21.1 (1996), pp. 76–84. ISSN: 1365-3032. DOI: 10.1111/j.1365-3032.1996.tb00838.x.

[73] Alfréd Rényi. "On measures of information and entropy". In: *Proceedings of the 4th Berkeley symposium on mathematics, statistics and probability*. Vol. 1. 547. 1961.

[74] David F. Rhoades. "Offensive-Defensive Interactions between Herbivores and Plants: Their Relevance in Herbivore Population Dynamics and Ecological Theory". In: *The American Naturalist* 125.2 (Feb. 1985), pp. 205–238. ISSN: 0003-0147. DOI: 10.1086/284338.

[75] Pawel Romanczuk, Iain D. Couzin, and Lutz Schimansky-Geier. "Collective Motion due to Individual Escape and Pursuit Response". In: *Physical Review Letters* 102.1 (Jan. 2009), p. 010602. DOI: 10.1103/PhysRevLett.102.010602.

[76] David Ruelle. *Statistical Mechanics: Rigorous Results*. Google-Books-ID: 2HPVCgAAQBAJ. World Scientific, Apr. 1969. ISBN: 978-981-4495-00-4.

[77] C. Runge. "Ueber die numerische Auflosung von Differentialgleichungen". In: (June 1895). DOI: 10.1007/bf01446807. URL: https://zenodo.org/record/2178704.

[78] M. Saiful Islam et al. "Parental effects on the behaviour and colouration of nymphs of the desert locust Schistocerca gregaria". In: *Journal of Insect Physiology* 40.2 (Feb. 1994), pp. 173–181. ISSN: 0022-1910. DOI: 10.1016/0022-1910(94)90089-2.

[79] Andrea Saltelli. "Making best use of model evaluations to compute sensitivity indices". In: *Computer Physics Communications* 145.2 (May 2002), pp. 280–297. ISSN: 0010-4655. DOI: 10.1016/S0010-4655(02)00280-1.

[80] Andrea Saltelli et al. *Global sensitivity analysis: the primer*. John Wiley & Sons, 2008.

[81] Andrea Saltelli et al. "Variance based sensitivity analysis of model output. Design and estimator for the total sensitivity index". In: *Computer Physics Communications* 181.2 (Feb. 2010), pp. 259–270. ISSN: 0010-4655. DOI: 10.1016/j.cpc.2009.09.018.

[82] G. H. Schmidt and R. Albutz. "Identification of solitary and gregarious populations of the desert locust, Schistocerca gregaria, by experimental breeding (Caelifera: Acrididae)". In: *Entomologia generalis* (1999). ISSN: 0171-8177. URL: http://agris.fao.org/agris-search/search.do?recordID=US201302927413.

[83] Claude E Shannon. "A mathematical theory of communication". In: *The Bell system technical journal* 27.3 (1948), pp. 379–423.

[84] Birgitta Sillen-Tullberg and Olof Leimar. "The Evolution of Gregariousness in Distasteful Insects as a Defense Against Predators". In: *The American Naturalist* 132.5 (Nov. 1988), pp. 723–734. ISSN: 0003-0147. DOI: 10.1086/284884.

[85] M. S. J. Simmonds and W. M. Blaney. "Effects of rearing density on development and feeding behaviour in larvae of Spodoptera exempta". In: *Journal of Insect Physiology* 32.12 (Jan. 1986), pp. 1043–1053. ISSN: 0022-1910. DOI: 10.1016/0022-1910(86)90124-1.

[86] Stephen J. Simpson, Alan R. McCAFFERY, and Bernd F. Hägele. "A behavioural analysis of phase change in the desert locust". In: *Biological Reviews* 74.4 (1999), pp. 461–480. ISSN: 1469-185X. DOI: 10.1111/j.1469-185X.1999.tb00038.x.

[87] Stephen J. Simpson, Gregory A. Sword, and Nathan Lo. "Polyphenism in Insects". In: *Current Biology* 21.18 (Sept. 2011), R738–R749. ISSN: 0960-9822. DOI: 10.1016/j.cub.2011.06.006.

[88] I. M Sobol. "Global sensitivity indices for nonlinear mathematical models and their Monte Carlo estimates". In: *Mathematics and Computers in Simulation*. The Second IMACS Seminar on Monte Carlo Methods 55.1 (Feb. 2001), pp. 271–280. ISSN: 0378-4754. DOI: 10.1016/S0378-4754(00)00270-6.

[89] Gustaf Söderlind. "Time-step selection algorithms: Adaptivity, control, and signal processing". In: *Applied Numerical Mathematics* 56.3 (2006). Selected Papers, The Third International Conference on the Numerical Solutions of Volterra and Delay Equations, pp. 488–502. ISSN: 0168-9274. DOI: https://doi.org/10.1016/j.apnum.2005.04.026. URL: https://www.sciencedirect.com/science/article/pii/S0168927405000954.

[90] Clive A. Spinage. "Locusts the Forgotten Plague Part II: History of Locust Plagues". In: *African Ecology: Benchmarks and Historical Perspectives*. Springer Berlin Heidelberg, 2012, pp. 533–569. ISBN: 978-3-642-22872-8. DOI: 10.1007/978-3-642-22872-8_11. URL: https://doi.org/10.1007/978-3-642-22872-8_11.

[91] A Steedman. *Locust handbook*. 3rd. Natural Resources Institute, 1990. ISBN: 0-85954-281-5.

[92] David W. Stephens and John R. Krebs. *Foraging Theory*. Vol. 1. Princeton University Press, 1986. ISBN: 9780691084411. URL: http://www.jstor.org/stable/j.ctvs32s6b (visited on 10/26/2022).

[93] Gregory A. Sword, Michel Lecoq, and Stephen J. Simpson. "Phase polyphenism and preventative locust management". In: *Journal of Insect Physiology*. Locust Research in the Age of Model Organisms In honor of M.P. Pener's 80th Birthday 56.8 (Aug. 2010), pp. 949–957. ISSN: 0022-1910. DOI: 10.1016/j.jinsphys.2010.05.005.

[94] P Symmons and Keith Cressman. "Desert Locust Guidelines 1. Biology and Behaviour". In: (Jan. 2001).

[95] Nessy Tania et al. "Role of social interactions in dynamic patterns of resource patches and forager aggregation". In: *Proceedings of the National Academy of Sciences* 109.28 (July 2012), pp. 11228–11233. ISSN: 0027-8424, 1091-6490. DOI: 10.1073/pnas.1201739109.

[96] C. M. Topaz et al. "A model for rolling swarms of locusts". In: *The European Physical Journal Special Topics* 157.1 (Apr. 2008), pp. 93–109. ISSN: 1951-6401. DOI: 10.1140/epjst/e2008-00633-y.

[97] Chad M. Topaz, Andrea L. Bertozzi, and Mark A. Lewis. "A Nonlocal Continuum Model for Biological Aggregation". In: *Bulletin of Mathematical Biology* 68.7 (July 2006), p. 1601. ISSN: 1522-9602. DOI: 10.1007/s11538-006-9088-6.

[98] Chad M. Topaz et al. "Locust Dynamics: Behavioral Phase Change and Swarming". In: *PLOS Computational Biology* 8.8 (Aug. 2012), e1002642. ISSN: 1553-7358. DOI: 10.1371/journal.pcbi.1002642.

[99] B. P Uvarov and Imperial Institute of Entomology. *Locusts and grasshoppers. A handbook for their study and control*. Imperial Bureau of Entomology, 1928.

[100] Boris Uvarov et al. *Grasshoppers and locusts. A handbook of general acridology Vol. 2. Behaviour, ecology, biogeography, population dynamics.* Centre for Overseas Pest Research, 1977.

[101] Milind G. Watve and Maithili M. Jog. "Epidemic Diseases and Host Clustering: An Optimum Cluster Size Ensures Maximum Survival". In: *Journal of Theoretical Biology* 184.2 (Jan. 1997), pp. 165–169. ISSN: 0022-5193. DOI: 10.1006/jtbi.1996.0267.

[102] Eric W. Weisstein. *CRC Concise Encyclopedia of Mathematics*. CRC Press, Dec. 2002. ISBN: 978-1-4200-3522-3.